NOAA Technical Memorandum ERL NSSL-90

SUMMARY OF AEC-ERDA-NRC SUPPORTED RESEARCH AT NSSL 1973-1979

J. T. Lee, Editor

Principal Authors:
J. T. Lee
Dusan S. Zrnic'
Robert P. Davies-Jones
Joseph H. Golden

National Severe Storms Laboratory
Norman, Oklahoma
March 1981

UNITED STATES
DEPARTMENT OF COMMERCE
Malcolm Baldrige,
Secretary

NATIONAL OCEANIC AND
ATMOSPHERIC ADMINISTRATION
James P. Walsh,
Acting Administrator

Environmental Research
Laboratories
Joseph O. Fletcher,
Acting Director

TABLE OF CONTENTS

LIST OF FIGURES

LIST OF TABLES

SUMMARY OF AEC-ERDA-NRC SUPPORTED RESEARCH AT NSSL 1973-1979[+]

Jean T. Lee, Robert P. Davies-Jones, Dusan S. Zrnic' and Joseph H. Golden*

Abstract

In 1973, the mutual interest in tornado wind and pressure structure witnessed the formation of a cooperative research program between the National Oceanic and Atmospheric Administration's (NOAA) National Severe Storms Laboratory at Norman, Oklahoma and the Atomic Energy Commission (AEC) with its successor organizations, the Energy Research and Development Administration (ERDA) and the Nuclear Regulatory Commission (NRC). This report presents an overview of the research and results generated through the coordinated effort.

This research proceeded along several lines - direct observations such as radar and photographic, indirect observations such as damage inferred wind flows, and modeling. Early stages of the research witnessed the emergence of Doppler radar as a viable observational tool through the development of: (a) real-time data processors; (b) high pulse repetition frequency system raising the maximum unambiguous velocity to ± 91.3 m s^{-1}; (c) expansion of mean velocity processor from 200 to 572 gate locations; and (d) development of real-time display of the intensity, velocity, and spectrum width. This led to the identification of a characteristic signature for the tornado mesocyclone and the tornado vortex. The mesocyclone signature was found to precede tornado sightings by an average of more than 20 minutes. The mobile Tornado Intercept Team development which made use of this information, is described. Results of these field observations, and photogrammetric analysis of movies taken of tornadoes are discussed. Horizontal windspeeds near 95 m s^{-1} were calculated through the tracking of debris clusters. Maximum vertical windspeeds near 60 m s^{-1} were found. Circulation values obtained in some tornadoes were on the order of 10^5 $m^2 s^{-1}$. Damage surveys are also discussed. Waterspout studies conducted to further the understanding of vortex motion, are described and detailed, as are aircraft penetrations of the vortex. A climatology of waterspouts was also obtained.

Progress in tornado modeling and comments on the design basis tornado are presented.

[+]The work was conducted under terms of Interagency Agreements AT(49-25)-1004, RES-76-106, AT(49-5)-1289, E(49-5)-1289 and EX-76-A-27-1289 between the granting agencies and NOAA.

*Dr. Joseph H. Golden is currently affiliated with the Environmental Research Laboratories in Boulder, Colorado.

SUMMARY OF AEC-ERDA-NRC SUPPORTED RESEARCH AT NSSL 1973-1979

1. INTRODUCTION AND HISTORY

Structures housing nuclear reactors must be designed to resist penetration by airborne projectiles and must survive intact through extreme loadings by wind and pressure. Maximum wind speeds and pressure differentials are associated with tornadoes. In FY 1973, support was extended by the Atomic Energy Commission (later the Energy Research and Development Administration and Nuclear Regulatory Commission) to NSSL's research on tornado distribution and wind speeds.

NSSL has two Doppler weather radars with fully steerable 9.1 m (30 ft.) diameter parabolic antennas. Their small angular resolution (1.2×10^{-2} radians or .8°) permits observations of small-scale weather phenomena such as tornadic storms. In addition, the highly sensitive systems can detect scatterers where only a few exist, thereby facilitating detailed measurement of wind velocity distributions.

Objectives of the joint program were defined as follows:

1) Modify the Doppler radar at Norman (NRO), Oklahoma, to obtain reliable estimates of tornadic wind speeds in the strongest cases;

2) Estimate tornado wind speeds through the acquisition and analysis of tornado movies;

3) Estimate wind speeds via analysis of tornado damage to structures for which engineering data is available;

4) Develop a wind speed distribution model through numerical simulation;

5) Develop a clearer understanding of vortex motion through *in situ* measurements on waterspouts;

6) Determine tornado and waterspout severity and distribution based on historical events.

Varying success has been achieved toward meeting these objectives, and results are detailed in the following sections. An historical overview of the program is given by the following list of "milestones":

1) Spring 1973: Mesocyclone signature identified in real time in single Doppler velocity fields.

2) May 1973: Initial section of a real-time radar data processor and display unit ("Ling") received, thereby paving the way for real-time digital processing of Doppler radar data.

3) May 24, 1973: Union City tornadic storm - first severe storm observed throughout lifetime by a Doppler radar. First major tornado life cycle photographed by tornado intercept teams; first clue of tornado vortex signature.

4) Sept. 1973: Doppler radar operated for first time with High Pulse Repetition Frequency (HPRF) (3,474.4 Hz) yielding a maximum unambiguous velocity spread of 91.3 m s^{-1} with maximum unambiguous range of 43.17 km.

5) Oct. 1973: Mean velocity processor (MVP) expanded to provide data at 512 gate locations instead of 200.

6) Spring 1974: Dual-Doppler capability brought on line with activation of Cimarron (CIM) Doppler radar.

7) Apr. 20, 1974: Del City, Oklahoma, tornado with first dual-Doppler coverage of a tornadic storm.

8) Summer 1974: Waterspout climatology study in progress. Successful interfacing of Ling system with Norman Doppler radar and real-time display of velocity spectrum and radial velocity.

9) Fall 1974: Waterspout program expanded to include waterspout penetrations by an instrumented aircraft, piloted by Dr. Peter Sinclair of Colorado State University.

10) Feb. 1975: Completion of waterspout climatology report.

11) Spring 1975: Switching time between high PRF and normal PRF operating mode reduced to less than two minutes from previous 15 to 30 minutes.

12) June 1975: First tornadic vortex signature identified in real time.

13) May 1976: First high PRF data collection in a tornadic storm.

14) June 1976: Tornado climatology statistics published.

15) Dec. 1976: Comprehensive report published on the Union City tornado of May 24, 1973.

16) Spring 1977: First high PRF data collection on a tornado.

17) Fall 1977: Tornado Spotter's Guide movie produced.

18) Dec. 1977: Publication of comprehensive report on engineering-oriented perspectives of tornadoes (prepared by Texas Tech University).

Photography was obtained (P) or Doppler radar data collected (D) on the following tornado cases:

1.	Kailua-Kona, Hawaii (P)	28 January 1971
2.	Union City, OK (P, D)	24 May 1973
3.	Norman, OK (P, D)	4 June 1973
4.	Fort Cobb, OK (P, D)	18 June 1973
5.	Salina, KS (P)	25 September 1973
6.	Parker, IN (P)	3 April 1974
7.	Xenia, OH (P)	3 April 1974
8.	Oklahoma City, OK (P, D)	8 June 1974
9.	Harrah, OK (P, D)	8 June 1974
10.	Luther, OK (P, D)	8 June 1974
11.	Great Bend, KS (P)	30 August 1974

12.	Alva, OK (anticyclonic) (P)	6 June 1975
13.	Stillwater, OK (P, D)	13 June 1975
14.	Dallas, TX (P)	26 May 1976
15.	Waurika, OK (P, D)	30 May 1976
16.	Central Iowa (P)	13 June 1976
17.	Quail, TX (P)	16 May 1977
18.	Shamrock, TX (P)	16 May 1977
19.	Sweetwater, OK (P, D)	16 May 1977
20.	Cheyenne, OK (P, D)	16 May 1977
21.	Altus, OK (P, D)	20 May 1977
22.	Tipton, OK (P, D)	20 May 1977
23.	Ft. Cobb, OK (D)	20 May 1977
24.	Binger, OK (D)	20 May 1977
25.	Del City, OK (P, D)	20 May 1977
26.	Arcadia, OK (D)	20 May 1977
27.	Piedmont, OK (P, D)	30 April 1978
28.	Vernon, TX (D)	10 April 1979
29.	Harrold, TX (P, D)	10 April 1979
30.	Seymour, TX (P, D)	10 April 1979
31.	Lawton, TX (P, D)	10 April 1979
32.	Wichita Falls, TX (P, D)	10 April 1979
33.	Orienta, OK (P, D)	2 May 1979
34.	Lahoma, OK (D)	2 May 1979
35.	Marshall, OK (P, D)	2 May 1979

2. DOPPLER RADAR

2.1 Radar System Development

Since 1973, the AEC provided major support for the development of improved Doppler capability on the NSSL's radar. The radar already had a fully coherent transmitter, but there were major engineering changes over a period of several years so that today the only components left of the old FPS-18 radar are the final power stage and support circuitry. A 30-foot parabolic reflector antenna and pedestal were custom built, and so was the entire receiver and signal processing circuitry. Figure 1 represents the system block diagram of the "Dopplerized " radar system. Local and coherent oscillators were replaced with stable, solid-state oscillators. A low-noise (noise figure 1.7 dB) parametric amplifier was installed at the front end. Two Gaussian-shaped filters were designed and built to match the transmitted pulse widths.

A first and second mixer were added and an automatic gain control loop (AGC) was provided to suppress the large dynamic range of the signals. This was needed in order to reduce saturation of the analog-to-digital converters.

Signal processing was developed along two lines: 1) Digital time series data recorded or Fourier analyzed on the minicomputer terminal; 2) On-line processing for spectral moment estimation of the mean velocity and Doppler spectrum width data. A pulse pair processor is currently used (see Fig. 1).

In 1973, a device that generates digital estimates of mean Doppler velocity of weather targets was built. This device, a phase change estimator, circumvented spectral calculations and processed echoes digitally in contiguous resolution

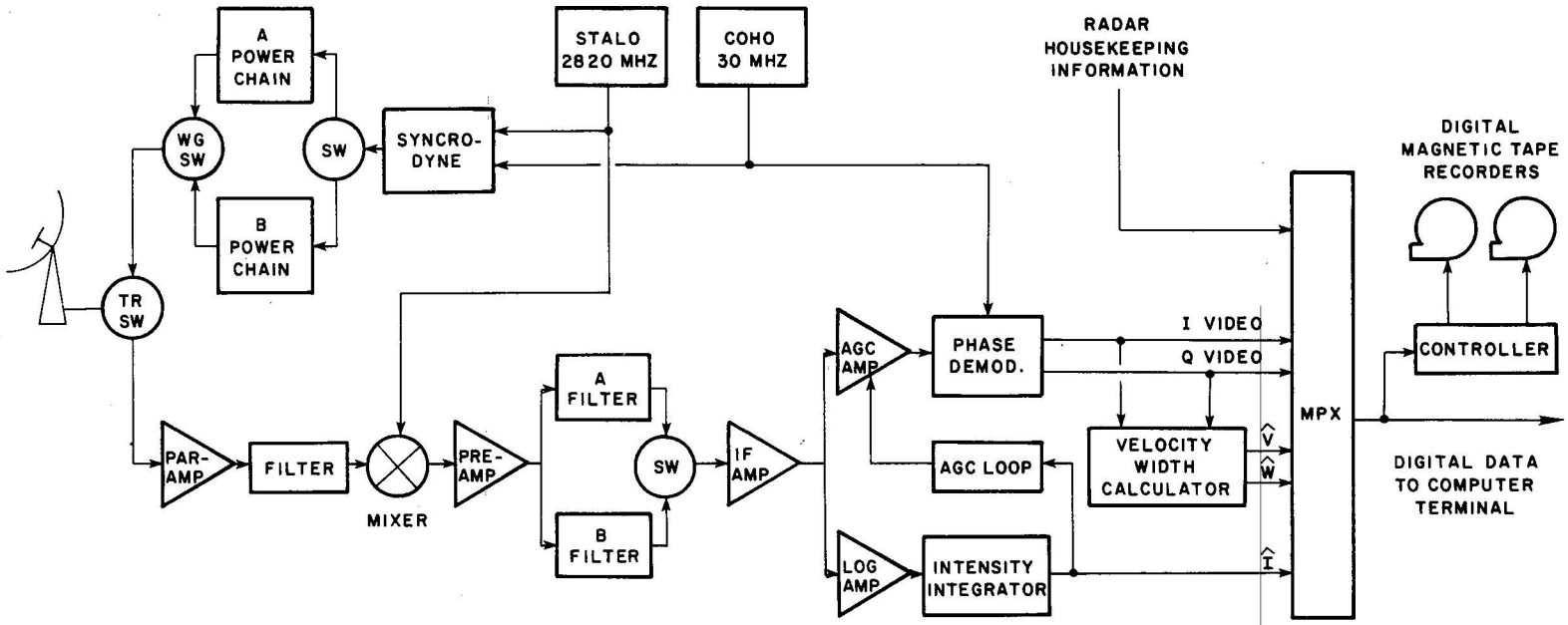

Figure 1. NSSL NRO Doppler radar simplified block diagram.

cells at the radar data rate. The phase of each echo was measured to within an octant (45°), thus the device was also known as octant change counter (Sirmans, 1972; Sirmans and Doviak, 1973). Although it was known that this device produced large errors in estimates and undesirable biases for velocities near the Nyquist limit, its simplicity and low cost prompted our choice at the time. The octant change counter proved very useful as it provided the first case of real time detection of rotating mesocyclones which are incipient to all major tornadoes (Burgess and Brown, 1976). Once the mesocyclone is detected from mean velocity measurements, time series data throughout the circulation are collected and Fourier analyzed in order to resolve tornadic wind fields.

The autovariance or pulse pair processor is about an order of magnitude more complex than the phase change estimator. But, because of its superior performance (lower standard error and level of bias) it replaced the phase change estimator in 1974.

Recording of time series data started in 1972 and has not changed much since, except that a second recorder has been added to avoid gaps in the time record during tape changes. Data from 16 contiguous range gates can be collected simultaneously (in low PRF), and as the antenna rotates, blocks of 16 gates can be stepped in range to cover the storm of interest. Fourier analysis of data yields velocity spectra from which the tornado wind speed and radius can be deduced (Zrnic' et al. 1978). Because the low PRF system has an unambiguous velocity of only ± 34 m s^{-1}, a second transmitter channel was modified to accommodate a higher PRF with a correspondingly larger (± 91 m s^{-1}) unambiguous velocity. These modifications included a new modulator, appropriate switching between the two transmitters, timing, and a second Gaussian filter.

The Ling minicomputer system was assembled to process and display the real-time data (Fig. 2). Two central processing units (CPU) with 16K x 16-bit memory each and an array processing unit (APU) are the essential components. A Vector General graphic display, a line printer, and a magnetic tape unit were the first peripherals. Recently, color displays for the three spectral moments and an additional 16-bit minicomputer were incorporated. On-line calculation of velocity spectra proceeds in the APU, and results for all 16 range gates can be presented on the graphics display. Also, an array of spectra, 16 range gates by 16 radials, each plotted in polar coordinate system, can be viewed on the graphics display. We are not certain which of the two displays (spectra at 16 range gates along a single radial or polar spectra at 16 ranges x 16 azimuths) is more advantageous for real-time identification and tracking of tornado spectra, since neither has been tried in real time.

2.2 Real Time Detection of Mesocyclones

NSSL's first real-time Doppler velocity processor (phase change counter) produced velocity contour maps of mesocyclone signatures during the Spring of 1973. The Marlow tornadic storm on June 4th produced a particularly large mesocyclone, and its reflectivity and isodop* signatures are clearly shown in Fig. 3. This storm's reflectivity structure exhibited a hook echo feature suggesting mesocyclonic circulation, severe weather, and tornadoes. Although the hook echo is identified

*An isodop is an isopleth of Doppler wind velocity measured by the radar.

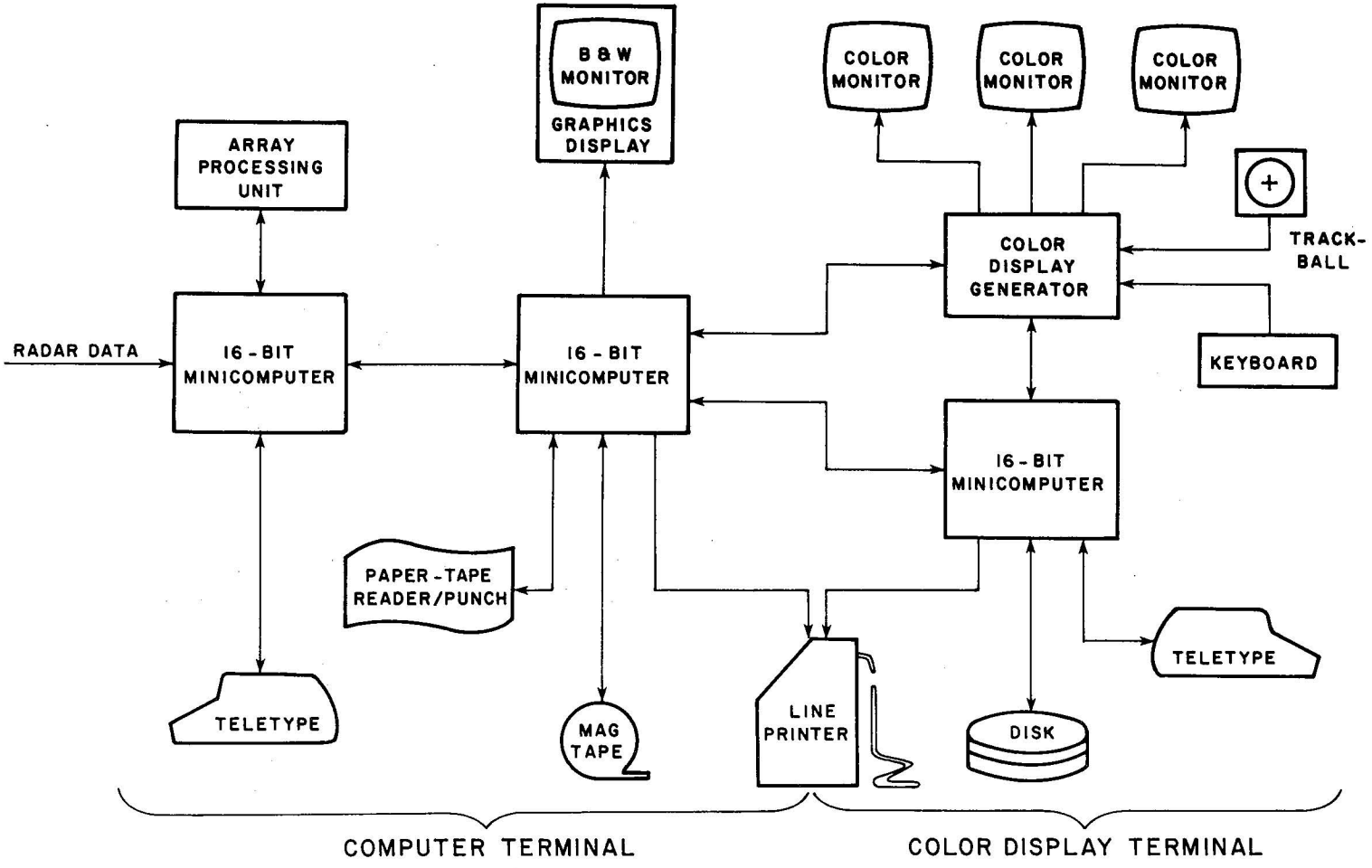

Figure 2. Computer terminal simplified block diagram.

usually as an appendage to the storm, it may be found within the storm, as in this case. Average storm height during data collection was 16 km; motions of signature and storm were equal (280°/13 m s^{-1}), with both considerably to the right of mean environmental wind (250°/12.5 m s^{-1}). East of the high reflectivity core, a low reflectivity notch extends well into the storm. Storm motion relative to the radar is slight, and therefore, isodop patterns indicate radial velocity relative to the storm. The nearly symmetric isodop signature characterizes circularly symmetric cyclonic rotation consistent with that inferred from the reflectivity pattern.

A second-generation radar real-time display, necessary in defining vortex characteristics, was developed at the National Severe Storms Laboratory in 1974. The three spectral moments are presented as a field of arrows shown by minicomputer-graphic display terminal interfaced to the NSSL 10-cm Doppler radar (Burgess et al., 1976). Arrow length is proportional to the logarithm of received power, arrow direction to velocity and arrowhead size to Doppler spectrum width.

The insert on Fig. 4 illustrates the above relations. Zero velocity is a horizontal arrow pointing right and nonzero velocities are proportional to angular rotation from the zero position (clockwise, negative, i.e., toward the radar, and conversely, counterclockwise, positive). The horizontal arrow pointing left corresponds to the maximum unambiguous velocity (±34 m s^{-1}) resolved by the radar. The display (Fig. 4) is a range vs. azimuth presentation of Doppler moments. The display sector can be changed quickly to check large areas of the storm for wind shear, turbulence and vortex motion. Note the mesoscale vortex in Fig. 4 at 187° and 71 km where the winds are 20 m s^{-1} toward the radar adjacent to 14 m s^{-1} away from the radar--a typical vortex couplet (see Section 2.3).

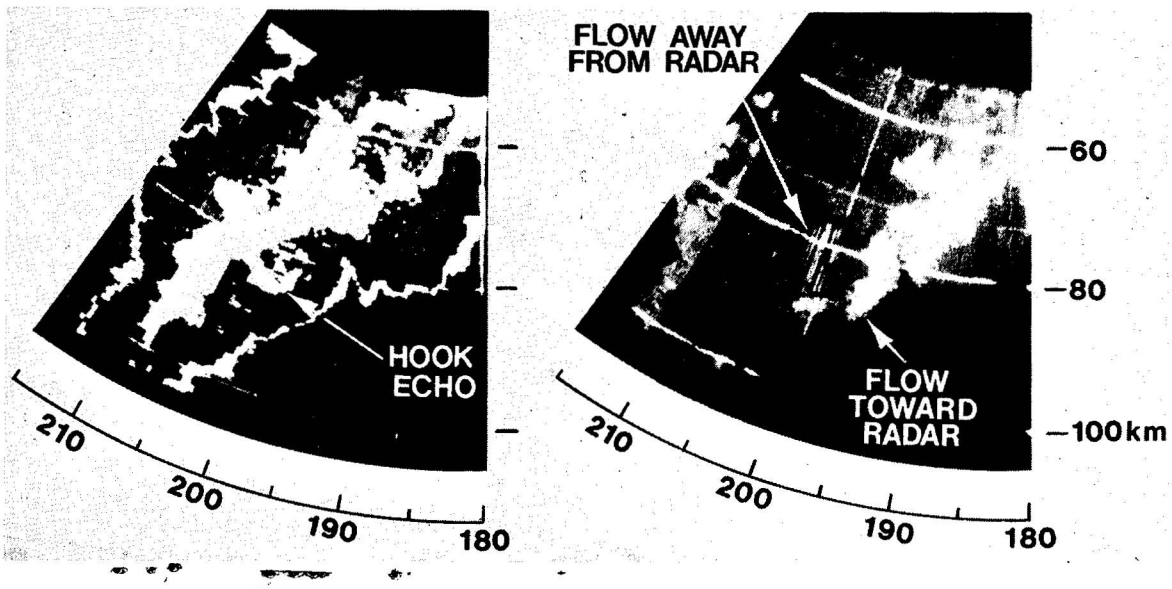

Figure 3. Storm reflectivity (a) and isodops (b) displayed on PPI at 2115 CST. The elevation angle is 1.9°, range marks correspond to 60, 80, 100 km. Reflectivity factor categories are: dim (<21 dBZ), bright (21-31), black (31-44), dim (44-57), and bright (>57 dBZ). Velocity categories are dim (<13 m s^{-1}), bright (13-21), and brightest (>21). Positive radial velocities are angularly strobed in brightness. Mesocyclone signature is between 194°-203° and 73-90 km.

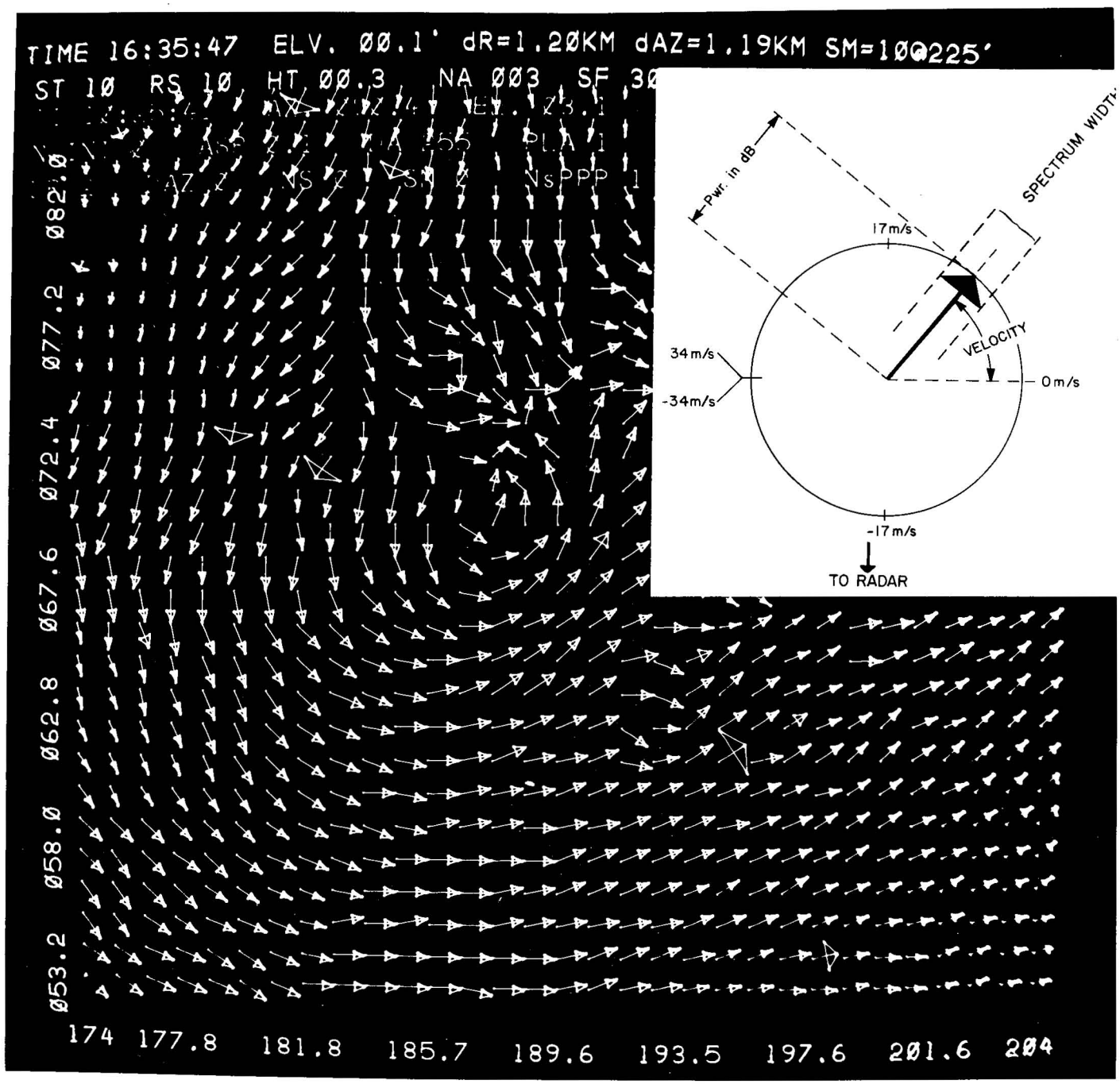

Figure 4. The multimoment Doppler display of a mesocyclone. Each arrow contains information of the three principal Doppler spectrum moments for a resolution volume. For interpretation of arrows, see insert in upper right corner (arrow length is proportional to received power, arrow direction to velocity and arrowhead size to Doppler spectrum width). Abscissa is azimuth and ordinate scale denotes range (km) from radar. "Housekeeping" information is at top of screen.

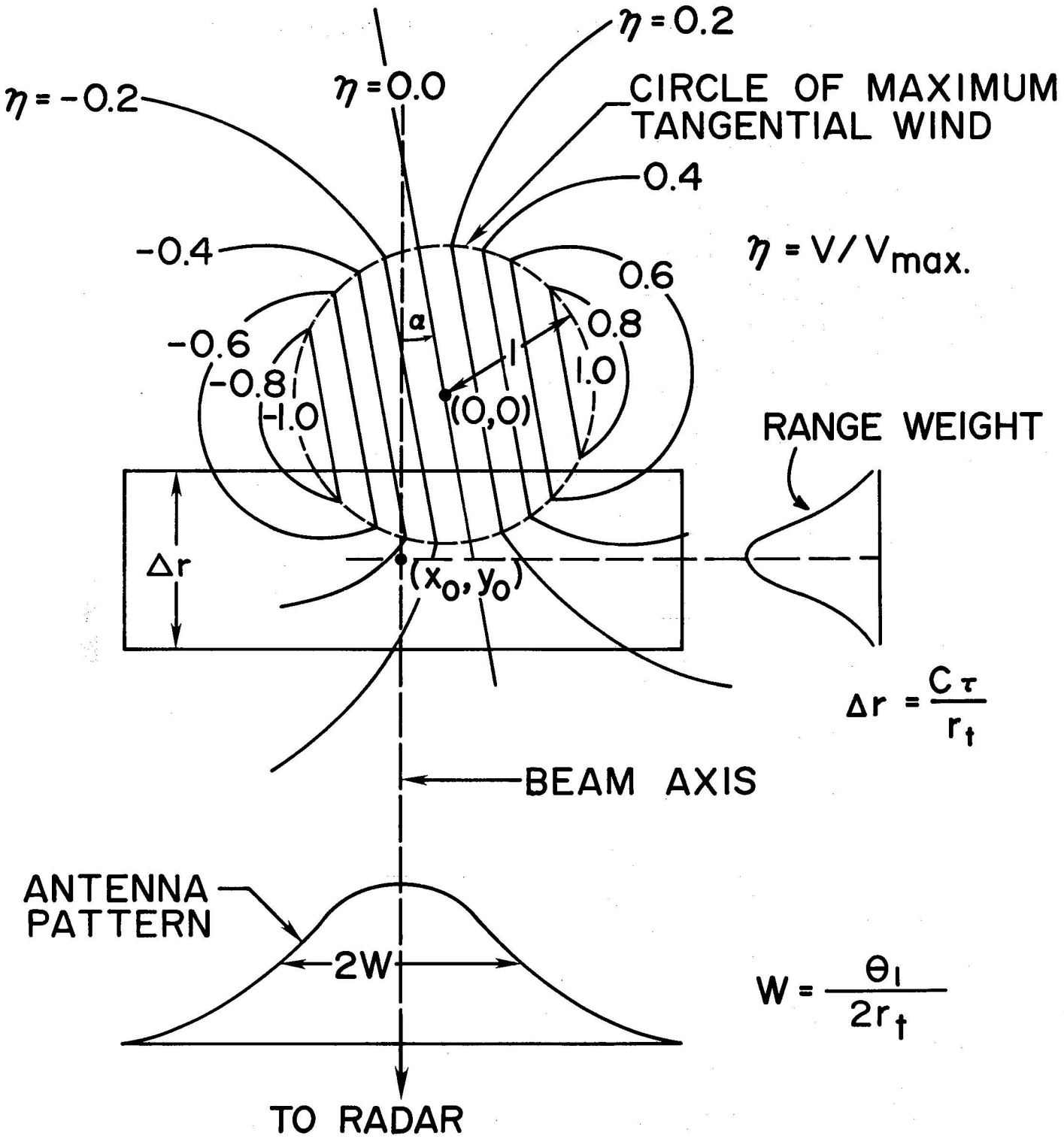

Figure 5. Plan view of idealized isodop pattern for a stationary modified Rankine vortex located at a range large compared to vortex diameter. η is Doppler velocity normalized to peak tangential wind. Radar is located towards the bottom of the figure. Resolution volume, antenna and range weighting functions are depicted. The angular tilt α determines radial component of flow into (α<0) or out of (α>0) the vortex.

2.3 Spectra of Model Vortices

It can be shown that non-translating cyclones have isodops forming a symmetric couplet of closed contours with equal number encircling positive and negative velocity maxima (Fig. 5). If the inner portion of the vortex is a solidly rotating core, its tangential velocity linearly increases with radius to a maximum. Outside this maximum, the velocity decreases (roughly) inversely with the radius. The isodop contours of such a combined Rankine vortex are circular sections connected with straight lines (Fig. 5). Patterns like these have been observed many times, and an example is shown in Fig. 6 for a tornadic storm that touched down in Del City, Oklahoma, in 1977 (Zrnic' and Istok, 1980).

The pattern in Fig. 5 is typical of a vortex, be it a mesocyclone or a tornado. When the radar resolution volume is small compared to the vortex, the mean velocities form an isodop pattern (Fig. 6) resembling the theoretical one. However, if the resolution volume is comparable to the vortex size, the vortex signature must be sought in the velocity spectrum.

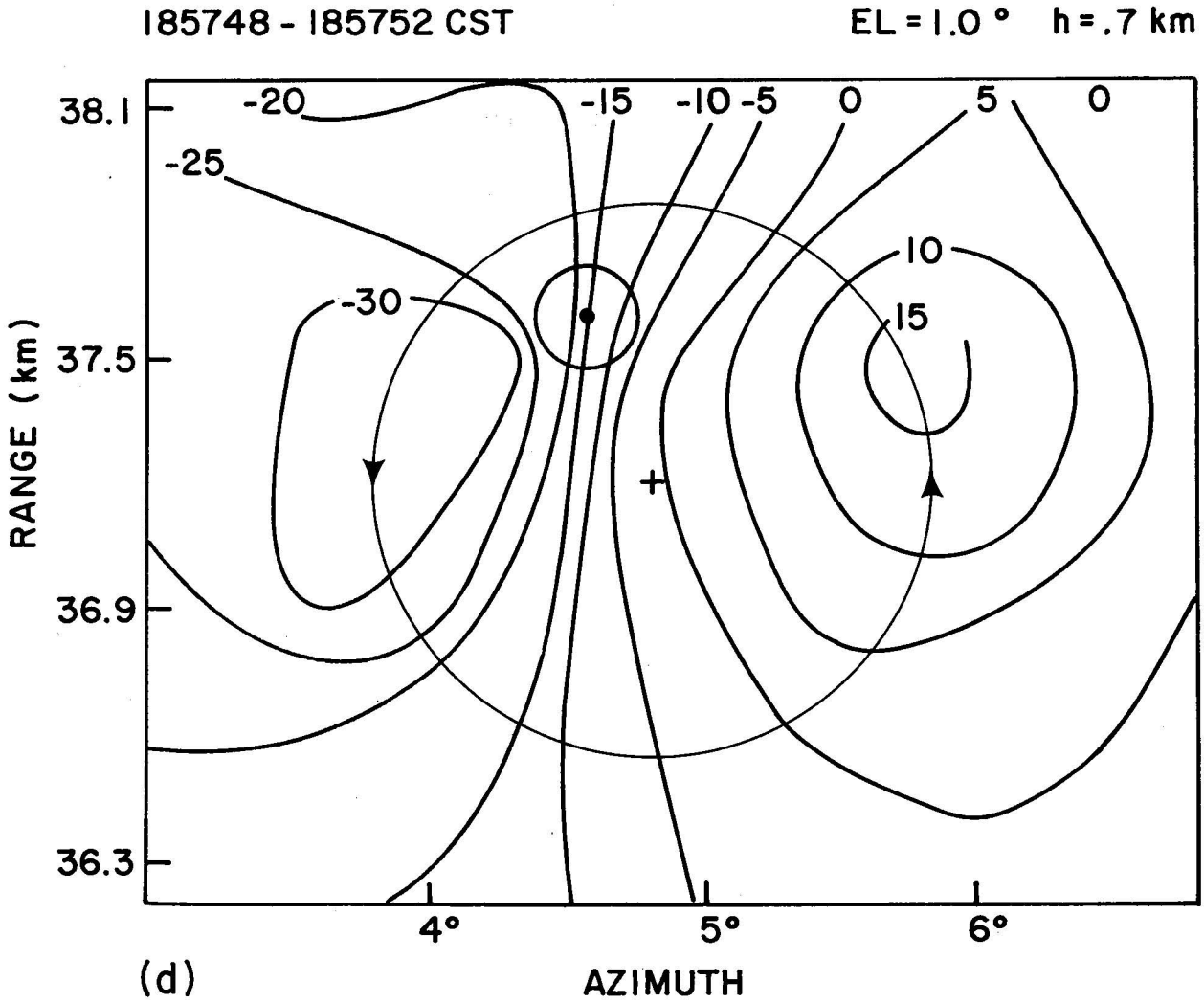

Figure 6. Position of the Del City tornado (small circle drawn to scale) with respect to the mesocyclone signature. Contours are drawn from data spaced 0.6 km in range and 0.2° in azimuth. Mean radial motion of the mesocyclone is removed. The notation and time correspond to the ones in Fig. 9.

In order to relate expected Doppler spectra of tornadoes to radar measurements, spectra for a model tornado circulation (Fig. 5) were calculated (Zrnic' and Doviak, 1975). The vortex is approximated by a combined Rankine model, with provision made for particle inflow or ejection. Positions of maximum radial and tangential velocities are coincident and the radius of their location is referred to as maximum wind radius. Given model reflectivity and Doppler velocity fields, the simulation program calculates mean Doppler spectra for specified pulse volumes. Both two-dimensional, as in Fig. 5, and three-dimensional integration of the Doppler velocity field is feasible; however, comparison revealed that negligible difference in spectra from the two integrations results if the vortex is invariant with height. Hence, all calculations were obtained from the two-dimensional model. Although the tornado may have nonuniform reflectivity, we assume (for simplicity) the reflectivity to be either uniformly distributed throughout the pulse volume or to have a Gaussian-shaped profile with control over the peak position and width. This allows us to account for nonuniformities, at least on a pulse volume to pulse volume basis; while with the Gaussian profile, radial nonuniformities can also be accommodated. Other parameters, such as tornado radius and position within the pulse volume, are variable.

2.4 Spectra of Three Tornadoes

Digital radar samples from three tornadoes were recorded and Fourier analyzed. A von Hann weighting function (raised cosine) was applied to data prior to a discrete Fourier transform. The von Hann weight offers a good compromise between the width of spectral main peak and the size of sidelobes. Specifically, the rapid sidelobe decay reduces contamination of high velocity peaks by strong signal, low velocity components.

Detailed analyses of spectra from the three tornadoes have been completed. Two of the tornadoes--the Union City and the Stillwater--were very strong and destructive while the third, Del City was less intense. Data from the two large tornadoes were collected with the regular PRF, and since the ± 34 m s^{-1} radar unambiguous velocity was smaller than the velocity span in the tornadoes, velocity folding was introduced in the simulated spectrum. Tornado position relative to the pulse volume, the maximum velocity and radius were determined from the least squares fit between simulation and data.

Fitting was done on linear and on logarithmic spectrum points. Logarithmic fit is better if spectra are free of artifacts because logarithms of exponentially distributed powers have equal variances--thus every point influences the overall root mean square difference (r.m.s. error) equally. The true velocity spectra are (unfortunately) corrupted by a dozen or so causes and the contamination shows mostly in weak spectral skirts. Therefore, fitting on linear data, which weights stronger powers more, offers advantages.

When centered on the beam axis, the Rankine vortex model predicts a bimodal spectrum, the so-called tornado spectral signature (TSS), which was verified experimentally several times. Shown in Fig. 7 are Rankine model vortex spectra matched to data by a least squares fit. The examples of spectra are from the Stillwater and the Union City "maxi"-tornadoes. Note the similarity of the spectra, even though the radial distance (range) to the two tornadoes is quite different. Tornado parameters deduced from the fit are listed in Table 1.

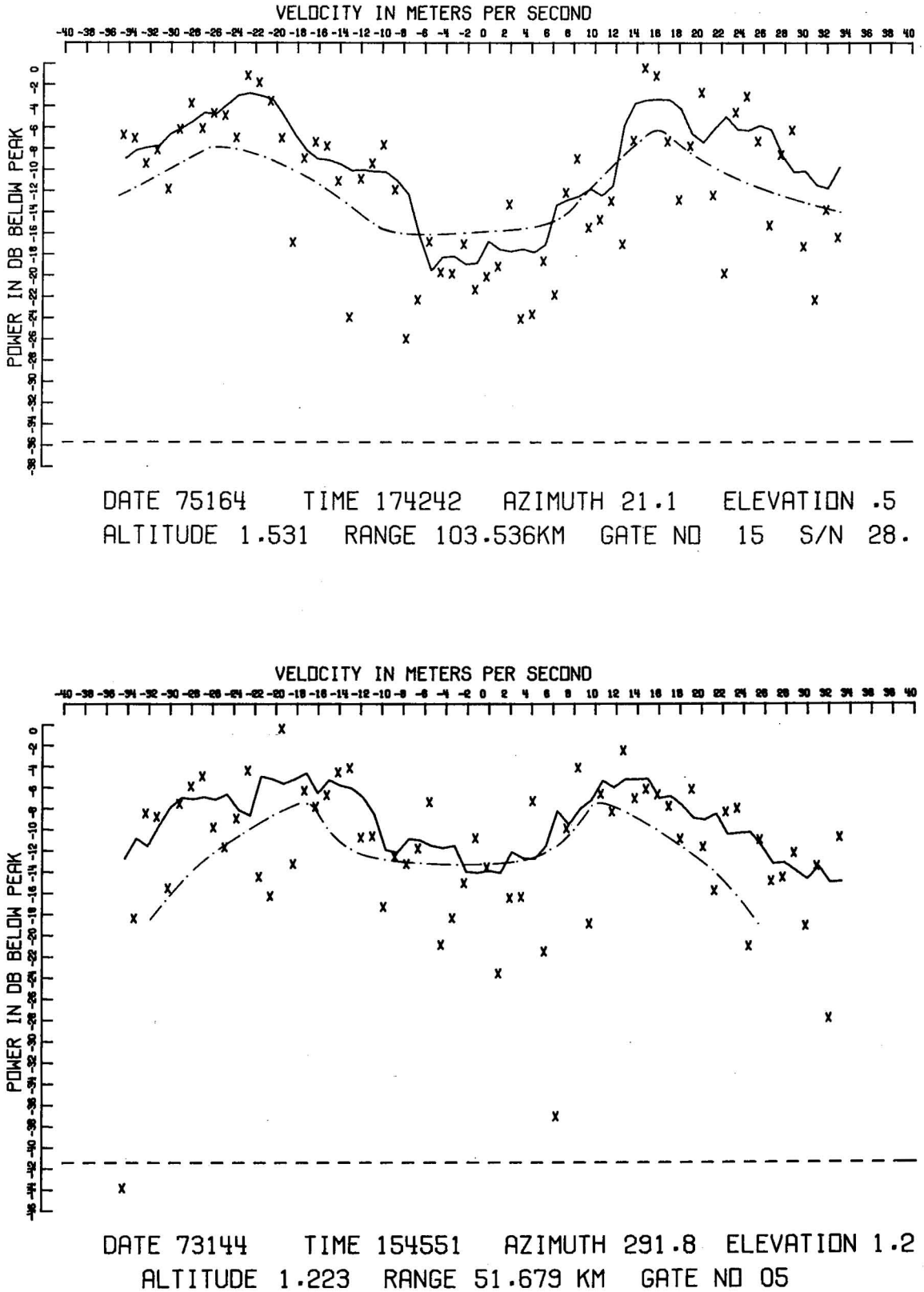

Figure 7. Power spectra on logarithmic scale: (a) Stillwater spectrum; (b) Union City spectrum. Both tornadoes are estimated to be centered on the beam axis. Least squares fit (dash-dot lines) is performed on logarithms of power. Solid lines are five-point moving averages of power. Dashed straight line is the receiver noise level.

Table 1. Tornado characteristics deduced from Doppler spectra.

Storm	Distance to Storm	Tornado Diameter	Maximum Tangential Wind Speed	Height of beam center above ground
Union City 24 May 1973	51 km	200 m	72 $m \cdot s^{-1}$	1.2 km
Stillwater 13 June 1975	103 km	300 m	92 $m \cdot s^{-1}$ 85 $m \cdot s^{-1}$	.63 km 1.5 km
Del City* 20 May 1977	34 to 40 km	130 to 250 m	22 to 35 $m \cdot s^{-1}$	.15 to 3 km

* Tornado parameters are superimposed on the damage path in Fig. 10.

In the Stillwater case, two spectra nearest to the tornado were simultaneously fitted in a least squares sense. Simulated model vortex spectra and real spectra show very good agreement, not only for the two where the fit was made, but also for adjacent gate locations (Fig. 8). Resolution volumes corresponding to any of these simulated spectra are assumed to have uniform reflectivity within the volume. Differences in echo power from each resolution volume are accounted for by forcing each simulated spectrum to have power equal to its matching data spectrum. Asymmetry of spectral peaks (Az 21.1°; range 104.136 km) about zero velocity suggests that targets were centrifuged outward with a velocity of 13 m s^{-1}.

The only high PRF (maximum unambiguous velocity ±91 m s^{-1}) data collected of a tornado were during the Del City storm. Over a hundred spectra from the Del City storm were individually examined in order to find the tornado spectral signature. In seven scans the tornado signature was identified (Zrnic' and Istok, 1980). Sample spectra from three adjacent azimuthal locations, where the signature was found, are presented in Fig. 9. Superimposed on the figure are the best fitted model spectra. Both three-point running average and raw spectral points were fitted with occasional differences in the final result. The parameters deduced from the smoothed spectra had a better self-consistency; hence, those are reported here. Uniform- and donut-type reflectivity profiles were tried. The reflectivity of a donut profile is a function of vortex radius only and in our case an offset (from tornado center) Gaussian curve is used to control the position and shape of reflectivity maximum (Zrnic' and Doviak, 1975). More often the donut profile resulted in somewhat better fit. This is to be expected because the two "degrees of freedom" (position and width) allowed easier adaptation of reflectivity to nonuniformities caused by debris. Further support for this conclusion comes from the fact that model spectra with donut reflectivity match the data better at lower altitudes. In Fig. 9a the fitted model has a donut Gaussian shaped reflectivity. To illustrate the small difference in the model spectra due to the two profiles, both model spectra (uniform and a donut shaped reflectivity) are shown in Fig. 9b.

Tornado location determined from the spectral fit is superimposed on the damage path obtained by survey teams (Fig. 10). Also on the figure are maximum measured velocities V_m, maximum tangential velocities V_t and heights of the scans above ground. Estimated radii of wind maxima range from 65 to 125 m, and are drawn to scale on Fig. 10. The area between I-35 and the railroad tracks was not surveyed since it was not easily accessible to ground crews. Along the county road the damage stopped at Oakdale School, and the path was picked up again northwest of there.

The path deduced from Doppler spectra shows a gradual curving. It seems likely that the vortex responsible for the wide damage path weakened, but it is not clear whether it stayed continuously on the ground or if it was replaced by a new tornado. The relative position of the tornado (whose spectrum is shown in Fig. 9a) with respect to the isodops of the mesocyclone is shown in Fig. 6. A photograph of the tornado taken a few minutes before the times of our observations contained multiple vortices. However, the spectral data concerning multiple vortices are inconclusive.

We emphasize that the Del City tornado produced damage of intensity F2 or less. Corresponding maximum tangential winds deduced from Doppler spectra were 35 m s^{-1}. These values are deduced from logarithmic plots of spectra (Fig. 11) obtained from windowed (von Hann) data. In this example, the sharp drop at 65 m s^{-1} (i.e., at the maximum velocity) is evident and agrees well with model

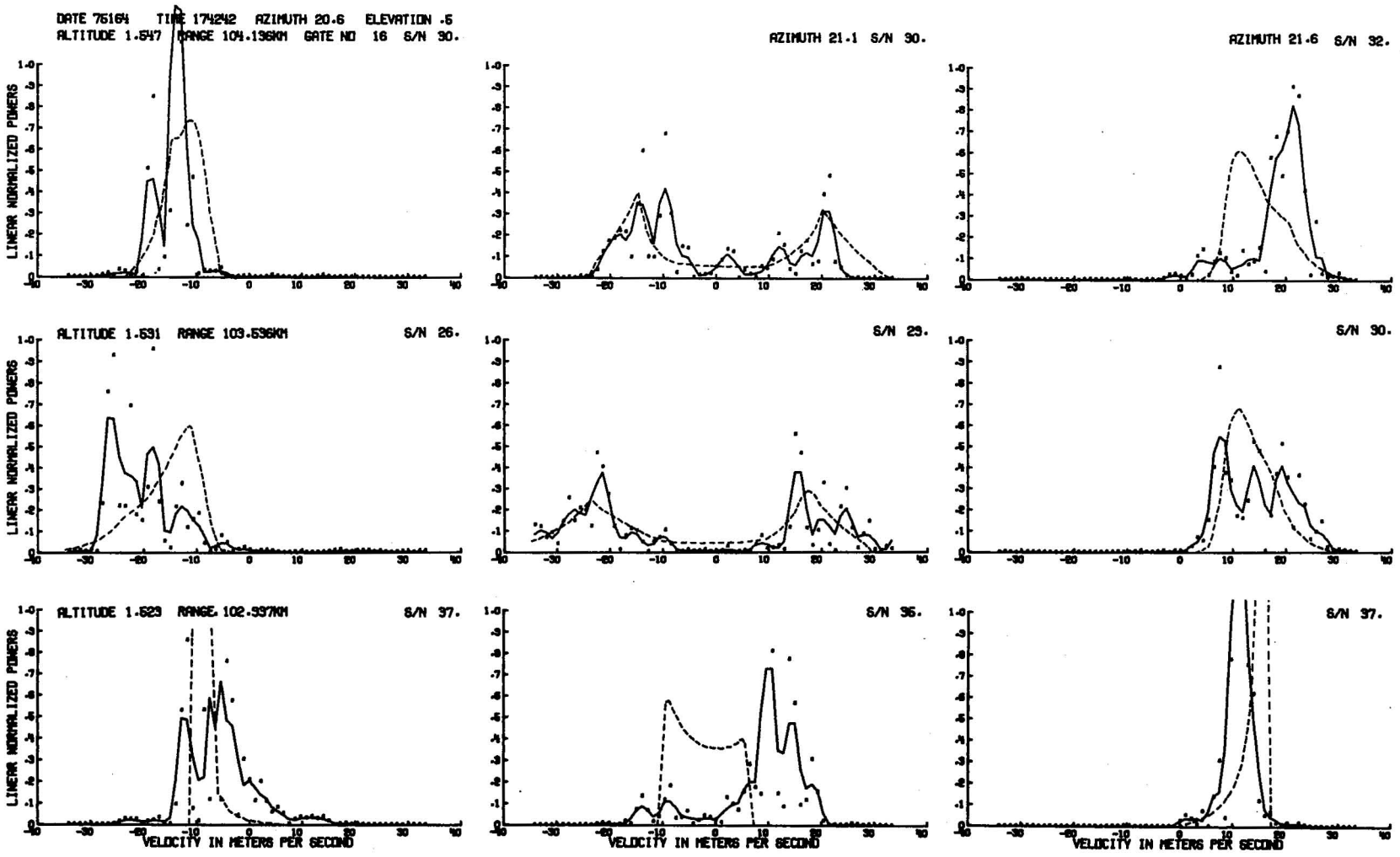

Figure 8. Spectra from three consecutive azimuthal and range locations for Stillwater tornado. Dots show spectrum estimates from recorded time series data, weighted with a von Hann window. Solid lines are three-point running averages. Dashed lines are simulated spectra. The mean square difference between data and simulated spectra is simultaneously minimized for two spectra (Az. 21.1° and range of 103.5 and 104.1 km). Resolution volume depth is 150 m, range gate spacing 600 m, and antenna beamwidth 0.8°. The tornado is located between the two upper middle gates. Tornado parameters obtained from these two fitted spectra are used to compute the remaining 7 simulated spectra. Height above ground for these spectra is 640 m.

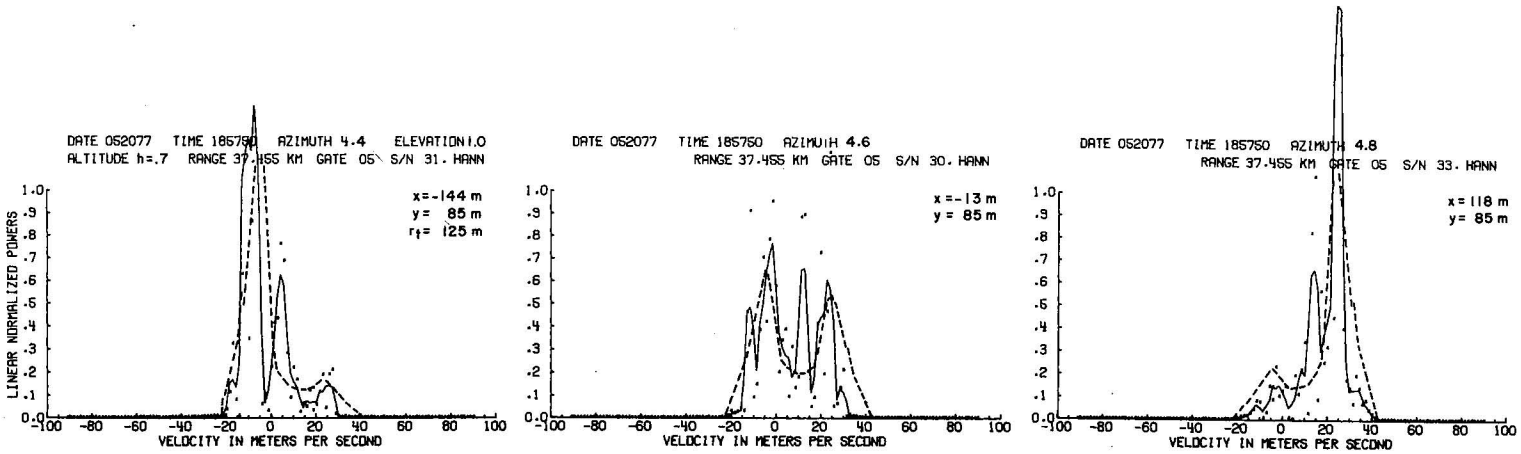
DATE 052077 TIME 185750 AZIMUTH 4.4 ELEVATION1.0
ALTITUDE h=.7 RANGE 37.455 KM GATE 05 S/N 31. HANN
x=-144 m
y= 85 m
r_t= 125 m
DATE 052077 TIME 185750 AZIMUTH 4.6
RANGE 37.455 KM GATE 05 S/N 30. HANN
x=-13 m
y= 85 m
DATE 052077 TIME 185750 AZIMUTH 4.8
RANGE 37.455 KM GATE 05 S/N 33. HANN
x= 118 m
y= 85 m
LINEAR NORMALIZED POWERS
VELOCITY IN METERS PER SECOND

(a)

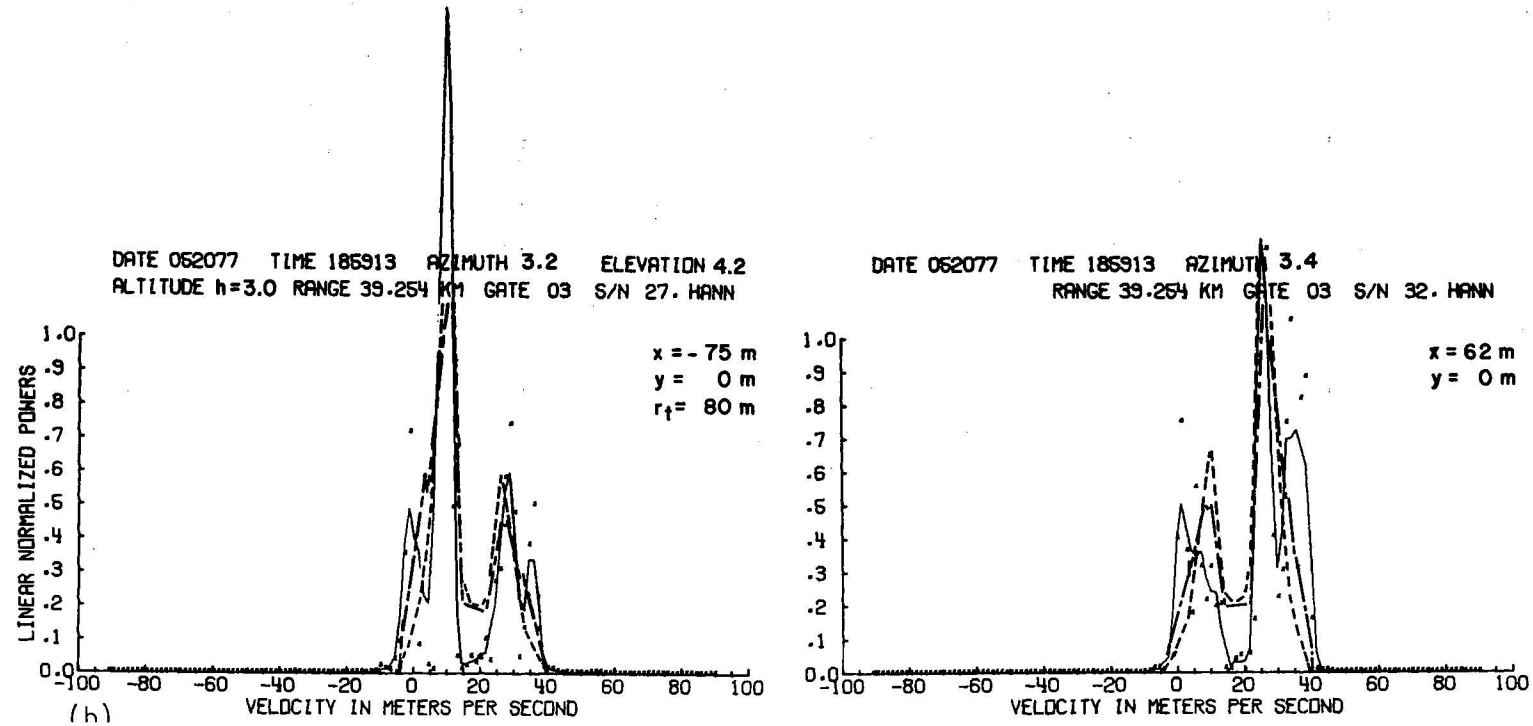
DATE 052077 TIME 185913 AZIMUTH 3.2 ELEVATION 4.2
ALTITUDE h=3.0 RANGE 39.254 KM GATE 03 S/N 27. HANN
x = - 75 m
y = 0 m
r_t= 80 m
DATE 052077 TIME 185913 AZIMUTH 3.4
RANGE 39.254 KM GATE 03 S/N 32. HANN
x = 62 m
y = 0 m
LINEAR NORMALIZED POWERS
VELOCITY IN METERS PER SECOND

(b)

Figure 9. Doppler spectra of the Del City tornado. Dots are squared magnitudes of Fourier coefficients for time series that were weighted with a von Hann window. Solid lines are three-point running averages. Dash-dot lines are best fit model spectra with uniform reflectivity while the dash lines are for a donut of Gaussian shaped reflectivity. The signal-to-noise ratio is in dB, and x (azimuthal distance) and y (range distance) are coordinates of the tornado center with respect to the resolution volume center; r_t is the radius of maximum wind and the altitude h (height) is from ground level to beam center in km. Spectrum in (a) for 4.6° azimuth indicates that the vortex is almost centered on the beam axis. Best fitted model spectra for both the uniform and donut reflectivity are illustrated in (b). (The indicated elevation angle is a few tenths of a degree too high.)

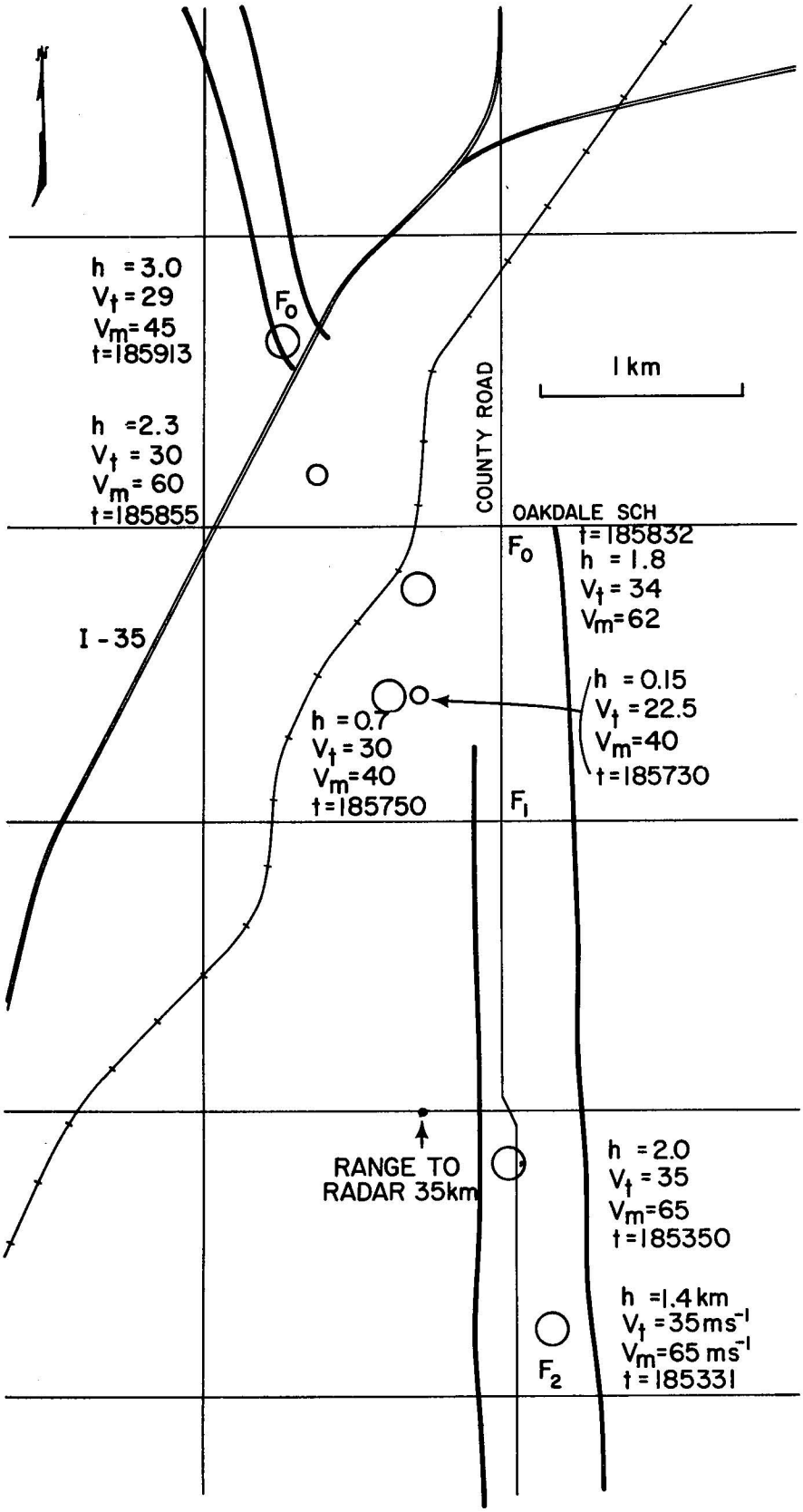

Figure 10. Tornado position for the Del City storm (circles drawn to scale), as deduced from the Doppler spectra, superimposed onto the damage path. Height (km) of beam center with respect to ground is h, V_t is the tangential speed (m s^{-1}) while V_m is the absolute maximum speed. The damage scale is Fujita's F scale. County roads (square grid) are 1 mile apart.

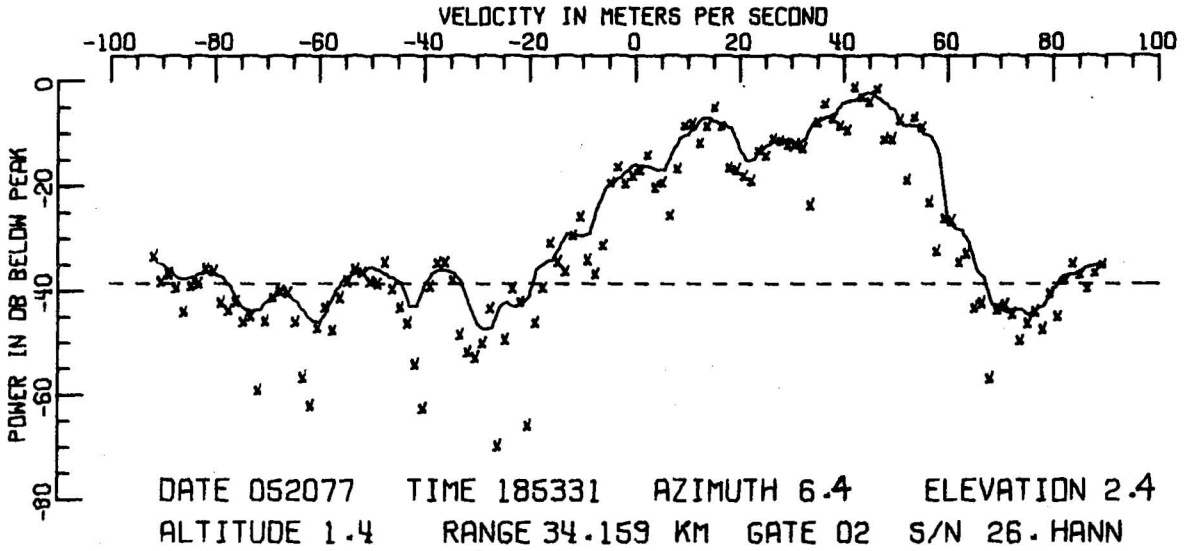

Figure 11. Plot on a logarithmic scale of a tornado spectrum (Del City). Spectral powers are marked with x's and a 5-point running average is drawn for visual clarity. The dash line, 40 dB below the spectrum peak, is a noise level estimate.

predictions. While higher wind speeds could not be ruled out on the basis of spectral measurements, the damage survey indicates that our values are quite realistic. Much less certain is the deduced radius of maximum winds (65-125 m), because it relies heavily on the model. Nonuniformities in reflectivity, tilting of the vortex and variances with height, and targets in sidelobes are just a few effects that do occur but are not accounted for.

Accuracy of measured velocities approximately equals the Doppler spectrum resolution which is 1.5 m s^{-1}. The pointing error of antenna beam is less than .1° which corresponds to about 50 m at the tornado location. Errors in slant range are quite small (<30 m), but the relative error (i.e., position of the tornado within the gate) could be 100 m. Errors in deduced radii of maximum winds are difficult to assess; however, the inferred radii between 65 and 125 m are plausible considering that the damage path width is between 200 and 500 m. A check for consistency was made by assuming that F0 (>18 m s^{-1}) and higher winds caused the damage. If this is the case, then a 100 m assumed radius combined with measured maximum velocities and a Rankine profile would result in a path width of about 500 m, as observed by the survey team in the first part of the path (Fig. 10). To illustrate the sensitivity of deduced radii, we present in Fig. 12 the rms error of spectrum data (normalized powers), fitted to the model, versus the maximum wind radius. A change by a factor of 2 in radius results in less than 3.6% change in error. Because this minimum is broad, spurious effects can easily enter. Thus, the uncertainty in radius could be tens of meters.

3. ENGINEERING STUDIES OF TORNADO DAMAGE

Engineering studies of tornado damage were performed by the Institute for Disaster Research (IDR), Texas Tech University, and a complete history of this work will be contained in a separate IDR report. The Institute for Disaster Research summarized their findings in NOAA Technical Memorandum ERL NSSL-82, entitled "The Tornado: An Engineering-Oriented Perspective." The reader is

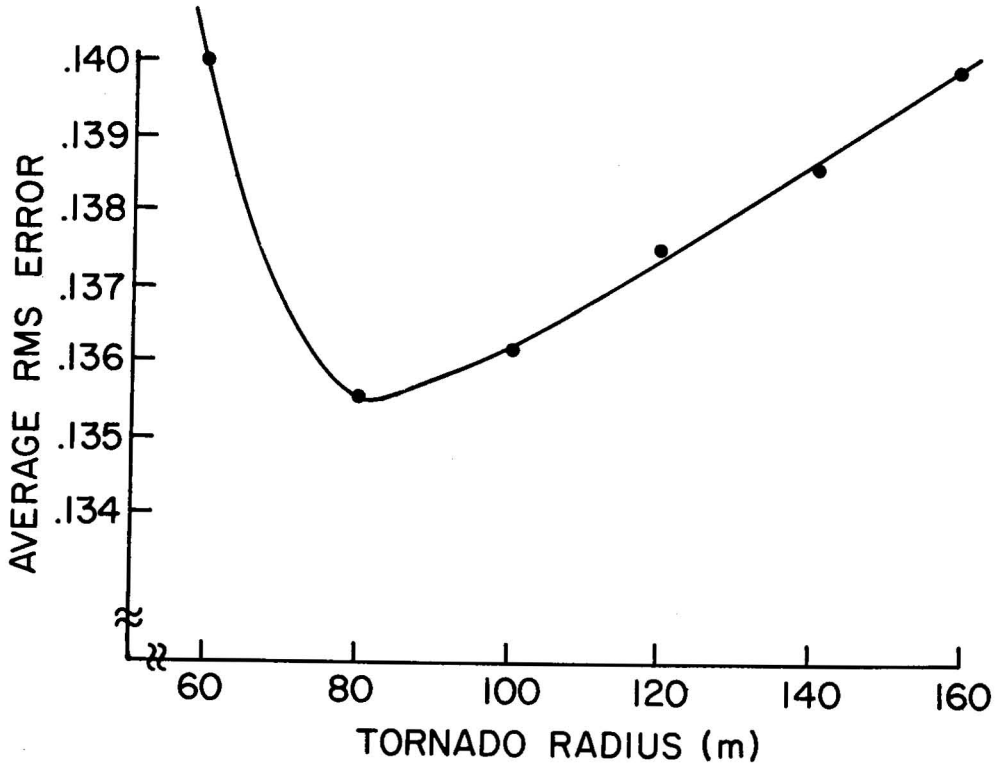

Figure 12. Behavior of the rms error between fitted spectra and data as a function of tornado radius (Del City tornado).

referred to the complete report for details, but the abstract, reprinted below, outlines IDR's principal conclusions.

> "Six years of investigations, evaluations and reporting of windstorm damage events have provided engineers with their own perspective of the tornado. This perspective is presented in a manner which is intended to enhance both the engineer's and meteorologist's understandings of the phenomenon. In addition, the presentation of an engineering-oriented perspective of the tornado serves to establish and demonstrate the feasibility of designing buildings and facilities against tornadoes.
>
> Included in the presentation are fundamental concepts of tornado-building interaction phenomena which are designed to assist the meteorologist in understanding and interpreting wind damage, and to assist the engineer in assessing wind resistance of building construction. Illustrations which establish roof to wall anchorages, foundation anchorages, and windward wall windows and doors as failure initiation points are valuable to the damage investigator and designer. Major sections on tornadic windspeeds and atmospheric pressure change advance the engineering-oriented perspectives that (1) buildings fail at relatively low windspeeds, (2) no conclusive evidence can be found that ground level windspeeds exceed 250 mph (112 m/s), (3) most building damage is caused by winds in the 75-125 mph (34-56 m s^{-1}) range, and (4) atmospheric pressure changes in tornadoes play only a minor role in the damaging mechanism. The performance of housing in tornadoes reveals that certain types of housing can be relatively good indicators of wind speeds in the lower ranges [150 mph (67 m s^{-1}) and less], but that

housing damage is an unreliable indicator of windspeed at larger windspeed values. Further, garage, porch, roof overhang, and gable orientation can present unfavorable survival conditions, thereby inviting structural failure, which can lead to erroneous conclusions relating to windspeeds and windfield geometry.

Technical discussions of tornado-generated missiles and unusual events lead to the conclusion that unusual events associated with tornadoes can be explained by current perceptions of the tornado as defined by winds and atmospheric pressure change. Missile trajectories established from field studies are compared with engineering models to establish rational assessments of missile events."

4. ACQUISITION AND ANALYSIS OF SEVERE STORM AND TORNADO FIELD OBSERVATIONS

4.1 Tornado Intercept

4.1.1 History of Tornado Intercept

Tornadoes, because of their infrequency, short lifetimes, small size, and destructivity, are not easily observed and measured. Eyewitnesses are seldom trained meteorologists and consequently pay scant attention to attendant cloud structures or to the sequence of events preceding the tornado. They also do not move with the storm so their observation time is limited. Tornadoes are too small to be resolved by radars and mesonetworks, although these sensors furnish important data on the parent stormsandDoppler radar can provide information, via spectral analysis, of tornadic winds within its resolution volume (see Section 2). Anemometers directly in the path of the storm are frequently damaged, and microbarographs respond too sluggishly to the rapidly passing vortex. Almost all the data on the tornado scale has been gathered from visual and photographic records and damage surveys. Lack of observational data and clear physical knowledge of the phenomenon has hindered the construction of sound tornado theories and models (Lilly, 1965; Morton, 1966). This has led Lilly (1975) to name the tornado as "perhaps the last frontier in tropospheric meteorology - the only intense and easily identifiable phenomenon whose internal structure and dynamics remain highly speculative". Although chance eyewitnesses have occasionally taken revealing tornado movies, much knowledge has also been gained from visual observations made by trained meteorologists in pursuit of tornadoes.

Ward (1961) and Donaldson and Lamkin (1964) were among the first to document successful ground intercepts (i.e., close range approaches) of tornadoes while Bates (1962, 1963) had similar successes from the air. These investigators went into the field only occasionally and did not obtain high-quality photography although they made skillful observations. Mobile ground teams have also been used to pursue hail storms, either to collect freshly fallen hailstones (Browning et al., 1968) or to study the sequence of precipitation events as the updraft passed overhead (Auer and Marwitz, 1972). Close range airborne observations by Rossow (1970) and Golden (1974a,b,c) have revealed many interesting properties of waterspouts.

The Tornado Intercept Project (TIP), a cooperative effort between the National Severe Storms Laboratory (NSSL) and The University of Oklahoma (O.U.), began in the spring of 1972 (Golden and Morgan, 1972). TIP is based in Norman, Oklahoma. Its formation represented an unprecedented commitment to severe storm intercepts, and an attempt to combine close range visual observations with data from other sensors such as radar. Tornado "chasing" quickly became a favorite pastime for a few meteorology students, fascinated by the sublime appearance and coherent structure of rotational storms. The skills developed and the observations made by many a self-funded impromptu intercept team, relying heavily on its own visual observations for guidance, have greatly supplemented the knowledge gained on official intercepts (e.g., Moller et al., 1974; Smith, 1974; Burgess, 1976a). Oklahoma University's formal participation in TIP during the period 1976-1979 has been summarized in a series of reports (Kimpel et al., 1976, 1977; Bluestein et al., 1978; Bluestein, 1979, 1980).

4.1.2 TIP Goals

The original goal of approaching within close range of tornadoes with conventional automobiles has been achieved many times since 1972. The continuing goals of the Tornado Intercept Project are:

a. To obtain high quality movies of tornado debris clouds so that tornado winds can be measured photogrammetrically.

b. To obtain accurate times and locations of tornadoes and document changes in vortex size, shape, and tilt for use in Doppler radar analyses, and other studies. Precision times and locations allow the tornado to be placed accurately relative to the radar echo, and permit relations between the tornado and parent storm to be investigated.

c. To observe and document photographically the evolution of storms with the ultimate intent of constructing descriptive models of tornadic storms based on visual and radar appearances.

d. To obtain visual and photographic records of tornadoes and their parent clouds; also of changes in cloud structure and sequences of events spanning tornadoes. Such qualitative observations provide an important "real world" starting point for tornado models.

e. To measure the wind, thermodynamic and electrical fields near tornadoes.

4.1.3 Personnel and Equipment

Each TIP field team consists of a team leader and three other members. The team leader has the final word on all in-vehicle decisions and is responsible for his team's safety and performance. He also chooses the intercept route, based on the availability of roads, visual storm observations, and information received from base (NSSL). Team members are assigned driving, documentary, photographic, and navigational duties. Emphasis is placed on accurate entries of time, location, and records of photography and visual observations in a log (usually a tape recording). A large van with windows on all sides is the best type of vehicle because it offers good visibility, ample space and easy accessibility to the equipment. Items carried into the field include maps, tape recorders, an

insulated chest containing dry ice (for hail collection if the opportunity arises), meteorological instruments, 16 mm movie cameras,[1] 35 mm slide cameras, intervalometers, tripods, and various other photographic accessories and supplies. Each van is equipped with FM radio and a radio telephone. FM communications with base (NSSL) are routed through a repeater located at the 440 m level on a tall television tower 40 km north of NSSL.[2] Beyond the FM system's range (115 km from the repeater), the radio telephone is used when an operator is within range and the channels are not busy; otherwise a public telephone has to be found whenever updated information is needed. Direct, short-range, intervehicle communications, provided by a second FM radio channel, enable teams to exchange information during intercepts of storms which lie beyond the repeater's range. Replacing the radio telephone with a 6 MHz shortwave AM radio link has been discussed, but never implemented. Due to a close range skip zone, shortwave radios would not replace the FM system. However, they could extend radio range by several hundreds of kilometers. Planned field tests to determine whether storm-generated static would block this communication channel were never carried out.

The Nowcaster is the NSSL-based person who communicates with the team leaders. His duties include preparing a 0 to 9 hour forecast by 1000 CST, and monitoring the weather throughout the day when the potential for severe storm development exists. His aids are the NAFAX weather maps (both analyses and prognoses), the standard teletype data reports, half-hourly satellite photographs, visual observations from the Intercept teams and NSSL radar and rawinsonde observations. By keeping abreast of the latest developments, the Nowcaster seeks understanding of the current state and tendency of the atmosphere. He relays the latest nowcast and radar information to the field vehicles, obtains their opinions and current visual observations, and directs the vehicles to the most strategic locations. Usually, the team leader and Nowcaster agree on strategy; however, if they fail to do so, the Nowcaster makes the final decision. The Nowcaster is also the link between the Intercept teams and other participants in NSSL's Spring Observational Program. Field reports of tornadoes are relayed to the Doppler radar meteorologists (and also to the local National Weather Service Office for public warnings) while information concerning echo positions, motions, characteristics, and Doppler radar signatures of mesocyclones and tornado vortices flow out to the field.

At times during the last few years the Nowcaster has served six teams simultaneously. TIP has fielded four teams (two long range and two restricted to the area of best radar coverage) with goals as outlined in Section 4.1.2. The primary goals of the other teams were to collect hail (National Center for Atmospheric Research) and to record electrical parameters and tornado acoustics (NSSL-University of Mississippi). The Nowcaster also exchanges information with unofficial intercept teams who telephone him.

---

[1] Larger format (e.g., 35 mm) movie cameras have not been used because they are too bulky. 16 mm cameras can be hand-held, thereby permitting movies to be obtained under extenuating circumstances.

[2] For the 1979 season, a second repeater, installed on a mountain 110 km WSW of NSSL, was linked into the system to extend range, but this repeater worked only intermittently.

4.1.4 Project History

B. J. Morgan,[3] a Notre Dame University engineer, provided the impetus for initiating the project by proposing ground interceptions of tornadoes using a flatbed trailer and an armoured vehicle (tank) system. The flatbed trailer would be driven to within visual range of a tornado on the basis of storm observations by the passengers, aided by radio link with a radar site. Thereafter the tornado would be tracked visually from the mobile station which would close into a strategic position. Then the tank would be unloaded and driven on an intercept course through the tornado. Instruments on the tank would measure the important meteorological variables. NSSL decided to fund the project on a limited basis initially to find out whether field teams could approach within close range of tornadoes using conventional automobiles. This goal was achieved successfully during 1972 (Morgan, 1972; Golden and Morgan, 1972), even though there was a dearth of tornadoes that year. The idea of driving a tank through a tornado was dropped because of (a) the number of bridges in the Oklahoma road network which could not support the tank's weight, (b) the uncertainty whether the tank would survive an encounter with a tornado, and (c) anticipated lawsuits with landowners. Nevertheless, the Intercept Project survived because the goals outlined in Section 4.1.2 proved to be both practical and worthwhile. Volunteer teams, mainly from The University of Oklahoma Meteorology Department, have made valuable contributions to the Project from its onset.

Morgan also proposed that an optical rangefinder be used to determine the range to tornadoes. However, rangefinders capable of measuring 15 km distances accurately were found to be too large to mount on a chase vehicle.

In 1972, the field teams communicated with base via telephone, and the only weather information at the NSSL-based coordinator's "fingertips" were the WSR-57 radar data and the standard teletype reports. Figure 13 shows how new communication and sophisticated weather monitoring equipment, and more vehicles have been added to the program over the years.

4.1.5 The Strategy

To maximize intercept chances, teams enter the field well before severe weather develops and often even before the formation of echoes on NSSL's WSR-57 radar scope. Immediately after the 1000 CST forecast (or even before when conditions warrant), the initial status of each team is resolved. Choices are (a) dismiss the teams, (b) place them on standby at NSSL, (c) dispatch them to a designated standby location in the field, or (d) vector them toward a target storm. Since the initial decision may prove to be a vital one, much depends on the forecaster's ability to assess the probability of severe storms during the day, and the prime time and location for development. On potential or actual severe storm days, the status of each team is updated frequently until the mission is terminated, either because of darkness or because of lack of suitable target storms within range. When storms fail to form by the predicted time, the teams are tempted to drive home early. However, the present policy is to remain in the field until dusk because of several instances of rapid storm development in regions just vacated by returning teams.

---

[3]Morgan participated in TIP during 1972-73.

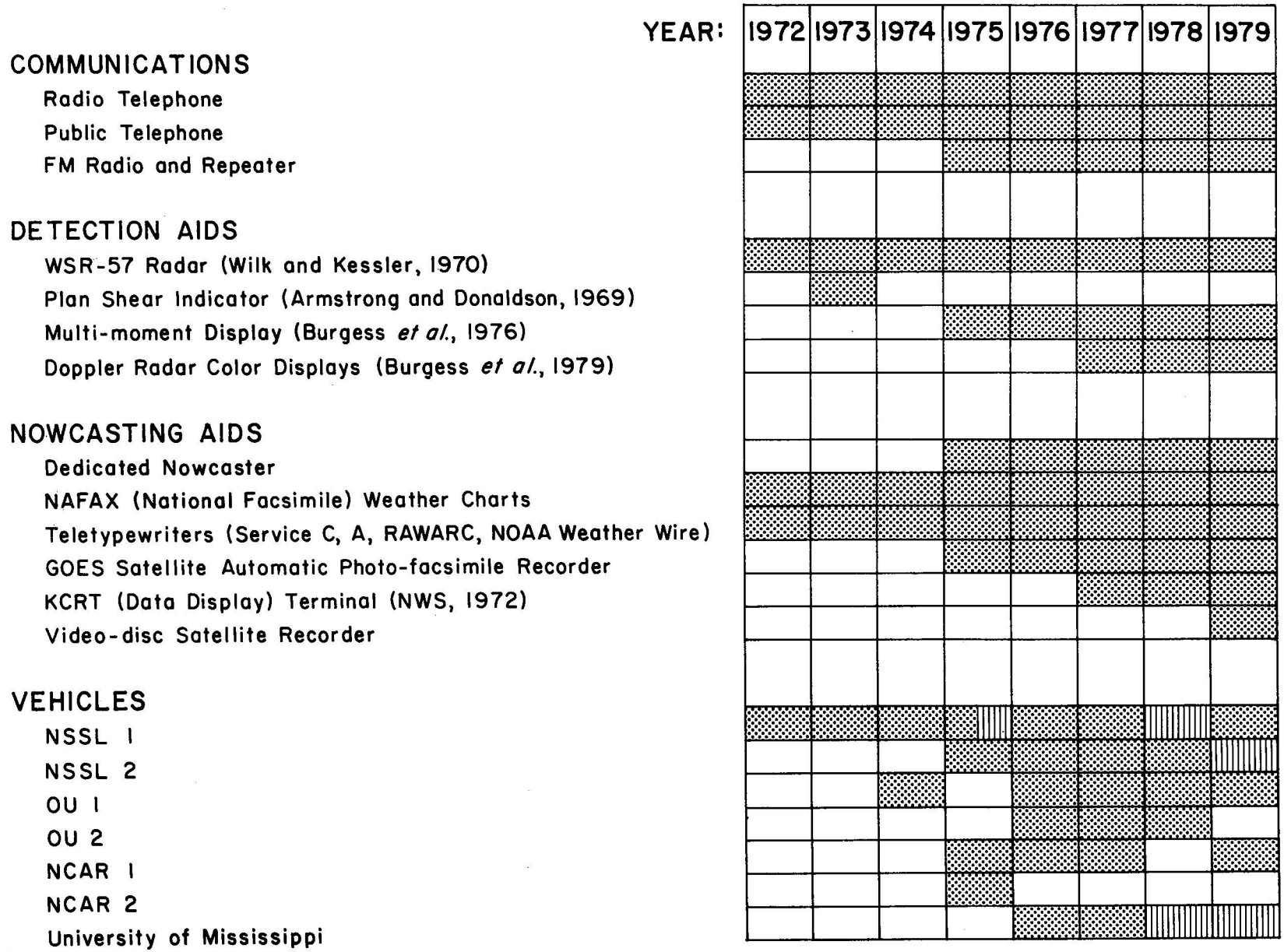

Figure 13. Intercept aids and vehicle participation; 1972-79. Hatching denotes vehicle equipped for meteorological and/or electrical measurements.

After storms have developed, the intercept strategy is founded on vehicle positions in relation to storm locations and movements, and expected weather developments. Unless a decision is made to forego existing storms in favor of ones which are anticipated in a different region, a target storm is chosen for each vehicle based on the storm's accessibility and its tornadic potential. As a field team approaches a storm (Fig. 14), it maneuvers around the precipitation core and takes up a tracking position on the storm's right rear flank.[4] Driving through the core is avoided whenever possible because bad driving conditions force the vehicle to slow down, large hail and strong winds may be encountered, and the team may drive "blindly" out of the precipitation core into the path of a tornado. [Incidentally, lightning, traffic accidents, and flash floods are probably greater hazards to field personnel than the tornado.]

As target distance decreases, the Intercept crew's own visual observations become increasingly important and their reliance on relayed radar information diminishes. This is fortunate since communication channels are often unavailable. The crews have become experts in interpreting cloud features, assessing the tornadic potential of a storm, picking out the part of a storm most likely to spawn a tornado, and recognizing visual precursors of tornadoes. [In fact, many successful private intercepts have been made by individuals acting solely on visual observations.] Once a tornado or suspicious cloud feature has been spotted (Fig. 15), the team positions itself ahead and to the right of the extrapolated track (and should leave itself an escape route to the south or east). This vantage point generally offers the best visibility because the tornado is silhouetted against a light background, and there is least likelihood of intervening precipitation[5] (Fig. 16). Teams which have pursued tornadoes from behind have experienced poor

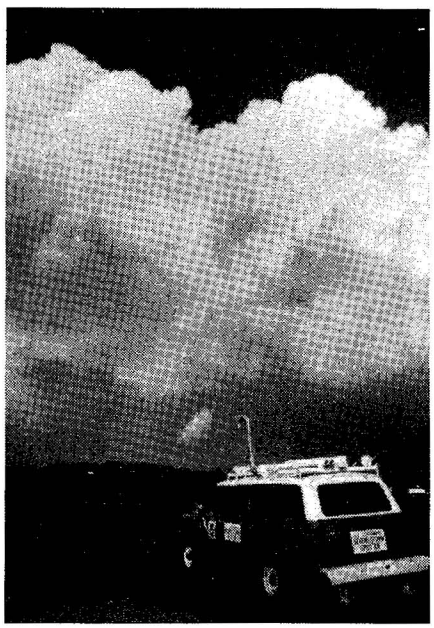

Figure 14. An NSSL instrumented vehicle proceeding towards a storm.

[4]Throughout this report, the precipitation core (low level, high reflectivity echo core on radar) is regarded as the center of the storm.

[5]Southeastward moving storms are a problem because the teams have to reposition frequently to avoid being overrun by the storm.

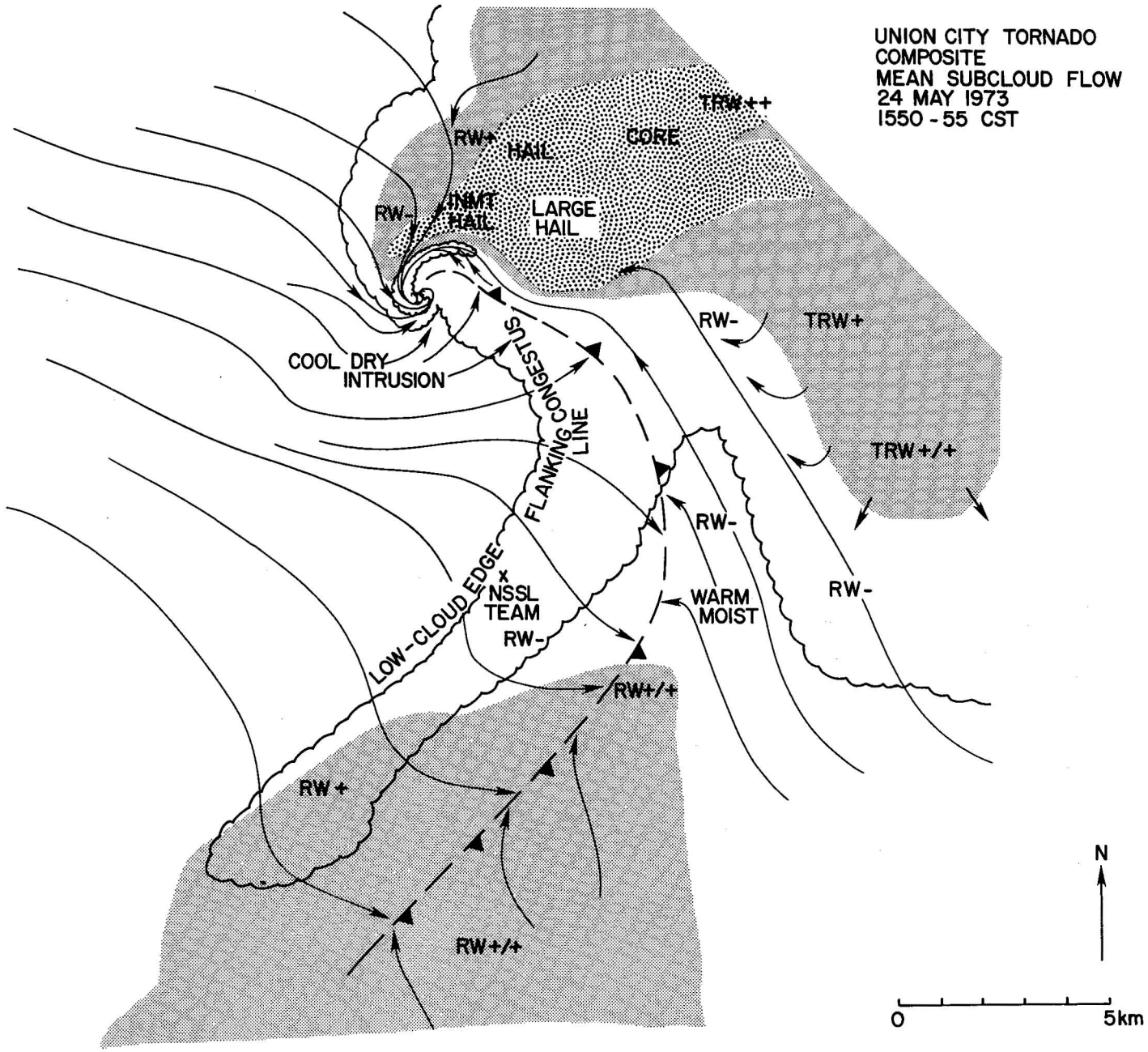

Figure 15. Position of NSSL Intercept Team relative to tornado (at "T"), rain, and hail at Union City, Oklahoma (5-24-73). Tornado was moving east-southeast at this time (from Golden and Purcell, 1978a).

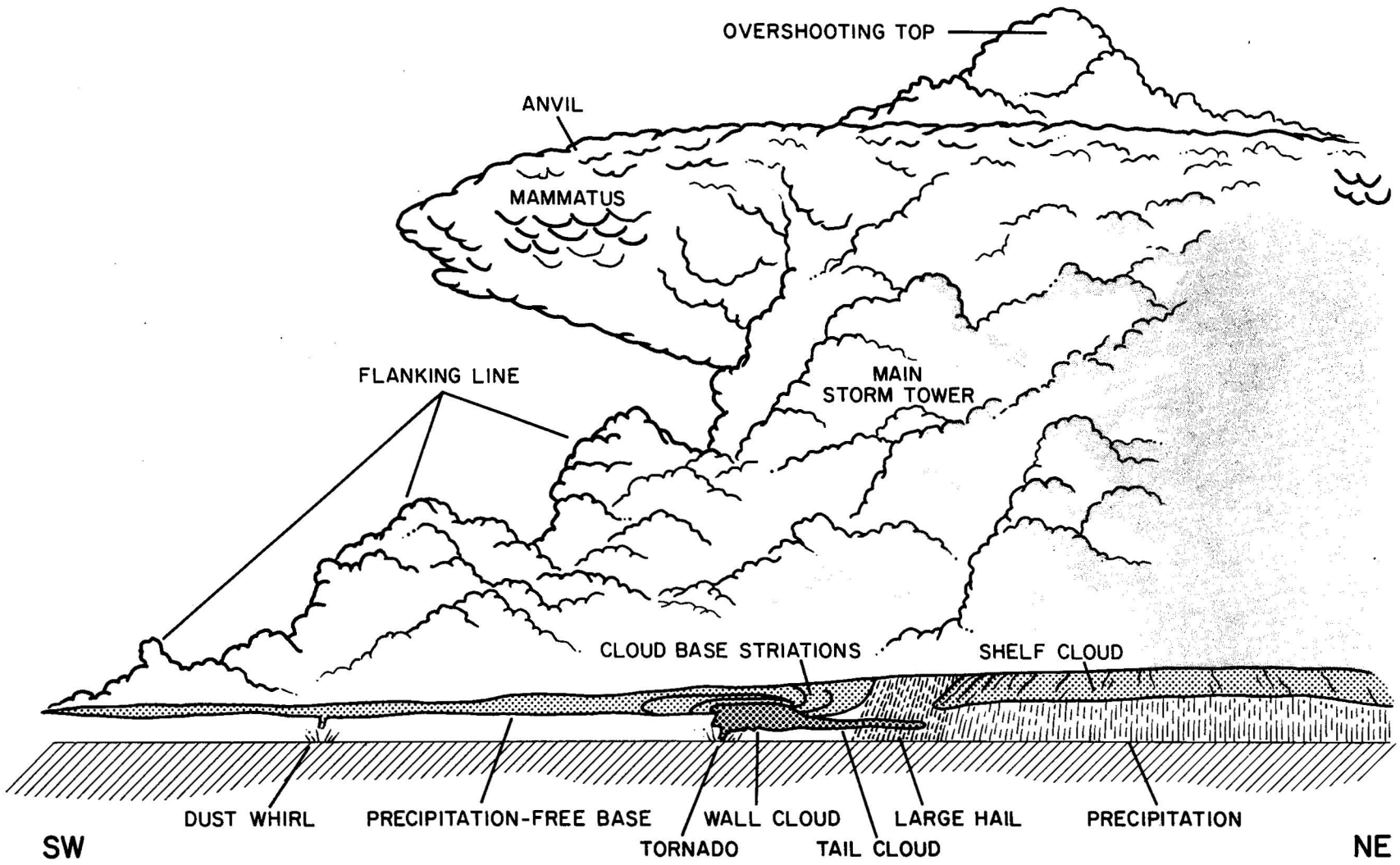

Figure 16. Composite view of a typical tornado producing cumulonimbus as seen from a southeasterly direction. Horizontal scale is compressed. All the features shown cannot be seen simultaneously from a single location. (Diagram by C. Doswell .)

photographic contrast and road obstacles due to fallen debris. Out of the hundred or more hours which each team spends in the field each spring, the opportunity to film a tornado at close range presents itself only for a few minutes. Thus, much of the success of the entire season depends critically on the crew's alert and skillful performance in rare but crucial situations. Also, a poor strategy decision during any part of the chase may be costly. Individual intercepts have been described by Golden (1976a), Moller et al. (1974), Smith (1974), and Gannon (1973).

Even though most of Oklahoma is covered by a network of section roads spaced one mile apart and oriented north-south and east-west, these roads are avoided except as a last resort. Because they are unpaved, they become treacherous when wet. Also, they rarely cross over creeks and rivers. Thus, the Intercept vehicles stay on major highways practically all the time. Lack of roads in desired directions has impeded the crews on numerous occasions.

In some years, one field team has been given a different mission, namely to take time lapse movies of storms from 60-120 km away for the purpose of correlating changes in overall storm structure with the severe weather developments observed by the close range teams (Bluestein and Metzler, 1980). Generally, the best distant view is from the west because the air is drier behind the storms, there are less intervening clouds, and the convective towers are not hidden by other storm features.

Up to this writing, emphasis has been placed on acquiring visual and photographic data. In 1973, "chaff"-bearing-rockets were launched to 1 km heights to introduce radar detectable tracers into severe storm inflows. The University of Wyoming participated in our 1975 program by sharing the use of their vehicle, instrumented for measurement of pressure, temperature, dewpoint, and other meteorological variables (Fig. 14; Martner, 1975). NSSL purchased this vehicle from the University of Wyoming in 1978 for TIP use. Other experiments could be attempted, provided that the equipment is portable and set-up time is minimal (one or two minutes). Longer preparation times are impractical because stops must be limited in duration so that the vehicle can reach and maintain the optimal position for viewing tornadoes as they travel, and because the majority of tornadoes are short-lived.

Possible measuring systems for future field use include short wavelength (K band) Doppler radar, Doppler lidar (laser equivalent of Doppler radar), an instrumented remote-control model airplane, and instrumented "toy" rockets. These devices may be carried on an airborne platform. Although less mobile than aircraft, ground vehicles have been used so far because they are more economical, safer in strong winds, and can stop at will.

4.1.6 The Chances

Because the intercept teams guide themselves visually over the last few kilometers of storm intercepts, their chances of success depend critically on local terrain and vegetation. The ideal "intercept country" is relatively flat with few trees so that distant cloud features at low elevation angles are visible. The region should also be sparsely populated, have few large lakes and rivers, and

have a dense road network so that the teams have good mobility. The local storm environment is also important; the presence of haze, low overcast, or extensive rain areas obscure the target storm and make intercepts practically impossible. Fortunately, in Oklahoma (and other Great Plains States), the storms are usually clearly visible (especially in late spring and summer). Eastern Oklahoma has many hills, lakes, and trees to impede the chasers but the farm lands of Western Oklahoma are almost ideal. Intercepts are easier in late spring than in early spring because of improved visibility and slower-moving storms.

The field teams are sent out on roughly 30% of the days during the two month period (normally 15 April to 15 June) of NSSL's Spring Observational program. On an average chase, a team drives roughly 600 km and spends between 8 and 9 hours in the field. A field team which is permitted to range up to 240-320 km from base typically has a successful "chase" (i.e., observes one or more tornadoes) about once in every seven outings. Almost all successful intercepts have been made in the Western half of Oklahoma or in the Texas Panhandle. Since tornadoes are rare and often unpredicted, teams are sent out even when chances for tornado formation are considered slight. Even when tornadoes are not seen, the missions are often scientifically valuable. Table 2 indicates that severe storms have been intercepted on 42% of field days. On the remaining days, either nonsevere thunderstorms were observed (43% of days), or no storms developed (15%).

Because of the time consumed in making a morning forecast, deciding upon the initial strategy, and travelling to the area where severe storms are anticipated, the teams are often not in position to make intercepts before 1300 CST. Fortunately, only 7% of Oklahoma tornadoes occur during the first half of daytime (0700-1300 CST). After 1900 CST, lighting rapidly becomes too low for photography (if intervening precipitation and clouds have not created an earlier dusk). Thus, we define those tornadoes which occur between 1300 and 1900 CST (50% of the total) within 240 km of Norman as pursuable. The frequency of pursuable tornadoes in Oklahoma is roughly one to two per 10,000 km^2 per two month severe storm season. Hence, in an average season there are 18 pursuable tornadoes and 7 pursuable tornado days. About 23% of pursuable tornadoes have been sighted by field teams (both official and private) during the eight years, 1972-1979. This percentage would have been slightly higher if some teams had not been assigned to cover the area of best multi-Doppler radar coverage, and had been free to leave this area at will.

4.1.7 Project Accomplishments

After two years it became apparent that tornadoes could be observed with sufficient frequency to make pursuit worthwhile. Counting both official and private intercepts, more than 130 Great Plains tornadoes (76 officially confirmed[6]) have been observed during the last eight years (1972-79). In most cases, close range observations of tornadic storms began well before actual tornado formation. The results and conclusions of TIP's extensive observational program are as follows:

a. Wind speeds of three tornadoes have been measured photogrammetrically from high quality movies taken by TIP teams (Section 4.2). Maximum measured wind speeds in these tornadoes range from 60 m s^{-1} to 90 m s^{-1},

b. Conceptual storm models, based extensively on visual observations, have been compiled. (To be presented in a forthcoming NSSL Tech. Memo.)

[6]Only 30 of these 76 fall into the "pursuable" category described in Section 4.1.6.

Table 2. Breakdown of TIP field days by year and by phenomenon observed [Severe storm (tornado), nonsevere storm or no storm at all]. Also given are number of NSSL and OU vehicles participating each year and range restriction.

Year	# NSSL Vehicles	# OU Vehicles	Range* (km)	# Days in Season	# Intercept Days	Severe Storm (Tornado) Days	# Nonsevere Storm Days	# No-storm Days
1972	1	0	240	65	17	5(2)	8	4
1973	1	0	200	62	12	6(1)	5	1
1974	1	1	115	62	16	10(4)	5	1
1975	2×	0	240	62	19	7(2)	8	4
1976	2+	2	320	67	22	7(4)	13	2
1977	2+	2+	400	76	30	14(8)	10	6
1978	2	2	345	76	30	13(2)	12	5
1979	2	1	240	79	13	4(4)	8	1
TOTAL				549	159	66(27)	69	24

*Range limit applies only to NSSL vehicles.
+One vehicle mainly restricted to Doppler radar coverage area.
×One vehicle assigned to long range photography.

c. Time lapse photography has revealed that entire convective towers rotate.

d. Rarely is any lightning seen near (closer than 2-3 km) or within tornadoes (Davies-Jones and Golden, 1975a,b,c).

e. Most tornadoes are close to, but outside, precipitation areas. A few are embedded in precipitation, however. Large hailstones often fall near the tornado, generally on its left forward side.

f. The tornado usually forms in a region of the storm where the cloud base has always been free of precipitation and lightning. Thus, there is no observational evidence to support theories which require cloud-to-ground lightning (Vonnegut, 1960) or a burst of precipitation (Rossmann, 1960; Danielsen, 1975; Eskridge and Das, 1976) to initiate tornadoes.

g. The tornado generally develops from convective towers on the storm's right rear flank. The tornado may be located very near the edge of its parent cloud (Fig. 17).

h. Strong tornadoes form from wall clouds (Fig. 18). Thus, wall clouds--when present--identify potentially very dangerous parts of the storm.

i. Gradual evaporation of cloud is often observed in the wall cloud, first to the rear of the tornado and then slowly propagating around its right side (Lemon and Doswell, 1979). This observation apparently indicates the presence of a developing unsaturated rear flank downdraft. Intense upward motions seen ahead and to the left of the tornado indicate that the tornado is located near an updraft-downdraft interface.

j. Relatively isolated storms are the best tornado producers (Fig. 19), presumably because they are not competing with neighbors for available warm, moist inflow air.

k. In some cases, surface weather features pinpoint small areas of maximum tornado threat. Tegtmeier (1974) showed that favored locations for tornadoes are the northeast sides of developing small scale lows and the moist sides of bulges in the dryline (Fig. 20).

Figure 17. Tornado near edge of cloud at Quail, Texas, 16 May 1977.

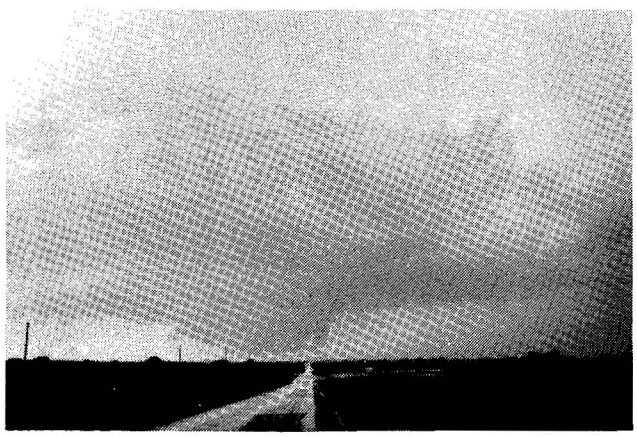

Figure 18. Wall cloud (discrete lowering of cloud base).

l. Anticyclonic tornadoes definitely exist (Fig. 21; Burgess, 1976a).

m. TIP storm observations and photography have been incorporated in a training movie (NOAA, 1977) and slide collection (NOAA, 1980) for tornado spotters.

n. The Intercept team's documentation of the Union City's tornado position in time and space and its tilt with height helped establish Doppler radar's tornadic vortex signature.

o. The life cycle of tornadoes has been clarified, and interesting changes in damage intensity and debris configuration as tornadoes evolve have been observed (Fig. 22).

p. A new type of severe storm, which fails to fit the classical model, has been identified (Davies-Jones et al., 1976; Burgess and Davies-Jones, 1979).

q. TIP has provided vital information to Doppler radar meteorologists involved both in the Joint Doppler Operational Project and in the analysis of research data. For example, well documented TIP tornado observations verified 11 out of 34 experimental tornado warnings issued solely on the basis of Doppler radar observations during 1977 (Burgess et al., 1978).

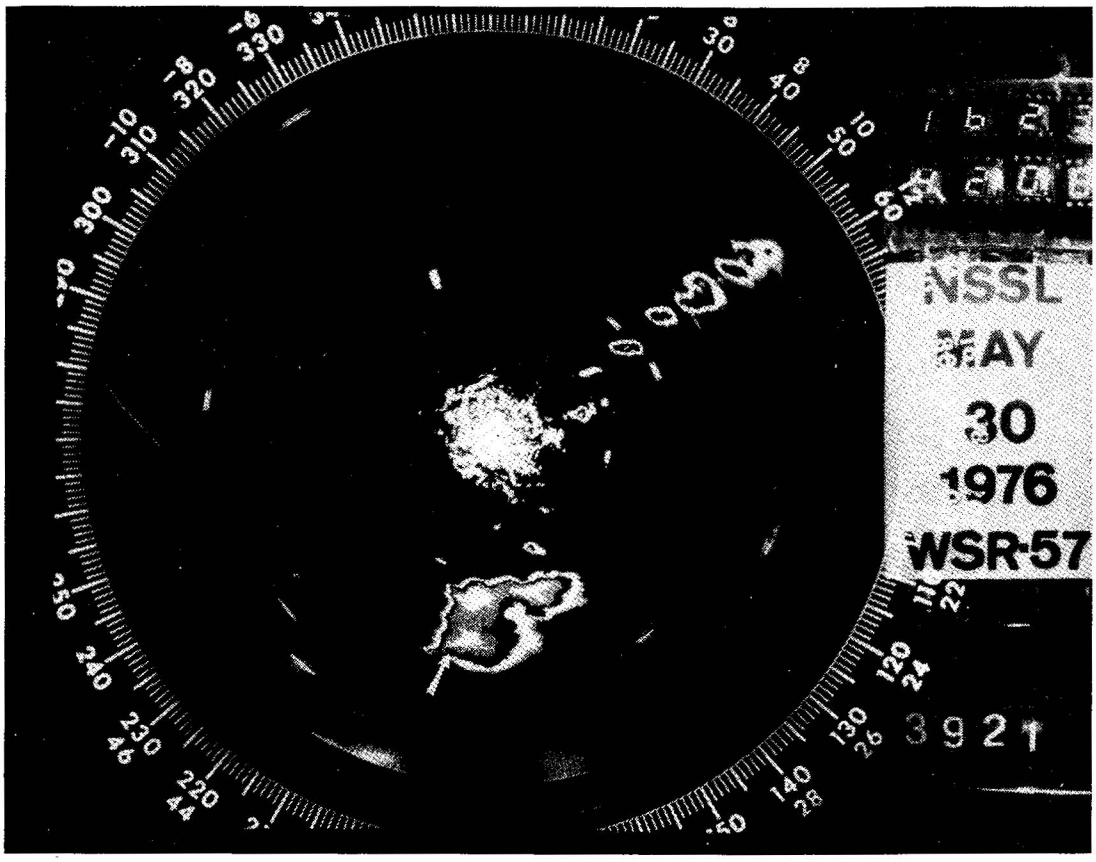

Figure 19. Radar display of a tornadic storm recorded at Norman, Oklahoma on 30 May 1976. Range to edge of scope is 200 km. Position of tornado is indicated by arrow.

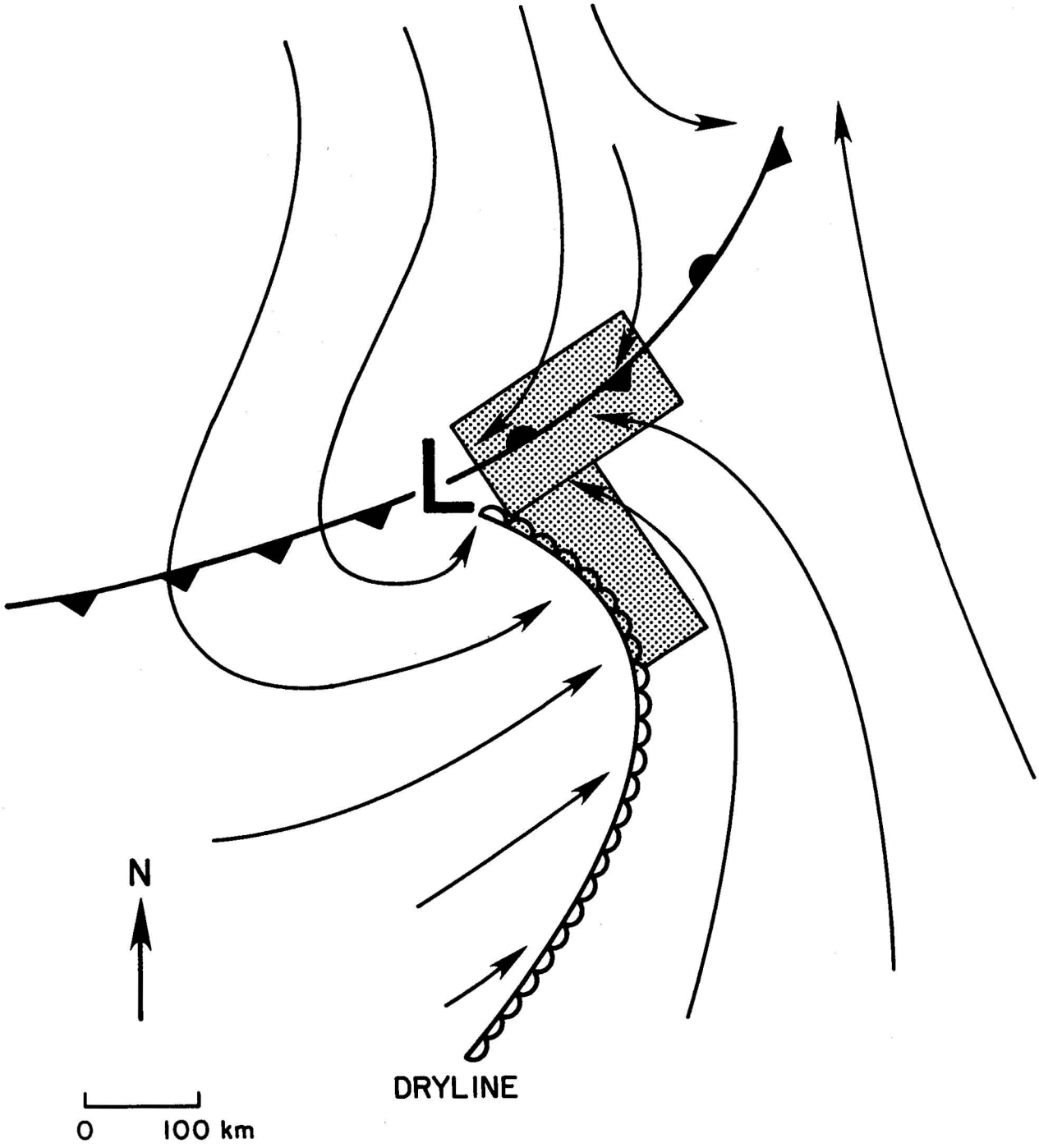

Figure 20. Schematic of surface flow features for a case where small scale low and dryline bulge are present simultaneously. Stippling indicates maximum threat areas. Typical scale drawn in bottom right corner.

4.1.8 Project Appraisal

Obtaining debris movies has proved more difficult than first anticipated. Nevertheless, high resolution, analyzable 16 mm movies of three tornadoes have been obtained. Tornadoes have been filmed on other occasions but photogrammetric analyses of these movies were not performed because either the tornado was too distant (or too near on one occasion!), the contrast too poor, or the tornado travelled over terrain devoid of potential debris material. The movies obtained by TIP are more valuable scientifically than those taken by chance eyewitnesses because high-resolution film and skillful photography permits small features to be seen and tracked. Sending meteorologists into the field is beneficial in many other ways too. Intercept teams can record accurate times--difficult to obtain post facto--of tornadoes and hailfall, and they can collect hailstones for scientific analysis (Knight and Knight, 1974; 1976). The rise rate of convective towers measured photogrammetrically can be compared to vertical velocities measured by Doppler radar. The everchanging visual outlines and motions of the clouds which they see and record on film contain valuable information about severe storm structure, and the dynamical processes which foreshadow tornadoes. Many fruitless tornado theories would never have been conceived if the instigators had witnessed tornadogenesis firsthand. The field crews also may make fortuitous discoveries of great research value such as the first proven anticyclonic tornado (Burgess, 1976a).

TIP personnel have noticed that, not only the frequency, but also the character of storms varies greatly from year to year. For instance, in 1972 and 1973, the most common tornadic storms were the isolated, slow-moving supercell and the "dryline" storm. Such storms can be intercepted relatively easily because there are no nearby storms to confuse the situation and because the tornado is usually highly visible from most directions. In other years, the tornadic storms primarily have been embedded in squall lines, and other types of tornadic storms have also been recognized. Thus, the continuance of the project over many years has enabled a broad base of knowledge to be acquired,[7] and has avoided the pitfalls of drawing definitive conclusions from a limited sample of storms. Our conceptual models of severe storms probably will continue to evolve as we observe still more storms. The Intercept observations and high quality Doppler radar data collection become especially valuable when they complement one another. However,

Figure 21. Anticyclonic tornado near Alva, Oklahoma (6-6-75). Note condensation funnel (white) at top center. Photograph courtesy of J. Leonard and E. Sims.

[7] This knowledge is being summarized in an NSSL Technical Report, currently under preparation.

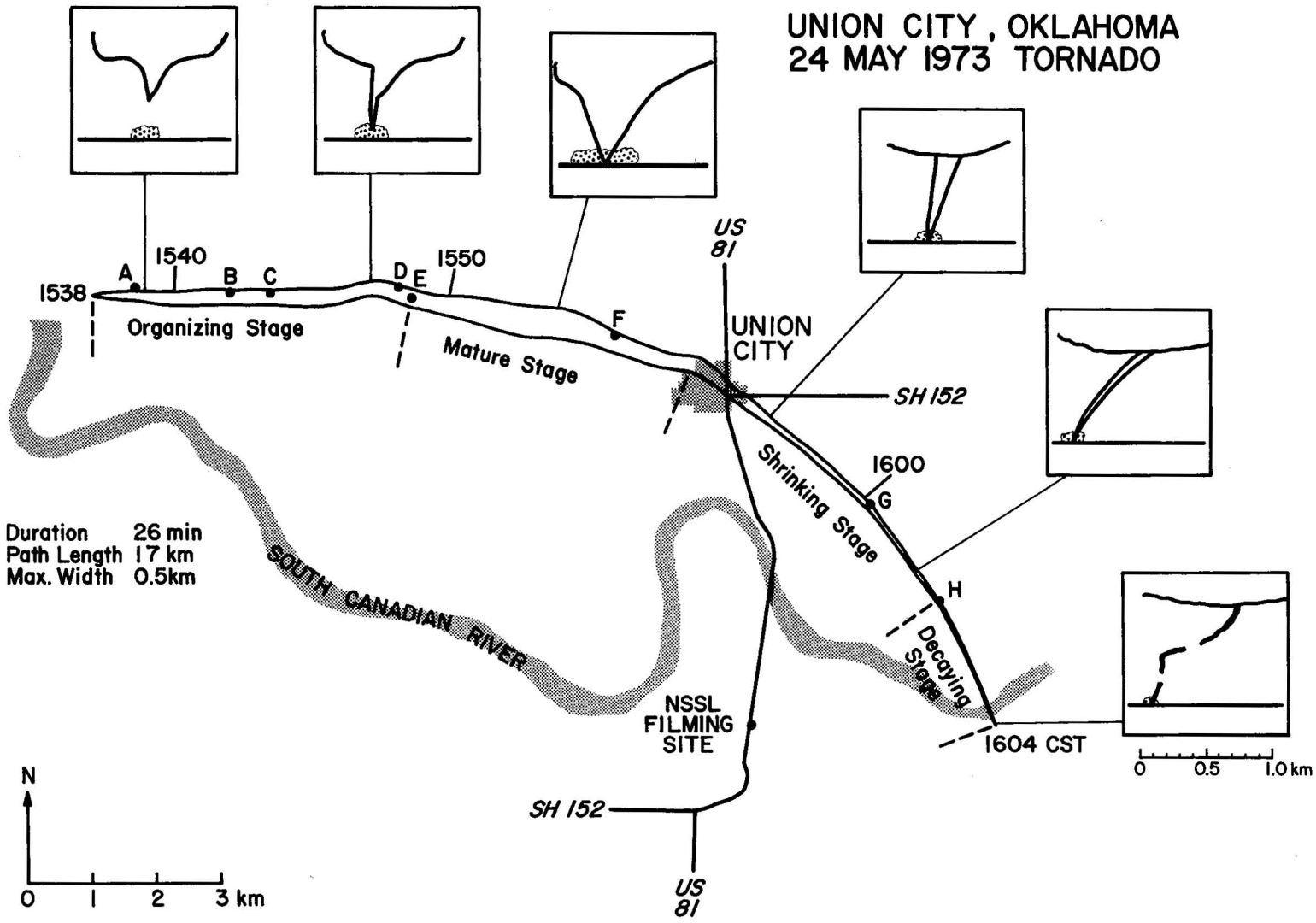

Figure 22. Damage path of the 5-24-73 Union City, Oklahoma tornado with sketches of the funnel at different life cycle stages (from Golden and Purcell, 1978a).

only a few severe storms each year are ideally placed for accurate, high resolution, multiple Doppler radar data collection,[8] and these storms may spend only a part of their lives in the "prime Doppler area." Because tornadic storms exhibit considerable variability, many more cases with simultaneous high quality Doppler radar and visual observations are needed (i) to separate the crucial factors in tornado formation and maintenance from incidental factors which are present sometimes but unnecessary, and (ii) to explain why some mesocyclones spawn "maxi"-tornadoes while others, seemingly just as intense, produce only weak tornadoes (if any).

In the future, man will attempt new techniques for measuring tornadoes and, perhaps will even try to modify them. The art of tornado interception will be important logistically to the success and safety of these field experiments.

4.2 Photogrammetry

4.2.1 Photogrammetric Analysis Technique

The motions of identifiable features (large debris, dust aggregates, cloud tags, etc.) in close range tornado movies can be measured using photogrammetric techniques. The analysis measures directly those velocity components, which are perpendicular to the camera principal axis, through painstaking tracking of air motion tracers across a carefully controlled, projected image. Image plane distances are converted to actual distances through accurate mapping of the tornado damage track and a survey from the photographic site of landmarks appearing in the movie.

A 16 mm copy of the film is cut at judicious intervals so that film loops 50 to 250 frames long can be made. Every frame or two the positions of air motion tracers relative to fixed landmarks are recorded. This procedure automatically compensates for camera movement. For scaling purposes the image plane distances between landmarks are also measured. Changes in camera focal length due to zooming are accounted for by repeating the scaling procedure whenever necessary.

A certain minimum of information is required before any tornado photogrammetry analysis can be performed (Morgan, 1974). Specifically, this includes: (a) the location of the camera during filming, (b) camera framing rate, and (c) damage track of the tornado. Nonessential but useful information consists of the vertical and horizontal angular orientation of the camera during filming, camera focal length, and intersection of the optical axis of the camera with the film (principal point). Basic photogrammetric techniques in meteorological applications have been described by Saunders (1963), and by Morgan (1974), who outlined a complex, digital approach to tornado photographic data analysis. The analysis procedures employed by NSSL follow those of Saunders (1963) with the added assumption that β (camera elevation angle) is less than 10°, and that all points used in the study lie within 10° of the lens horizon-principal plane intersection. This assumption means that, on each film loop, distances on the photograph can be related to angular separations by a single scale ratio with less than six percent error (this can be shown by mathematical analysis of Saunders' equations).

---

[8] The prime coverage area for the permanent NSSL dual-Doppler network is only 10,000 km^2 (Davies-Jones, 1979). Thus, intercept teams have had to venture further afield to gain experience and skill.

The scale ratio for each loop is determined as follows:

(1) The exact positions of the camera and the tornado's damage track are located precisely on a scaled, up-to-date topographic quadrangle map during a photographic site survey.

(2) From the camera site, azimuth (ϕ) and elevation angles (θ) of conspicuous permanent landmarks on the film horizon are determined to 30" accuracy, using a transit.

(3) An approximate lens horizon is established from interpolation amongst the elevations of several landmarks.

(4) The horizontal distance, Δx, between the images of two landmarks is measured. The scaling factor, S, is given by

$$S = \frac{\Delta\phi}{\Delta x} \quad , \qquad (1)$$

where $\Delta\phi$(in rads) is the azimuthal separation between the two landmarks. With S established, the position of the lens horizon is checked.

(5) The (horizontal) range from the camera site to the center of the tornado, D_o, is then found by measuring on the topographic map the straight line distance from the camera site to the point where the line-of-sight through the tornado intersects the known path.

(6) Distances in the image plane are related to distances in the object plane containing the tornado by the scale ratio $1:D_oS$.

The above method measures "raw" velocities, i.e., those computed using a constant scaling factor, S, and a constant tracer-camera separation distance, D. In many cases, the raw velocities may contain significant error, and corrections must be applied by incorporating local variations of S and D into the calculations (Forbes, 1978). First, use of a wide-angle lens in the original photography, or pincushion distortions in the camera or projector lenses, may require the use of local scaling factors for different segments of the frame. Second, objects closer to (further from) the tornado than D appear to be moving faster (slower) than their actual speed. To correct the scale ratio for this effect, the true horizontal range to the tracer has to be approximated from factors such as the tracer's elevation angle, its azimuthal angular separation from the tornado axis, the tilt of the vortex with height and an estimate of the object's radial distance from the axis. If the tracer is in a roughly circular orbit, then its radial distance can be measured photogrammetrically at the time when its apparent horizontal velocity vanishes. Eyewitness photography from several vantage points, if available, can be used to establish the three-dimensional vortex tilt and geometry.

The photogrammetric technique measures only the two velocity components normal to the line of sight. Thus, the net wind speed measurements (in the film plane) are low estimates of the actual speeds, except where the third component (along the line of sight) is small compared to the others.

Even after the scale ratio corrections, two fictitious velocities arise because of tracer motions parallel to the camera axis. First, apparent vertical velocity (i.e., change in elevation angle) in the film plane may arise in part from the horizontal motion of the tracer towards or away from the camera. The

false contribution to apparent upward motion is $-\dot{Y} \tan \theta \sec(\phi-\phi_0)$ where $\dot{Y}$ is the horizontal velocity component parallel to the optical axis (positive away from the camera) and ϕ_0 is the azimuth angle of the principal point. For $\dot{Y}$ = 100 m s^{-1}, $\theta = 5°$ and $\phi-\phi_0 = 0°$, the vertical velocity error is -9 m s^{-1}. For a cyclonic tornado, this effect causes apparent subsidence on the right side and apparent ascent on the left side of the image. Second, apparent horizontal velocities in the film plane (i.e., changes in azimuth angle) also arise partly from horizontal motions parallel to the optical axis. This fictitious velocity component is due to perspective (lines of sight diverge outwards), and is given by $-\dot{Y} \tan(\phi-\phi_0)$. Because of this effect, features on the far (near) side of the tornado appear to be traveling faster (slower) than they really are by as much as 10 m s^{-1} (for $\dot{Y}$ = 100 m s^{-1}, $\phi-\phi_0 = 6°$).

For a vertical tornado, the total velocity at a point can be broken into the following components: tornado translation velocity ($\vec{V}_{tr}$) and radial (u), tangential (v), and vertical (w) velocities in cylindrical coordinates centered on the vortex axis. The translation velocity along the surface is easily obtained from the tornado's motion across the image plane and the known orientation of the damage path (unless the tornado is traveling directly toward or away from the camera). The apparent horizontal and vertical velocities of a tracer are simply determined from its estimated range, and measured horizontal and vertical displacement in the image plane. Removal of the fictitious components of these velocities is often not feasible because it is impossible to estimate $\dot{Y}$ reliably in many cases (see below).

If the tornado is assumed to be cylindrically symmetric and the debris has negligible radial velocity, then the vortex-relative horizontal velocity in the image plane varies quasi-sinusoidally as the debris orbits around the funnel. The tangential velocity, v, is proportional to the amplitude of the sine wave. Forbes (1978) has generalized this technique to deduce both u and v, but apparently failed to take into account the fact that radial distance changes with time in the case of $u \neq 0$. The tangential velocity can be deduced confidently when the data fit the sine curve well; however, in many tornadoes, asymmetries are marked and the cylindrical coordinate system does not apply to the vortex geometry. Note that $\dot{Y}$ can be estimated reliably, and the fictitious components can be removed from the apparent horizontal and vertical velocities, only for tracers with negligible radial velocity.

Because u is generally much smaller than v and w except very close to the ground, it is usually difficult to infer from the measured velocities (particularly, because debris tends to be centrifuged outwards). Inflow along the surface frequently appears to be concentrated in a single (asymmetric) band of dust feeding into the vortex. When this band lies normal to the optical axis, inflow velocities near the ground can be measured.

The types of tracers must be identified because of possible differences between tracer speed measurements and actual air motions. Note that (a) heavy debris velocities are dependent on inherent tracer properties (e.g., mass, shape, orientation, exposed surface area, tumbling or non-tumbling motion, etc.) and respond relatively slowly to wind changes within the local environment traversed; (b) dust parcels (aggregates) may change shape and optical density characteristics may vary rapidly as a result of radial shear in tangential velocity, making accurate tracking of apparent centroids difficult; (c) funnel-wall perturbations may be wave motions (Ward, 1972; Davies-Jones and Kessler, 1974), and their apparent speed may represent a phase velocity rather than actual airflow;

(d) cloud features may change shape due to evaporation and condensation, causing the motion of the centroids to be unrepresentative of actual air motion; and (e) even though suction vortices may be regarded as vortex lines carried with the airflow, their measured displacements only yield the air velocity component normal to their axes (which may be greatly contorted and changing orientation rapidly).

The wind fields presented below represent temporal composites over roughly 30 seconds or less. Each velocity measurement is an average over at least one-third of a second. Tracer type is identified for each measurement.

NSSL has performed photogrammetric analyses of nine tornado movies, five of which were taken by chase teams and four by chance eyewitnesses (Table 3). Three Intercept Project movies, all of which contain multi-vortex tornadoes, were obtained during Project SESAME '79 and are currently being analyzed in-house and elsewhere. The results of the other analyses are given below (and also in Golden, 1976c).

4.2.2 Union City, Oklahoma tornado May 24, 1973

A large tornado devastated Union City, Oklahoma (population 500, location 48 km WNW of NSSL) in the late afternoon of 24 May 1973. The tornado had an overall path length of 16 km, a maximum path width of 500 m and a lifetime of 25 minutes. Its complete life cycle was photographically documented from the NSSL Intercept vehicle, which had stopped 5 km south of Union City (Golden, 1976a). Additional photographic documentation and meteorological observations were provided by two Oklahoma University student teams (Moller et al., 1974). Golden (1976b) and Golden and Purcell (1978a) have shown that the tornado's life cycle appears in many respects to resemble key features of the Florida waterspout life cycle. Major differences are apparently the vortex and parent cloud scales, and to a lesser extent, vortex lifetimes and intensities (Golden, 1974a,b). The tornado shrunk rapidly in diameter at all levels while passing through Union City, increased its northeastward tilt, and changed course from east at about 9 m s^{-1} to southeast at 15 m s^{-1}. On the next day, the damage path was extensively surveyed both from the air and the ground.

All debris tracking west of Union City was performed during a two-minute interval when the mature tornado was about 4 km west of town, and 6 km northwest of the camera site. The rotating debris cloud was somewhat asymmetric with respect to the tornado's center. Surface damage analyses indicated that debris particles at this time were composed primarily of dust and small bits of vegetation. Therefore, trajectories derived from tracking these aggregates of light debris particles should be representative of the actual air motion. The debris aggregates had dimensions of 10-30 m. The bulk of the debris velocity data (Fig. 23) were obtained to the right of the funnel wall, at elevations from 75 to 145 m (the lowest 55-80 m of the tornado's debris cloud circulation west of Union City was obscured by an elevated railroad track and shrubbery in the foreground.)

We introduce a horizontal coordinate x', defined as the projection of radial distance from the tornado onto that vertical plane normal to line of sight which bisects the tornado. Figure 23 shows contours of the x' component of horizontal wind plotted on an x' vs. z (height) cross section. The maximum windspeed (80 m s^{-1}) is located 90 m above the ground and 80 m from the tornado axis. Between x' = 80 m and 180 m the windspeeds do not decrease monotonically along constant height lines. However, the secondary windspeed maxima outward from x' = 90 m in Fig. 23 may be due to temporal changes in the tornado's flow structure

Table 3. Tornado movies analyzed by NSSL.

Tornado	Date	Taken By	Maximum Measured Wind speed ($m\ s^{-1}$)	Occurred at Height (m)	Official F Scale Damage Rating of Tornado	Reference
Kailua Kona, HI (Tornadic-waterspout)	1-28-71	Eyewitness	56	40	-	Zipser (1976)
Union City, OK	5-24-73	NSSL	80	90	F4+	Golden and Davies-Jones (1975) Golden and Purcell (1976, 1978a)
Salina, KS	9-25-73	Eyewitness	59	45	F5	Zipser (1976)
Xenia, OH	4-3-74	Eyewitness	95	200	F5	Golden and Purcell (unpublished)
Great Bend, KS	8-30-74	Eyewitness	85	80	F2	Golden and Purcell (1975, 1977)
Alva, OK (Anticyclonic tornado)	6-6-75	Private chase team	<60?	?	F1	Unpublished
Seymour, TX	4-10-79	NSSL	77	15	F2	To be published
Seymour, TX	4-10-79	G. Moore	90	30		To be published
Orienta, OK	5-2-79	OU	76	50	F2	To be published

+Should have been F5 according to Davies-Jones *et al.* (1978).

during the 20-30 sec of film data composited. The dashed arrows in Fig. 23 indicate the approximate debris-aggregate trajectories in the x'-z plane. Below the level of primary horizontal windspeed maximum, the debris have upward velocity components of 13-30 m s^{-1} for x' = 100 m. This implies that as small debris particles were picked up off the ground on the tornado's south side, they accelerated (with the wind) upward and outward before orbiting around the tornado's east side. Using values of x' at which the x'-component of debris velocity changes sign, and assuming that the orbits were approximately circular reveals that the tracked debris were located between 180 and 220 m from the funnel axis. Thus, the primary horizontal windspeed maximum of 80 m s^{-1} was located at a true radial distance of roughly 200 m from the tornado's center.

A composite, scaled outline of the Union City tornado funnel with cloud-tag motion vectors superimposed is given in Fig. 24. Approximate radius from the funnel center has been noted for each major cloud streamer. (Since the cloud-tag speeds are those actually measured in the image plane, only those near the tilted center line of the funnel represent true tangential velocities.) Figure 24 indicates that the upper peripheral cloud-tags were rotating around the tornado funnel with speeds ranging from 15 to 40 m s^{-1} at radii of 300-700 m outward from the funnel at cloudbase level. These velocities compare favorably with those measured at similar elevations by NSSL's single Doppler radar. Visual observations from the NSSL Intercept vehicle of peripheral cloud rotation about the upper southeast quadrant of the funnel indicate that cloud elements were sinking and evaporating. This downward motion is confirmed in Fig. 24 and is in excess of 8 m s^{-1} halfway up the funnel, near its closest edge. Using triangulation with photography of eyewitnesses to obtain the funnel cloud's surface location at 5-6 different points west of Union City, it was determined that the funnel's surface location lay within the one-third to one-quarter mile wide damage swath. Furthermore, the funnel cloud's intersection with the ground had a distinct tendency to be near the north boundary (i.e., left side) of the tornado damage path.

The tornado continued southeastward after devastating Union City, and, as it entered its decay stage, destroyed a large wooden frame house. At that point, the tornado was about 4 km ENE of the NSSL intercept vehicle location. Large amounts of debris from the house could be followed around the tornado at various elevations for several successive frames on the film. As the tornado continued onward, ejecting suspended debris as it went, it crossed fields with standing rainwater and drew water into its circulation. Figure 25 shows a composite side-view of debris velocities, plotted relative to the mean shape and location of the

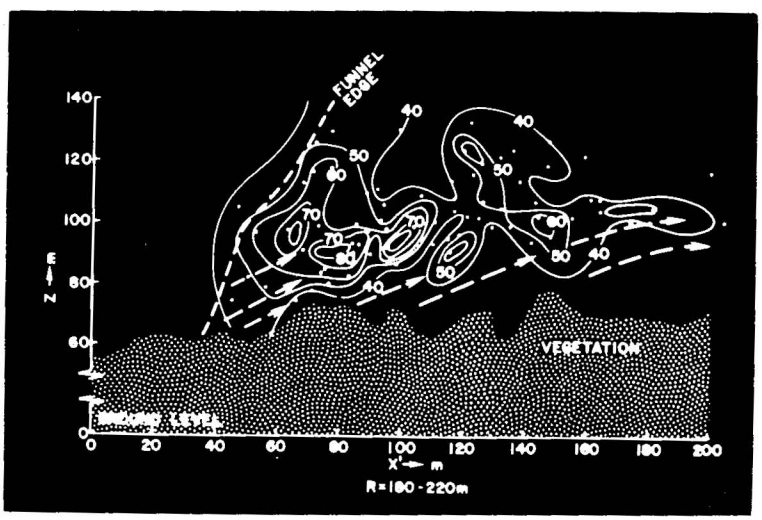

Figure 23. Profile of photogrammetric horizontal windspeeds in Union City tornado. Isotachs in m s^{-1}. Abscissa, x', is projected distance from funnel's center measured normal to camera's principal axis; R is range of true radial distances from tornado's center. See text for details. After Golden and Davies-Jones (1975).

tornado's temporary spray sheath. Most debris particles are believed to have been large pieces (≥ 1 m^2) of white wooden siding and roofing material from the farm house. At that time, most of the debris to the left of the spray vortex had already been suspended for at least one revolution.

The orbits of debris particles in Fig. 25 appear quite different from those earlier in the tornado's lifetime (compare with Fig. 23). In its later decay stage, the tornado's radius of rotational influence was much smaller and the debris orbits appear highly eccentric (see Golden and Purcell, 1976, 1978b; Davies-Jones et al., 1976, 1978, for more details). Those debris particles in Fig. 25 which change direction in the film plane are marked with radial distance values, R. These values apply only for the point in the orbit at which x' is a maximum. Horizontal windspeeds in the debris were 25 m s^{-1} at 130 m upstream from the vortex center and around 60 m s^{-1} within 50 m of the vortex center at elevations between 50 and 80 m. The horizontal windspeed reached at least 65 m s^{-1} at a radial distance of roughly 25 m (compare with results in Fig. 23). Most of the debris tended to sink as it passed ahead of the vortex, and strongest rising motions were found just to the north of the spray vortex axis. It appears that the tornado's flow structure became increasingly asymmetric in both rotational[9] and vertical components.

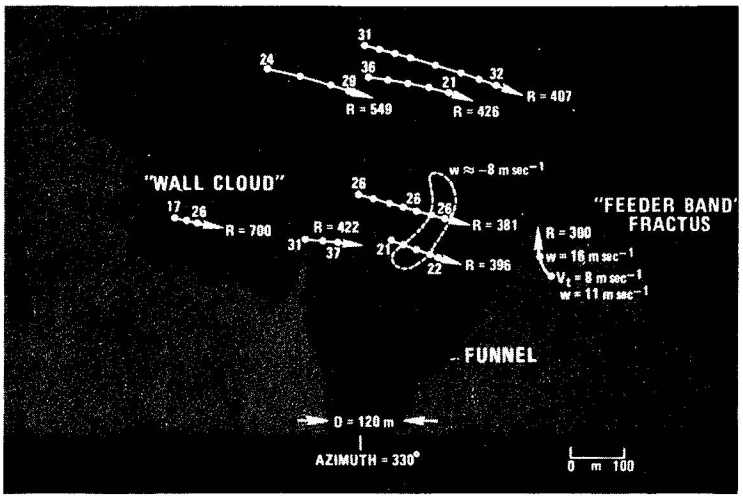

Figure 24. Scaled outline of Union City tornado funnel with cloud tag trajectories in wall cloud superimposed. Representative cloud tag velocities (m s^{-1}) and radii (m) are indicated along each trajectory. Note pronounced sinking motion, up to -8 m s^{-1} (dashed region) on SE side of funnel and rising motion into base of "feeder band" of clouds spiralling into upper funnel from NE. After Golden and Davies-Jones (1975).

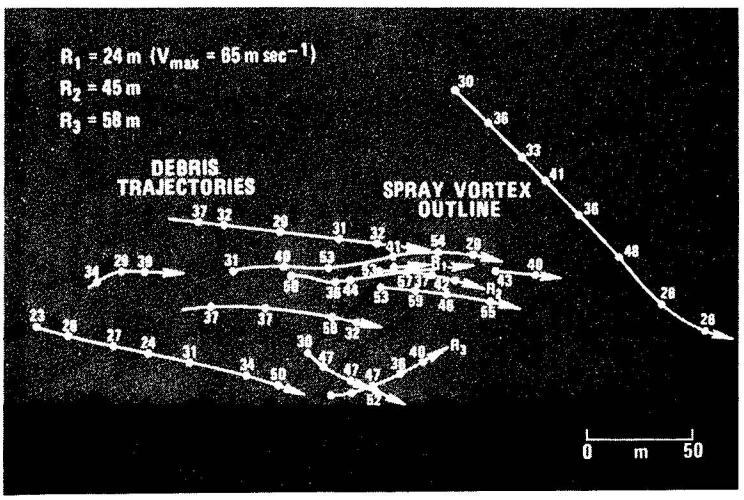

Figure 25. Cross section in x', z plane showing debris particle trajectories and photogrammetric windspeeds, when tornado was SE of Union City (4-5 km ENE of NSSL intercept vehicle). Outline of spray vortex is shown, distance scale is at lower right, and those trajectories for which distance determination was possible are listed in upper left. After Golden and Davies-Jones (1975).

[9]The rotational wind component is the horizontal wind vector relative to the vortex, rather than the ground.

Using representative maximum windspeeds and estimated radii from Figs. 23 and 25, we computed the circulation in the tornado's debris cloud before and after it passed through Union City. The circulation values obtained were 100 x 10^3 and 10 x 10^3 m^2 s^{-1}, respectively. For comparison, Hoecker's (1960a,b) data indicates that the circulation of the 1957 Dallas tornado was 19 x 10^3 m^2 s^{-1}. The large circulation west of Union City is due principally to the large vortex width at this stage. The circulation in the upper peripheral cloud tags around the tornado funnel decreased when the tornado was small, southeast of Union City, to 28 x 10^3 m^2 s^{-1}, or one-fourth of the cloud-tag circulation computed when the tornado was much larger west of Union City. Larger circulation values of 7 x 10^4 to 35 x 10^4 m^2 s^{-1} were measured on a larger scale within the tornado's parent mesocyclone by Doppler radar (Lemon et al., 1978).

4.2.3 Salina, Kansas tornado - September 25, 1973

Zipser (1976) performed a photogrammetric analysis of an eyewitness movie of the 25 September 1973, Salina tornado. By tracking cloud tags, funnel perturbations, and debris aggregates rotating around the tornado funnel at various radii and elevations, he obtained photogrammetric windspeed measurements at several different times during the Salina tornado's lifecycle. Maximum horizontal velocities in cloud tags were about 49 m s^{-1} at an elevation of 350 m and a radius of 200 m; maximum vertical velocities were 45 m s^{-1} at z = 700 m, R = 350 m. Maximum net windspeeds in the debris cloud were reported by Zipser to be about 69 m s^{-1} at z = 70 m, R = 114 m; maximum vertical motions in the debris cloud were +31 m s^{-1} at z = 125 m, R = 100 m. However, because two separate dust aggregates were mistakenly identified and tracked as one, Zipser's maximum wind speed, also reported by Golden, (1976c), was subsequently found to be too high. The revised maximum measured windspeed is 59 m s^{-1}.

4.2.4 Kailua-Kona, Hawaii tornadic-waterspout - January 28, 1971

Zipser (1976) also performed a detailed photogrammetric wind speed analysis of a large tornadic waterspout, which swept ashore on the coastline of Kona, Hawaii on 28 January 1971. The large waterspout developed a few kilometers offshore from Kona and moved northward, making landfall in the main business district of Kona. Zipser tracked spray aggregates and large debris elements visible in an eyewitness movie a few seconds after the vortex made landfall. There were many discrete elements of debris which were rapidly produced from many buildings in the downtown section of Kona. The derived debris trajectories indicate that most of the large debris was generated in a shallow region of inflow accelerating into the vortex from its right rear-side. The maximum measured velocity was 56 m s^{-1} at z = 38 m. The photogrammetric windspeed estimates above the spray vortex region of the Kona waterspout could not be obtained because of the lack of suitable tracers around the upper portion of the funnel. Note that the maximum vertical and net velocities in the Kona waterspout's spray vortex shortly after landfall were comparable to those of the Salina tornado's debris aggregates. Additional details of the flow structure in the Salina tornado and Kona waterspout are given by Zipser (1976).

4.2.5 Xenia, Ohio Multivortex tornado - April 3, 1974

One of the largest, most intense, destructive tornadoes of the massive 3-4 April 1974 outbreak struck the heart of Xenia, Ohio. Fortuitiously, an outstanding super-8 movie was taken by an eyewitness, Mr. Bruce Boyd, as the tornado was moving northeastward through the Arrowhead subdivision of Xenia, where many

houses were destroyed or literally blown away. Throughout Mr. Boyd's film coverage there was no evidence of the condensation funnel reaching the ground. Instead, the huge vortex was characterized by an evolving series of 2-6 "suction vortices." Individual vortices tended to form rapidly in the right-rear quadrant of the parent vortex, accelerate around the vortex in the direction of storm translation and weaken as they moved into the left-front quadrant. This evolution of suction vortex intensification, acceleration and decay occurred in completely different regions of the parent vortex than in a different tornado investigated by Agee et al. (1975).

Golden and Purcell (unpublished work) performed a photogrammetric analysis of the Xenia tornado movie, using detailed angular measurements of landmarks from a photographic site survey conducted by Texas Tech Institute for Disaster Research. This work was done independently of Fujita's (1975) analysis of the same movie. During most of the Boyd film sequences subjected to analysis, the tornado was composed of a series of writhing, serpentine vortex condensation filaments. These often became greatly tilted above 30 m elevation, in a sense opposite to their rotation about the parent vortex. During a short sequence of the Boyd movie, two intense "suction vortices" rapidly developed in the southeast quadrant of the parent vortex. The trailing "suction vortex," apparently at a larger radius than the first within the 220 m diameter boundary of the dust vortex, accelerated and overtook the first. The translational speed (relative to the ground) of the trailing "suction vortex" as it overtook the first was 70 m s^{-1} at about 75 m elevation (true radius was indeterminate). This value compares well with Fujita's (1975) tangential speeds of dust aggregates at similar elevations. The translation speed of the parent Xenia tornado vortex was 12 m s^{-1} (8 m s^{-1} across the film plane) during the filming sequence; this value was computed photogrammetrically by Golden and Purcell and is considerably smaller than that used by Fujita. Golden and Purcell found a maximum net velocity of 95 m s^{-1} at 200 m elevation in the Xenia tornado. The corresponding horizontal and upward windspeed components were 85 m s^{-1} and 41 m s^{-1}, respectively. Since the tornado's translation velocity in the film plane (8 m s^{-1}) was directed in the opposite direction to the maximum, ground-relative, horizontal wind velocity, the maximum rotational velocity was 93 m s^{-1}.

Golden and Purcell emphasized that the apparent debris motion in the Xenia tornado was strongly asymmetric with respect to azimuth (θ). Since Fujita's (1975) "off-center correction" requires axisymmetry (and also that all the debris lies at a constant radius from the axis), his deductions of tangential and radial wind speeds from the measured horizontal tracer speeds in the object plane appear questionable. Note, also, that his derived windfields do not appear to satisfy mass continuity.

Golden and Purcell also found that large debris elements the size and shape of rooftops (30 m) were centrifuged out of the vortex at low levels (30-40 m). Horizontal speeds of 60-70 m s^{-1} well outside the main debris cloud of the tornado (at $r \geq 100$ m) were obtained by tracking these large debris elements.

4.2.6 Great Bend, Kansas Tornado - August 30, 1974

Late in the afternoon of 30 August 1974, at least 12 tornadoes within a 65 km radius of Great Bend, Kansas were photographically documented during a two-hour period by a newsphotographer, Mr. Robert Dundas. All of the tornadoes except the first traveled toward the southeast. Dundas recalled that most of these tornadoes were first visible as a large intense dust whirl at the ground, with a very short

pendant at cloudbase (estimated at 1500 m MSL). In each case, dust spiralled helically upward to form a tall column, which, in the weaker vortices, became hollow at mid-levels. One of the largest and best-documented tornadoes occurred about 40 km west-southwest of Great Bend (Golden and Purcell, 1975, 1977). After approaching the fully developed tornado from the east, Dundas was able to position himself 2.7 km north of the vortex, which was receding slowly east-southeastward. High contrast, high resolution movies obtained by Dundas show the lower vortex column in remarkable detail. A subsequent site survey with the photographer revealed that the tornado passed through a dry maize field during the filming. The vortex was visible as a sloping, rotating column of dense dust and small debris particles.

A remarkable new finding on tornado boundary layer structure was a dark band of dust, about 35 m high, which extended into the vortex column's base from the west-southwest. The general flow along the dust band is illustrated by the trajectory in Fig. 26a. A more detailed view of the dust column's lowest 150 m with the dust band structure and photogrammetrically-derived flow trajectories is given in Fig. 26b. The large dust turret in the upper right was one of several which were centrifuged outward, began to sink and were rapidly drawn back into the vortex by strong low level inflow.

The dust band apparently outlined a major confluent inflow band of air accelerating into the vortex at low levels. Horizontal wind speeds near tree top level in the dust band increased from right to left in Fig. 26b, from about 25 m s^{-1} at 120 m outward from the vortex edge to 50-55 m s^{-1} for points within 16 m of the vortex edge. Photogrammetric analysis of a movie sequence preceding Fig. 26 indicates a thicker dust band, 75 m high, with larger rising motions increasing from 10 m s^{-1} at 225 m to 20 m s^{-1} at 20 m from the vortex column edge. Horizontal wind speeds increased rapidly inward along the dust band from 20 m s^{-1} to 50-60 m s^{-1} within 75 m of the vortex column edge. The dust band has appeared in a few other tornado photographs (e.g., those in Kessler, 1972), but its relationship to the vortex boundary layer flow structure has not been stressed. The dust band denotes

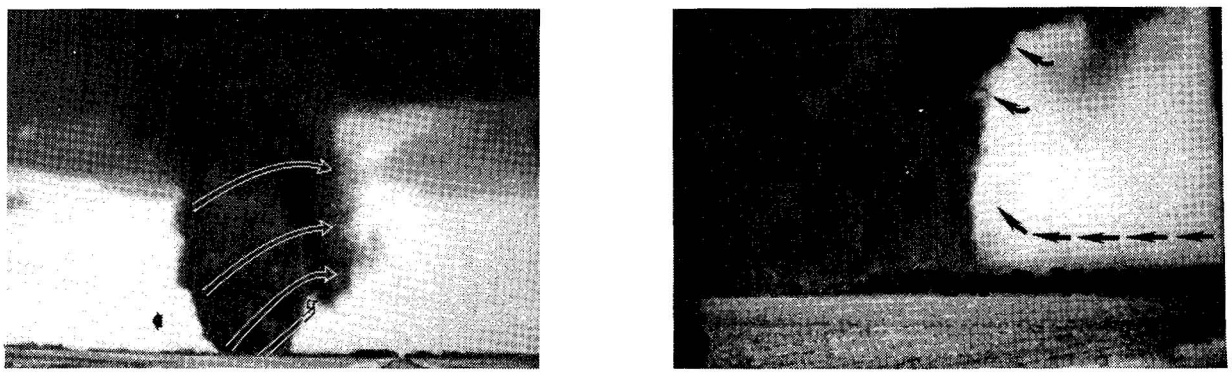

(a) *(b)*

Figure 26. (a) Enlarged movie frame of Great Bend tornado, looking south, with schematic debris aggregate trajectories superimposed. Tornado was moving east-southeast (bold arrow). (b) Enlarged frame from zoom movie sequence, illustrating asymmetric flow features in lower vortex region. Note concentrated dust band extending into vortex column base from the right (west-southwest). Schematic trajectories of flow in dust band and centrifuged dust turret are superimposed. (After Golden and Purcell, 1975, 1977.)

an inflow band of damaging winds, which extends outward from the edge of the tornado's debris cloud for considerable distance. Its existence reveals that tornado inflow can be markedly asymmetric.

Two scaled outlines of the tornado's dust column, with superimposed vertical distribution of photogrammetric velocity components, are given in Fig. 27. Wind speeds could be obtained only in the outer portion of the dense dust column outside the vortex core. Maximum measured net velocities there were at least 85 m s^{-1} at 80 m AGL. The corresponding radius was 150 m. Moreover, net velocities at 60-80 m s^{-1} were commonly found in the region 50-100 m AGL. Horizontal wind speeds increased rapidly with height from 40-50 m s^{-1} at treetop level to at least 75 m s^{-1} at 80-100 m AGL. Horizontal wind speeds decreased with height above the level of the maximum to 45 m s^{-1} at 205 m AGL and 30 m s^{-1} at 560 m AGL (Fig. 27a).

Rising motions increased very rapidly with height above treetop level to 60 m s^{-1} at 60 m AGL (Fig. 27b), implying upward accelerations of 3 g in the lowest 60 m. Such large vertical accelerations obviously obviate the hydrostatic assumption in modeling the lower vortex column. Maximum rising motions tended to occur at levels lower than maximum horizontal windspeeds. Although most

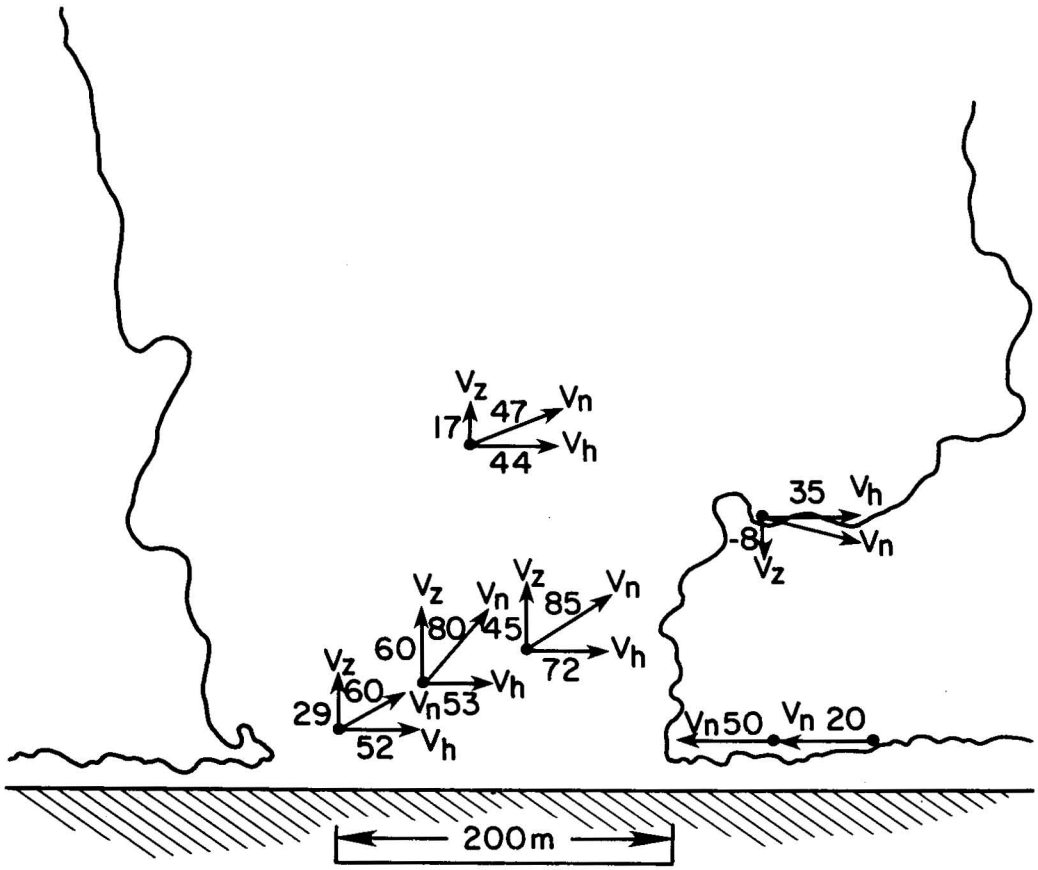

(a)

Figure 27. Scaled outlines of Great Bend tornado's dust column at two slightly different times, (a) and (b), with representative net, horizontal and vertical velocity vectors (units of m s^{-1}) superimposed. Velocities were derived photogrammetrically, as described in text. Compare with Fig. 26. (After Golden and Purcell, 1975, 1977.)

of the windspeed data were obtained by tracking dust-cloud turrets, somewhat larger rising motions were found in the darker recesses (folds) of the turbulent dust column (see Fig. 26b). Rising motions decreased rapidly with elevation above 100 m AGL to 15-25 m s^{-1}; moreover, at these heights, largest values tended to occur on the left (east) of the vortex column with weak sinking motions on the right (west) side. These vertical motion patterns shifted around the vortex column during other mature stage times.

Golden and Purcell (1975, 1977) concluded that the Rankine-combined vortex model and cyclostrophic flow assumption are not valid for the lowest 200 m of the Great Bend vortex column because of (non-steady) azimuthal asymmetries in both horizontal and vertical flow. The periodic changes of position of the asymmetric features occur on time scales of minutes, and do not appear rapid enough to allow these features to be treated as turbulent fluctuations superimposed on a basic, symmetric, steady vortex flow. Note that there was no evidence of suction vortices in either the damage survey or in the tornado movies.

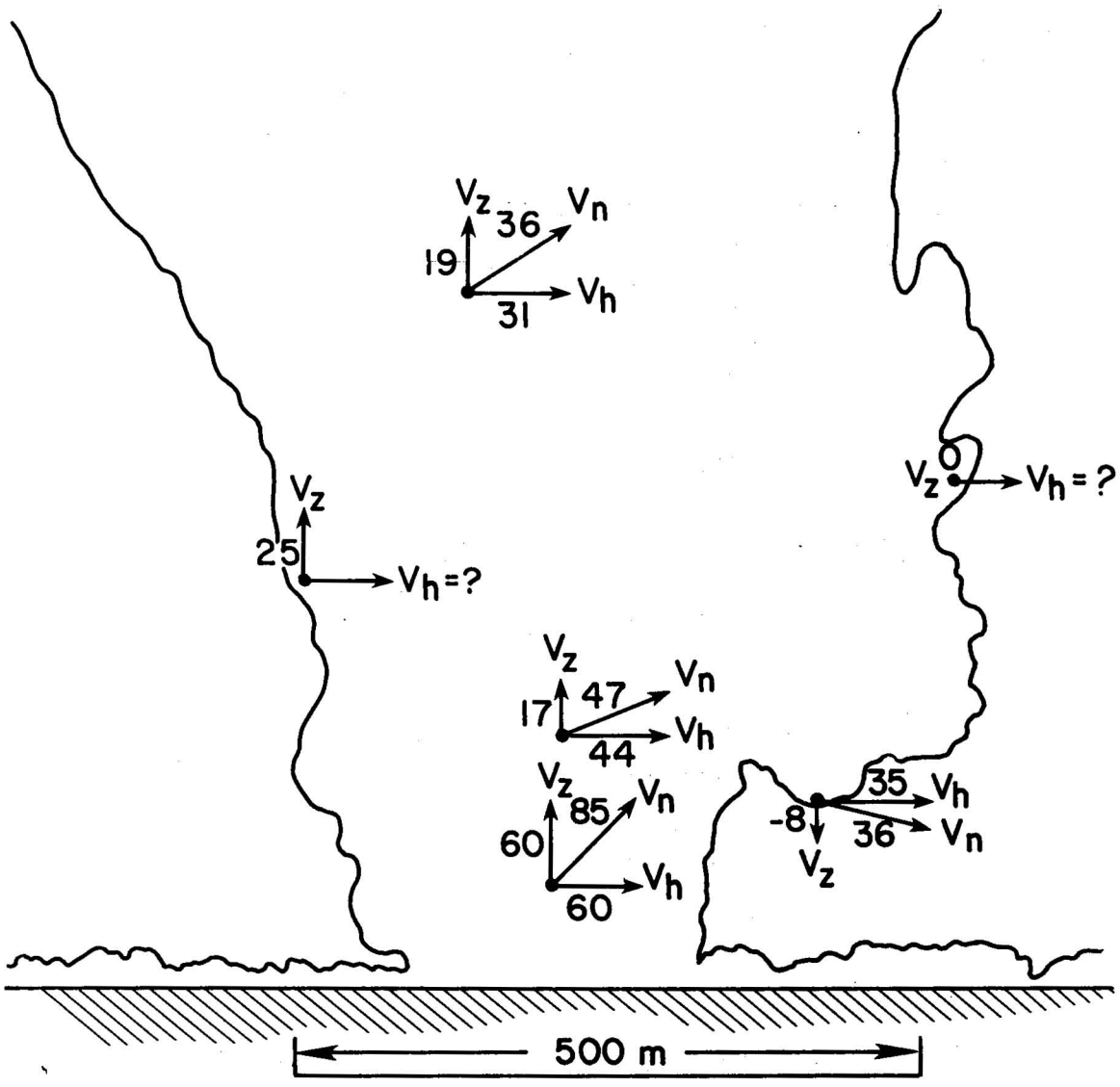

(b)

4.2.7 Alva, Oklahoma Anticyclonic Tornado - June 6, 1975

Just before 1900 CST, 6 June 1975, an anticyclonic tornado was documented by super-8 motion picture photography in northwestern Oklahoma by two students from Florida (Leonard and Sims), who were chasing storms as a hobby but were receiving guidance from NSSL (Burgess, 1976a). The anticyclonic tornado was observed on the right rear flank of a right-moving severe thunderstorm, which also produced two cyclonic tornadoes in the same general vicinity. The anticyclonic tornado was visible as a condensation funnel, which extended partway to the ground, and a surface-based dust cloud, which contained smaller embedded vortices (dust whirls) within it. Photogrammetric analysis of this movie was never completed because of significant uncertainties of the damage path location and subsequent uncertainties in the measured wind speeds. However, we now believe that the preliminary results of 60-70 m s^{-1} at low levels reported by Golden (1976c) are probably too high.

4.2.8 Seymour, Texas Tornado - April 10, 1979

On 10 April 1979, a large tornado was photographed near Seymour by the NSSL 2 Chase Team and by Mr. Gene Moore, who was working for NSSL under contract. Two excellent close range movies were obtained from different vantage points, and photogrammetric analyses are currently underway. Several smaller vortices rotating around the main funnel are visible in the movies. Preliminary results indicate that maximum wind speeds in Moore's movie (~90 m s^{-1} at 30 m AGL) are considerably in excess of the F2 rating given this tornado on the basis of damage assessments. Furthermore, the maximum wind speed in the NSSL 2 movie (77 m s^{-1} at 15 m AGL) occurred at a point in the tornado's path where the damage rating was F0. The wind speeds quoted in this case pertain to the ground-relative translation speeds of small suction velocities which revolved around the base of the main funnel at 80 m radius. Tornadoes which occur in open country, like this one, tend to be given low F scale ratings because of the lack of structures and tall vegetation in their paths. When F numbers are assigned to different segments of damage tracks, they often appear to escalate whenever the path crosses an urban area.

The parent storm of the Seymour tornado later spawned the infamous Wichita Falls tornado.

4.2.9 Orienta, Oklahoma Multivortex Tornado - May 2, 1979

In contrast to the Seymour tornado, this multivortex tornado did not have a primary funnel during the time when the main movie sequence was taken by the Oklahoma University chase team. Instead, it consisted of a series of suction vortices which tended to form on the front side of the parent circulation and decay on the back side. The sporadic nature of the new vortex formation gives the impression that the tornado was "leap frogging." The serpentine appearance of the vortex filaments, which at times wrapped around each other in pairs, make this movie extremely fascinating. Many wind speed estimates are in the neighborhood of 65 m s^{-1}, and one suction vortex had a translation speed of 76 m s^{-1} at 50 m AGL.

4.2.10 Conclusions

The highest wind speed measured thus far by NSSL is the 95 m s^{-1} net velocity measured at 200 m AGL in the Xenia tornado. Speeds almost as fast have been measured at much lower heights (15 to 50 m) in movies taken by the Tornado Intercept Project (see Table 3). Note that wind speeds measured photogrammetrically may be somewhat lower than actual maximum wind speeds because (i) the velocity component

along the camera axis is not measured (see Section 4.2.1), (ii) differences may exist between tracer motions and actual air motions, (iii) the locus of maximum winds may lie within an opaque dust column or in a region devoid of tracers, and (iv) the tangential wind velocity around suction vortex axes often can not be resolved.

In all tornadoes investigated, the highest measured tangential velocities have been within the lowest one to two hundred meters above ground. In the Great Bend tornado, upward speeds of 60 m s^{-1} at 60 m above ground were detected, implying upward accelerations of 3 g in the lowest 60 m. These rising motions decreased rapidly with elevation above 100 m, possibly in association with a vortex breakdown (Lewellen, 1976). Another feature of the Great Bend tornado was a band of dust which flowed rapidly along the ground into the vortex. Speeds of 50 m s^{-1} were measured near the tornado in this inflow. The presence of this dust band suggests that the low-level inflow into tornadoes is concentrated in a spiral jet rather than being axisymmetric. Similar bands have since been noted in other tornadoes.

Asymmetries in the vertical velocity fields around the funnel have been observed. Typically, cloud elements on the right-rear side of the tornado sink and evaporate whereas fractus clouds, spiralling in towards the funnel on the left front side, rise rapidly (Fig. 28). These observations have important implications for tornado theories (Lemon and Doswell, 1979). The observed asymmetries in vertical velocity may be associated partly with the tornado's tilt and partly with the slow intrusion of a rear flank downdraft into the vortex's circulation.

The Union City tornado was filmed as it evolved through its life cycle. Maximum rotational wind speed decreased from 80 m s^{-1} in the mature stage to 65 m s^{-1} in the shrinking stage. The major change between the two stages was the much smaller radius of maximum winds in the shrinking stage (25 m compared to 200 m), implying a significant decrease in circulation.

4.3 Other Experiments and Studies

4.3.1 Proposed Methods To Measure Tornado Parameters

Several methods, other than simple photogrammetry and fixed Doppler radar, have been proposed for measuring tornado parameters. These involve stereo photogrammetry, airborne Doppler lidar, remotely piloted vehicles, portable K band Doppler radar, instrumented toy rockets, special cameras to detect electrical glows around tornadoes, and instrument packages to be placed in the path of an approaching tornado.

NOAA's Wave Propagation Laboratory has developed a portable CW Doppler Lidar system with the capability of remote velocity measurement in small scale atmospheric vortices (Schwiesow and Cupp, 1976). This system has been used to measure dust devil winds from a land vehicle and waterspout velocities from an airplane (Schwiesow *et al.*, 1977). A tornado field program has not been undertaken yet owing to lack of sufficient funds. Because tornadoes in Oklahoma are a hundred times less frequent than waterspouts in the Florida Keys, and because they are not as easily approached, a successful lidar field experiment on tornadoes would require considerable flying time and an increase in the lidar's present range (1 km) to about 5 km.

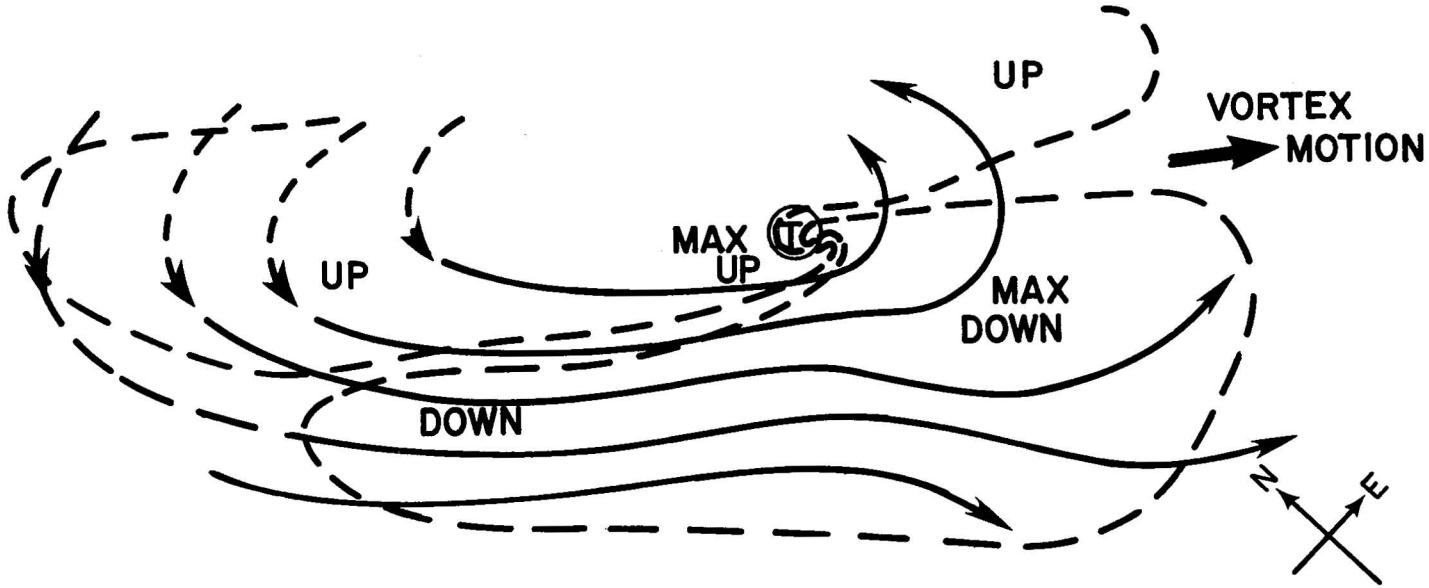

Figure 28. Schematic plan view of horizontal streamlines (solid lines) and low-level vertical motion patterns (dashed lines) around the decaying Union City tornado, deduced from photogrammetric analysis of debris motion and surface damage surveys (from Golden and Purcell, 1978b).

The feasibility of using a portable K band Doppler radar to measure tornado wind speeds has also been discussed by NSSL staff. To develop such a radar in-house would be very expensive, and an off-the-shelf radar would not meet required specifications.

A comparison of three different methods (photogrammetry, Doppler lidar, portable Doppler radar) for measuring tornadic wind speeds is interesting. The Doppler sensors measure velocity directly, whereas the photogrammetric technique depends on the determination of range from a damage survey (so that angular velocity can be converted into linear velocity) and on the differentiation of a distance-time graph. All three methods require close range approaches to tornadoes. In contrast to the other two systems, the Doppler radar has poor angular resolution, and hence broad Doppler spectra must be analyzed to estimate the extreme wind speeds within the sampling volume. Return from the highest speed targets may be indistinguishable from noise. The Doppler radar does have the advantage of less attenuation; thus, it can sense regions hidden from view of the eye, camera and lidar. The lidar is range limited because of attenuation; this is its biggest drawback. It has excellent angular resolution and holds an advantage over photogrammetry in its ability to measure speeds in "homogeneous media", such as smooth funnel walls. Photogrammetry requires the tracking of identifiable features. Note that the lidar and photogrammetry are complementary techniques in the sense that the lidar measures longitudinal (line of sight) velocity, photogrammetry the other two (i.e., transverse) components.

Current plans are to deploy a tornado-resistant instrument package, designed by Dr. Bedard (WPL[10]) to measure temperature, pressure, wind and electric corona current, in front of mesocyclones and tornadoes during future Spring Seasons.

The other methods proposed involve measuring variables other than wind. S. Colgate is developing tiny rockets, instrumented to measure temperature, pressure and electrical parameters, which can be fired through tornadoes from an airplane. NSSL is assisting Colgate during the field part of his program.

A team from the Argonne National Laboratory visited NSSL during the 1976 Spring season to attempt to launch a remotely piloted vehicle (RPV) into a tornado. Their intention was to introduce tracer material into the vortex and to measure its subsequent dispersal. No tornadoes were observed during the short time that the team was in Oklahoma.

Intercept teams have taken into the field a special cine super-8 sound camera with an optical lightning detector (photocell) mounted on top (Vonnegut and Pasarelli, 1978). The photocell's output is recorded on the camera's audio track. This special camera is designed to detect lightning or electrical glows which are too faint for the eye or camera to detect. The goal of collecting data on a tornado was accomplished on 10 April 1979 (Seymour, Texas tornado). Unfortunately, the camera's internal circuits generated noise on the audio track, and spectral analysis will have to be performed to separate this noise from any effects due to electrical activity in and around the tornado. In the meantime, attempts will be made to repeat the experiment, using an improved version of the camera.

---

[10]Wave Propagation Laboratory, ERL, NOAA, Boulder, Colorado.

4.3.2 Dryline Storms

Supercell storms have long been recognized as prolific producers of severe weather. Studies at NSSL have revealed a new type of severe storm which appears innocuous on radar, but which can be quite damaging. The "dryline" storm is a particularly distinctive unicellular storm which has been identified recently (Davies-Jones et al., 1976; Burgess and Davies-Jones, 1979). As the name implies, this type of storm is found near a dryline; however, most storms that form close to a dryline are not of this type. "Dryline" storms have small, weak, low-level radar echoes and appear deceivingly benign on radar. They have large intense updrafts at the storm rear, in some cases even behind the low level radar echoes. They generally travel in the direction of, but slower than, the mean wind. This type of storm contains a wide rotating updraft, so intense that most of the precipitation is carried downstream in the anvil rather than falling back through or out of the updraft. Hail and large raindrops falling from the downshear anvil reach the surface ahead of the main storm tower (the smaller drops evaporate while descending). Since precipitation does not fall out of the updraft into mid-level dry air entering the storm from the rear, cold air outflow at the surface is absent. The updraft may be either erect or tilted downshear. This storm type has a low precipitation efficiency and produces large hail, funnels, and minor tornadoes, but rarely (if ever) major tornadoes. To date, all "maxi"-tornadoes observed have formed from supercells, not from "dryline" storms.

4.3.3 Updraft Soundings

Davies-Jones (1974) and Davies-Jones and Henderson (1974, 1975) analyzed the data from NSSL mesonetwork upper air soundings which sampled thunderstorm updrafts. The four fastest updraft cases were associated with severe storms, and in one case the balloon entered a cell which had just produced a tornado. The conclusions from these investigations were that (i) strong updrafts have cores that are virtually undiluted, at least up to mid-levels, (ii) the vertical perturbation pressure gradient force usually acts in the opposite direction to the buoyancy force, (iii) although updrafts are warm core at mid- and upper-levels, air rising into the updraft at cloud base is often negatively buoyant and is moved upward, presumably, by the perturbation pressure gradient force, (iv) updraft speed is positively correlated with the relative warmth of the core and with the potential wet-bulb temperature, which is a measure of the static energy content of the air, (v) the average horizontal winds measured in the updraft and storm environment agree with conceptual Great Plains thunderstorm models, especially with regard to the weaker vector wind shears and more southerly winds in the updrafts.

These empirical findings are important because they confirm previous speculations on thunderstorm structure and because they provide verification for numerical models of severe storms. Simulation of rotating thunderstorm cells is necessary for realistic numerical studies of tornadogenesis (Smith and Leslie, 1979).

4.3.4 Study of Central Iowa Tornadoes - June 13, 1976

On 13 June 1976, an outbreak of tornadoes occurred near Ames, Iowa. Of particular interest was the existence of a pair of tornadoes, one cyclonic (F5) and the other anticyclonic (F3). The anticyclonic tornado formed 3 km SSE of the cyclonic one, and the tornadoes followed parallel, cycloidal tracks. Brown and Knupp (1980), with NSSL support, collected storm photography, conducted damage surveys and examined available rain gage and radar data (the tornadoes passed

through a rain gage network). The cyclonic tornado formed before and outlived its anticyclonically partner, and was the more intense vortex. At times, this tornado appeared to exhibit a vortex breakdown (see Section 5.3.1). Radar showed a cyclonic hook echo in the vicinity of the tornado pair. Such a vortex pair may be produced by an updraft drawing up a loop of an initially horizontal vortex tube, or by an updraft concentrating the cyclonic and anticyclonic shear vorticity on the right and left sides, respectively, of a low-level band of strong winds sweeping around a mesocyclone.

4.4 NSSL Tornado Damage Surveys

4.4.1 Objectives

The objectives of damage surveys were as follows:

(a) To determine damage paths from beginning to end.

(b) To determine the times that damage occurred at different points along path.

(c) To ascertain the severity and nature of damage to buildings, structures, trees and crops.

(d) To obtain photography (particularly close range movies) and tape recordings of tornadoes.

(e) To relate damage severity, path width and debris configurations to life cycle of damaging phenomenon (tornado, gustfront, hailswath).

(f) To position the tornado relative to the overall storm, hailshafts, rainshafts, lightning centers, gust fronts and cloud configurations.

(g) To document evidence of heavy missiles generated by the wind.

(h) To deduce tornado flow features near ground.

4.4.2 Procedures

4.4.2.1 Telephone Survey

Immediately after receiving first reports of damage within the domain of NSSL Operations from TV, NWS, Doppler radar signature, field teams, etc., a preliminary telephone survey was conducted to establish the extent and severity of damage. If warranted by the reports, the following day's operations were suspended and a command post in the NSSL Conference Room readied for briefing one to eight survey teams early the next morning for rapid dispersal to the damage area(s). They were briefed on the damage reports, given area assignment, maps, questionnaires and general instructions.

4.4.2.2 Notifying Engineers

The Institute for Disaster Research at Texas Tech University was notified immediately if there were confirmed reports of

(i) damage to the frames of engineered structures,

(ii) heavy missiles generated by the wind,

(iii) extensive damage to schools,

(iv) water loss (or lack of) from swimming pools, wells, ponds, etc., lying in a tornado path.

4.4.2.3 Aerial Surveys

Aerial surveys afforded the best overall perspective of entire damage tracks and revealed damage patterns not readily discernible to ground personnel. Private plane or helicopter overflights were conducted early the next day (before the debris had been cleaned up and rearranged). The crew generally consisted of four people, a pilot, a plotter who recorded the plane's track and damage locations on a sectional map, and two photographers equipped with 35 mm SLR cameras and normal and wide angle lenses.

Aerial photography proved to be tricky. The best results were obtained with the lens aperture nearly wide open (stopped down about two stops to enter the aperture range where the lens performed the best) and the exposure adjusted by varying the shutter speed. This way, the shutter speed was the fastest which conditions allowed. Exposures were bracketed (stopped down by 0 to 1-1/2 F stops) because light scattered by haze and other factors often caused the light meter to read too low. The haze problem was worst when taking photographs into the sun (i.e., for backlighting). Lens shades and haze filters helped to increase photographic contrast by reducing effects of lens flare and poor visibility. High resolution, intermediate speed, color film was used. Photographs from a helicopter were best taken when it was moving forward because hovering set up fairly severe vibrations. Color infra-red photography was tried without much success.

Flights criss-crossed the damage path because ground marks in fields were sometimes only visible when viewed from certain sun angles (e.g., when looking toward the sun). Flights were made at variable heights, with the highest at a few thousand feet to afford a comprehensive view of the track and the lowest at a few hundred feet to maximize details. The aircraft crews radioed back their initial findings to the command post for relay to the field crews via radio or phone.

All photographs were documented by photo number, subject, plane location, height and camera orientation. A tape recorder was taken along for logging this information as well as flight paths, general observations, etc. The aerial surveys were used for

(i) locating damage tracks and determining number of tracks.

(ii) mapping the total extent of all tracks.

(iii) discovering debris patterns and ground marks not readily discernible from the ground, e.g., suction swaths, fan-shaped diffluent or confluent patterns evident in downed wheat or fallen trees,[11] tornado tracks within swaths of straight line wind damage, etc.

---

[11] Diffluent and confluent patterns do not establish actual flow diffluence and confluence unless the objects were all felled simultaneously.

(iv) obtaining high-quality aerial photographs.

(v) assessing the intensity of the wind damage, and how intensity and debris configurations varied along and across the path. The variation of path width with distance along the track was also noted.

(vi) assessing the best locations for concentrated analyses by the ground teams.

4.4.2.4 Ground Surveys

Ground surveys revealed the extent of the damage, often not fully apparent from the air, and, in some cases, were required to confirm tornado paths which were not visible from an airplane. They also provided detailed information. Each ground survey team was equipped with maps, 35 mm cameras, rolls of color film, tape recorders, notebooks, pencils, questionnaires, government I.D. cards and boots (for protection against stepping on nails).

(i) Teams, which were going to restricted areas, obtained passes from the local law enforcement agencies. At this time, they contacted the local Civil Defense to pinpoint the time of the event and to ascertain an approximate track by talking to local officials. They also inquired whether there was any peripheral damage outside the main track. Street maps were obtained if available.

(ii) Contact with the local media was found to be helpful. They generally publicized NSSL's request for movies, still photographs and tape recordings of tornadoes. One team was assigned to make this contact.

(iii) Each team was responsible for obtaining data on the following in its assigned area:

(1) maximum damage severity, using the Fujita (F) scale as a guide (Fujita, 1971), and path width.

(2) damage variations across and along path.

(3) path width variation along path.

(4) nature of damage to buildings, trees, crops, etc. (The type of building construction was also noted.)

(5) objects which survived the winds relatively unscathed, although in midst of severe damage (e.g., water towers frequently withstand a tornado).

(6) the extent of damage to any engineered structures or schools in path.

(7) any evidence of tornado skipping.

(8) water removal (or lack of it) from swimming pools, wells, ponds, etc., in path of a tornado.

(9) evidence of buildings exploding in a tornado due to sudden drop in atmospheric pressure (all walls are blown outward by explosion whereas wind action, a far more common damage mechanism, causes the windward wall to fall inward).

(10) the variation of damaging wind direction across path at various locations along path. Methods for identifying wind directions are listed in Davies-Jones et al., 1978. For tornadoes, it was noted in particular if the vortical nature of the winds were evident, or if the tornadic winds appeared to have blown predominantly from one direction. If signs of circulation were obvious, rotation (cyclonic or anticyclonic) was noted. Twisted trees and houses rotated on their foundations were not used as indicators of the sense of rotation, but curvature in the "bounce marks" of heavy objects hurled by the winds was a reliable sign.

(11) Evidence of tornadic winds changing with height in the lowest few meters (see Davies-Jones et al., 1978).

(12) Heavy objects displaced by the wind. The final location of the object, point of origin (if this could be determined) and manner in which the object was moved (e.g., dragged, bounced, airborne, etc.) were logged. Also, potential missiles which were not dislodged by the wind were noted, and instances of bent steel such as trailer frames wrapped around telephone poles were documented.

(13) Missile penetrations such as straws driven into utility poles, wooden boards through house walls, etc.

(14) Any signs of scorching or dehydration produced by a tornado.

(15) Any microscale debris patterns and ground marks apparent in the fields (e.g., patterns described in Fujita et al., 1967, and Davies-Jones et al., 1978, also "suction" holes "dug" by tornado, and "stepping spots" where a small scale, stationary whirlwind appears to have acted).

(16) Relationship between damaging phenomenon and other storm features (established by eye witness interviews, see questionnaire in Fig. 29). Special efforts were made to find out the names and phone numbers of people who took close range tornado movies.

(iv) Each team noted the location of each observation, and recorded identification number, subject, location and camera orientation for each photograph. It also logged its route through the damage area.

4.4.2.5 Debriefing

A debriefing was conducted the day after the survey and the data was assessed. Each team prepared cleaned-up copies of their notes. Secondary surveys were conducted to fill in missing data or extend the initial survey as needed.

Fig. 29 NSSL Questionnaire Used on Damage Surveys.

Type of severe weather observed (tornado, windstorm, hailstorm, etc.)_____

_____

_____

Date of Survey_____ Date of Storm_____

Name_____ Sex____ Approx. Age_____

Address_____

_____

Phone No._____

Location at Time of Storm_____

HAIL

1. Did it hail at your location? Yes____ No____
   If no, go to question 10.

2. Time hail began:_____ a.m.____ p.m._____

3. If it hailed, would you classify the hailfall as

   heavy_____ moderate_____ light_____

4. Hail fell for _____minute(s).

5. What was the size of the largest hailstone (diameter in inches)?

   1/4 (pea)_____ 3/4_____ 1-1/2 (golfball)_____

   1/2 (marble)_____ 1 (walnut)_____ 2 or more _____

   If 2 or more, please specify exactly how large_____.

6. (a) Did the largest hailstones fall

   before smaller ones_____ after smaller ones_____ at same time as smaller ones_____

   (b) Did the hail fall

   before rain_____ after rain_____ at same time_____ no rain fell_____

7. What percentage of the ground was covered by hail?_____

8. Did you store any hailstones in your freezer, yes_____ no_____
or take photographs of the stones? yes_____ no_____

9. Was there anything unusual about the hailstones (e.g., unusual shapes, spiky surface, stones broke apart on impact, etc.)?

STRAIGHT LINE WINDS

10. Were there damaging straightline winds (i.e., winds not associated with a tornado) near your location? Yes_____ No_____

If no, go to question 15.

11. Time of damaging winds:_____ a.m._____ p.m._____

12. Wind damage was to: trees_____ buildings_____ crops_____

13. Describe wind damage (e.g., broken tree limbs, trees uprooted, concrete block wall collapsed,...)

14. From which direction did the damaging winds blow N, NW, W, SW, S, SE, E, NE (circle one)?

Tornado

15. Did you observe or experience a tornado? Yes_____ No_____
If no, go to question 33.

16. Time of tornado(es):_____ a.m._____ p.m._____

17. Number of tornadoes observed _____
Number of funnels aloft observed_____

Please describe sequence of events. Include the directions in which you saw the funnels, how each tornado formed, how it changed with time, how it decayed, etc.

18. Did you see small funnels or whirlwinds within or close to the main tornado? Yes_____ No_____

If yes, please sketch what you saw.

19. Did it hail at your location

(a) before the tornado Yes_____ No_____

(b) during the tornado Yes_____ No_____

(c) after the tornado Yes_____ No_____

20. Did it rain at your location

(a) just before the tornado Yes_____ No_____

(b) during the tornado Yes_____ No_____

(c) just after the tornado Yes_____ No_____

21. If it rained near tornado time, would you classify the rainfall as

heavy_____ moderate_____ light_____

22. Did you experience strong winds at your location?

(a) just before the tornado Yes_____ No_____

(b) during the tornado Yes_____ No_____

(c) just after the tornado Yes_____ No_____

23. Was there any damage at your location: None_____ Minor_____ Moderate_____ Major_____. Please describe nature of damage.

24. Did the winds shift near the time of the tornado? Yes_____ No_____
If yes, please describe how.

25 During the tornado were the winds at your location blowing

Toward tornado_____ Away from tornado_____ Neither_____

If neither, sketch wind direction relative to tornado.

26, Which way was the tornado rotating ?

Clockwise_____ Counterclockwise_____ Did not notice_____

(Note: for a counterclockwise tornado, you would have seen debris on right side of tornado moving away from you, and on left side moving towards you. For clockwise tornado, you would have seen the exact opposite.)

27. Did you notice a sudden cooling at your location? Yes_____ No_____
If yes and tornado was on ground, in which direction was the tornado at the time (N, NW, W, SW, S SE, E, NE) (circle one).

28. During the tornado did you hear the characteristic roar of the tornado (variously described as like very loud freight trains, jet engines, swarm of bees, etc.)? Yes_____ No_____. Or were the sounds like those normally associated with strong winds? Yes_____ No_____

29. Did you see any lightning near the tornado? Yes_____ No_____

30 Was most of the lightning

(a) near the tornado Yes_____ No_____

(b) in the darkest part (heaviest precipitation area) of the storm
Yes_____ No_____.

31. Did you see any electrical type glow in or near the tornado? Yes____ No____
If yes, please describe.

32. Where was the tornado relative to the darkest part (heaviest precipitation area) of the storm? (N, NW, W, SW, S SE, E, or NE) (circle one)

33. Did you receive a tornado warning? Yes____ No_____

34. If yes, by what means? Radio/TV____ Sirens_____ Police Car____
Other_____

35. Reaction to warning

_____ran outside to look for tornado

_____drove to community shelter

_____sought shelter inside house or cellar

---

36. Where did you take cover?

Community shelter_____ Storm cellar_____

Basement_____ Closet_____

Bathtub_____ Under heavy furniture_____

---

37. In which part of your house (if home at time) did you take cover?

____center ____corner

If corner, which one_____(e.g., SW, NE, etc.)?

38. If tornado passed directly over your location, please describe your experiences, expecially any sensations of rapid pressure and temperature changes during tornado passage.

39. Did you or anybody acquainted to you take movies, photographs or tape recordings of a tornado? Please list full particulars including names, addresses, phone numbers, etc.

40. Remarks, curious occurrences, heavy objects picked up by tornadoes, damage to structures witnessed, straw driven in tree trunk, other missile penetrations, etc.

4.4.3 Results

Since 1972, NSSL personnel have performed surveys of 92 tornado tracks in Oklahoma and Texas.[12] The tornadoes ranged in intensity from minor (F0) to devastating (F5), in width from a few tens of meters to 1.5 km, and in length from 1 to 100 km. Examination of each track ranged in scope from cursory to extremely detailed. A breakdown of these tornadoes by official F scale rating[13] is given in Fig. 30.

The primary aims of most of the surveys were to determine accurate paths and times for the tornadoes, to collect eyewitness photography, to make rough assessments of the tornadic intensity and, in some instances, to ascertain whether a

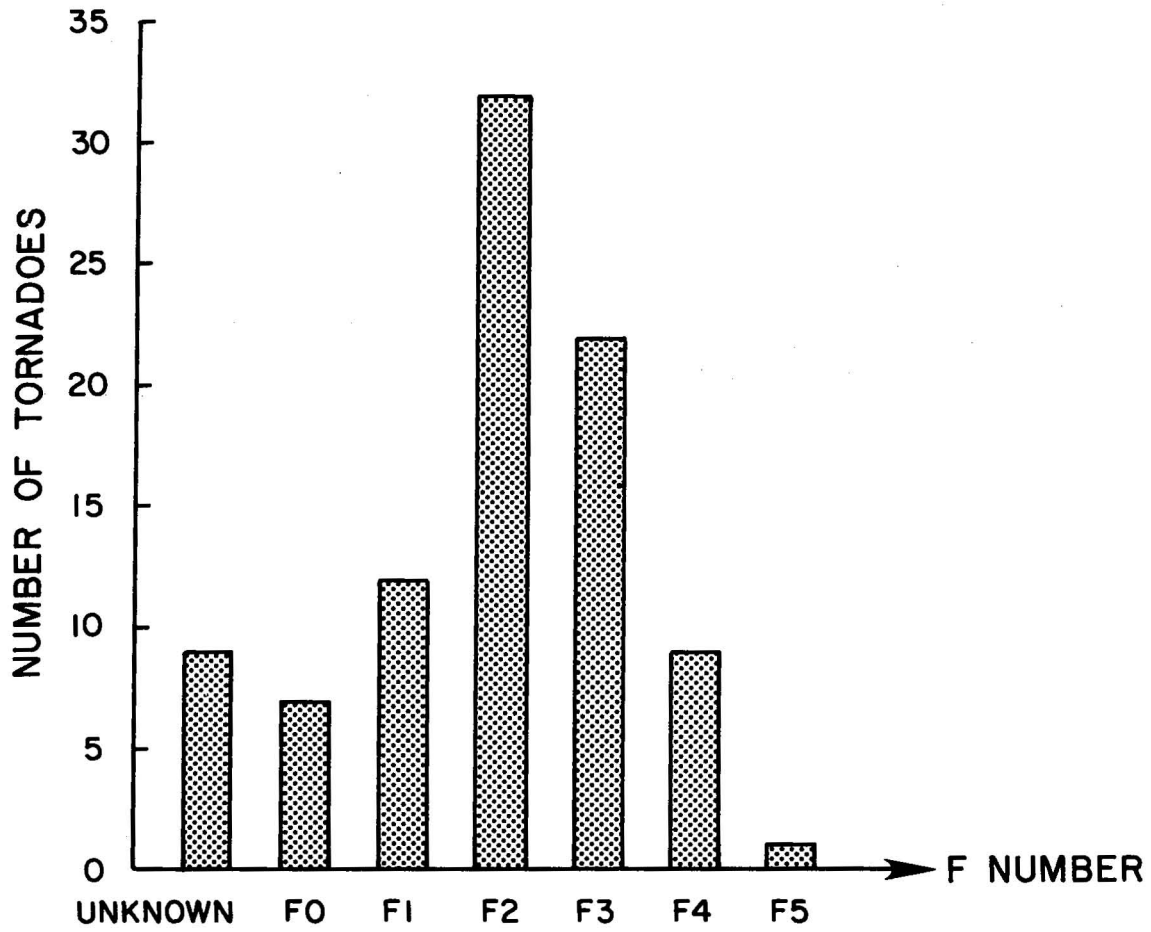

Figure 30. Statistical breakdown of the Oklahoma and Texas tornado tracks, surveyed by NSSL, by official F scale intensity. Of the 92 paths, only 83 were officially confirmed as separate tornadoes; hence, the remaining nine were never assigned an F rating.

[12] In addition, Golden and McCarthy (1975) performed aerial surveys of the damage in Kentucky, Indiana and Ohio from the 3 April 1974 tornado outbreak.

[13] Note that the Union City tornado was officially rated F4, but should have been rated F5 (Davies-Jones et al., 1978).

tornado occurred at all. This information was extremely valuable for Doppler radar and photogrammetric analyses.

We learned useful additional information. For instance, large hail often falls within a few kilometers of the tornado, usually on its left forward side. A few tornadoes are embedded in precipitation for their entire lives. Small scale, short-lived, but sometimes quite intense, tornadoes occur occasionally along gust fronts outside of mesocyclones. A few tornadoes occur during the developmental stages of their parent storms; in one case the tornado occurred five minutes before first radar echo. We know of other anomalous cases where tornadoes occurred at locations where the radar echo totally lacked indications of severe weather. Tornadoes were confirmed with a winter outbreak of severe weather (22 February 1975), which occurred in a region of low surface dewpoints (upper 30's in °F) and cool surface temperatures (upper 40's) just ahead of an intense warm front.

The questionnaires have established that eyewitnesses seldom recall any dramatic temperature changes coincident with tornado passage, and that the great majority of tornadoes have no dramatic electrical effects associated with them (although there may be a weak coronal discharge at the base of the funnel in a few instances). Tornado sounds are audible within 1.5 km typically.

Surprisingly sharp damage gradients are often observed in tornado tracks. In some weak tornadoes, the winds are clearly more intense at treetop level than near the ground. In the majority of cases, the damaging winds are predominantly from one direction, frequently along the direction of motion, although in some instances they blew at an angle to the path. Thus, debris from identifiable sources are usually seen strewn in a line along the track. On the periphery of the tornado, patterns suggesting radial inflow into a moving vortex are commonly seen. Note that many tornadoes inflict damage with little indication of any circulation in the damage patterns and could be mistaken for straight line winds except for their narrow damage swaths. In wide track tornadoes, however, signs of the rotary winds are far more obvious, with the damage on opposite sides of the track being caused by winds from opposing directions (in agreement with intuition). One wide track (F4) tornado surveyed ended abruptly during its mature stage (characterized by maximum size and intensity), without evolving through the shrinking and decay stages as almost all maxi-tornadoes do. The damage path was roughly a mile wide at the end. Suction marks (Fujita et al.,1967) have been observed in the tracks of a few large tornadoes. Damage features seen by Fujita (1979) in Midwestern corn fields are not clearly revealed in Oklahoma wheat fields, probably because wheat is more wind-resistant than corn.

The most detailed of NSSL's surveys was that of the 24 May 1973 Union City, Oklahoma tornado (Fig. 31, Davies-Jones et al., 1978). It was found that changes in tornado structure were accompanied by corresponding changes in damage intensity and debris configuration. Initially, damage was light over a 200 m wide path, but the vortical nature of the winds was clearly evident. During the tornado's mature stage, damage was severe and still showed signs of circulation across a path 500 m wide. Intriguing microscale patterns were seen in the wheat. In the shrinking and decaying stages, heavy damage occurred over a 100 m wide swath, there was evidence of strong radial inflow in the lowest meter above the surface, and the tornado left behind a deposition or "litter" line less than a meter wide. Generally, debris was thrown ahead of the vortex during these stages, with heavy objects coming to rest on the right forward side. Signs of circulation were no longer apparent in the debris configuration, and flow relative to the moving vortex appeared asymmetrical with the strongest winds on the right side of the

Figure 31. Damage on the west side of Union City, Oklahoma, inflicted by 24 May 1973 tornado. (Photo courtesy of the Oklahoma Publishing Co.).

funnel. A "laundry list" of heavy missiles generated by the tornado was compiled (Table 4). Boards found driven into soft ground in fields were first carried aloft by the tornado as buildings disintegrated, then dropped some distance away. Rossmann(1960) and Deissler (1977) have attributed this phenomenon to an intense, buoyancy-driven downdraft, but the debris orbits in the NSSL movies refute this hypothesis.

Table 4. Crudely estimated diameter (D), length (L), and weight (W), of heavy missiles generated by the Union City tornado. Units are MKS.

Missile	D (m)	L (m)	W (kg)	Remarks
7600 liter gas storage tank	1.5	3	700	Made of 6 mm steel. Airborne 400 m, then bounced 400 m.
Acetylene storage tank	0.4	1.5	65	
Steel container	1	1.2	60	
Steel I-beams		10	225	Carried 150 m.
Steel trailer frames		15	900	Width 4 m. Carried 50 m.
Cars and pickup trucks		5	1800	Width 2 m.
Car engine		1.2	250	Width 0.6m. Carried 300 m.
House roofs		10		
Telephone pole sections	0.36	3	100	

No cases of buildings exploding due to sudden change in atmospheric pressure, or of significant water removal from ponds or pools, or of "incredible" missiles have been observed by NSSL. The engineering aspects of damage surveys have been summarized in an NSSL Technical Memorandum by Minor et al. (1977). The F scale was found to be unrepresentative of tornado windspeed in the case of the Seymour tornado, which occurred in open country (see Section 4.2.8). In general, tough mesquite trees proved to be poor indicators of the ferocity of winds. For instance, the 1979 Wichita Falls tornado passed through the city, heavily damaging buildings in a 1.2 km wide path, but cut only a 100 m path through a mesquite patch within the city limits.

Some curious tornado stories have proved to be well founded. For instance, documented cases of wood penetrating metal (e.g., brakedrum, aluminum drill) have been uncovered by NSSL. Also, after the recent tornado outbreak of 10 April 1979, cancelled checks from Wichita Falls were recovered as far northeast as Bixby, Oklahoma (near Tulsa), a distance of 325 km. However, obvious scorching of vegetation, reported by Vonnegut (1960) and Silberg (1966), has never been observed by NSSL.

5. TORNADO MODELING

5.1 General

Two comprehensive and critical review articles on tornado dynamics (Davies-Jones and Kessler, 1974; Davies-Jones, 1981) have been written. These survey papers fulfill a need of scientists and engineers working in tornado problems by summarizing current tornado knowledge. The articles address all aspects of tornadoes, including their characteristics, relationship to parent storm, statistics, climatology, prediction, detection, measurement, and sources of rotation and energy. Tornado theories, and analytical, laboratory and numerical models are also discussed, as well as possible modification methods. A more succinct summary of the state of tornado knowledge was written by Kessler (1978).

5.2 Laboratory Modeling

A critical review of the current state of tornado vortex simulation has been given by Davies-Jones (1976). Of the various models examined, Davies-Jones concluded that the one developed by Ward (1972) at NSSL provides the most realistic simulation because of its dynamical and geometrical similarity to tornado cyclones.

Davies-Jones (1973) showed that the nondimensional radius of the turbulent vortex core in Ward's model is primarily a function of swirl ratio (ratio of typical tangential to vertical velocity) alone. Previous work (Ward, 1972; Jischke and Parang, 1974) had indicated that the core radius is primarily a function of inflow angle (or ratio of tangential to radial velocity) at the radial inlet. This new result showed that for given circulation and updraft radius, narrow vortices require high volume flow rates (but not necessarily high radial momentum fluxes as previously thought) for their maintenance. Davies-Jones also pointed out (from Jischke and Parang's (1974) data), that the experimental transition from a single wide vortex to a pair of concentrated vortices occurs at a critical swirl ratio (and hence, by implication, as the single vortex reaches a critical radius).

The fact that the swirl ratio, not the inflow angle, is the fundamental controlling factor in determining vortex structure contradicts the hypothesis that, for tornado formation, a large influx of radial momentum is required to converge the fluid against the opposing action of centrifugal forces. If the inflow layer is sufficiently deep, updraft volume flow rates may be high without correspondingly high radial momentum influxes, and a concentrated vortex will still form.

Jischke and Parang's (1975) measurements showed that the flow in Ward's model is, to a large extent, irrotational. They had previously shown (Jischke and Parang, 1974) that the experimental transition from a single wide vortex to a pair of concentrated vortices occurs at a critical swirl ratio in the range 0.45 to 0.7, the exact value depending on the Reynolds number. They also observed that a propeller placed at the apparatus axis showed no rotation, implying that the two vortices were not embedded in a third larger parent vortex centered at the axis of the system.

More details of the work in Ward's apparatus prior to 1976 are included in Davies-Jones' (1976) review. More recent work by Leslie (1977, 1979) investigated the effects of surface roughness on vortex structure. Leslie found that the

critical swirl ratio for transition to a greater number of vortices increases with increasing surface roughness. Thus, multi-vortex tornadoes are more likely to occur over smooth surfaces than rough ones. He also discovered that, in Ward's apparatus, increasing surface roughness yielded smaller core diameters (contrary to results in other types of vortex chambers).

5.3 Theoretical Modeling

5.3.1 Vortex Breakdown

"Vortex breakdown" refers to an abrupt change in the core structure of a vortex. Upstream of (or below) the breakdown, the flow consists of a high velocity, rapidly swirling jet. The core flow undergoes a transition to a new larger diameter with lower axial and swirl velocities. Above the breakdown point, flow along the axis is reversed, turbulence levels are higher and the central pressure deficit is reduced. The upper flow may be axisymmetric, or assume the forms of a spiral or a double helix. Breakdowns occur when the swirl ratio passes a critical value of order one. Laboratory investigations have shown that, although breakdowns may occur anywhere along the core, the region next to the ground (corner region) is a favored location. It is uncertain whether vortex breakdowns actually occur in tornadoes; however, photogrammetric data (Hoecker, 1960a; Golden and Purcell, 1977) as well as funnel shapes (Burggraf and Foster, 1977) strongly suggest that they do.

Burggraf and Foster (1977) received NSSL support to study theoretically whether breakdowns could occur in tornado-like vortices. Below a critical value of the "flow force" they obtained solutions which exhibited vortex breakdown, while for higher values of flow force abrupt transitions were absent in their solutions. Davies-Jones (private communication) supplied them with tornado photographs which appeared to capture a vortex breakdown in progress.

5.3.2 Vortex Instabilities

Many large tornadoes contain suction vortices (subsidiary vortices). Since suction vortices often appear to locate maxima in the wind, pressure deficit, and pressure change fields, they are extremely important features of the overall tornado. Are suction vortices a manifestation of a vortex instability? To help answer this question, Foster is currently investigating the stability of Long's (1961) vortex to non-axisymmetric perturbations (again with NSSL support). Long's vortex solution was chosen for the basic state because of its realism in describing the lateral spread of a vortex with height.

5.3.3 Vortex Boundary Layer and Core

Jischke and Parang (1975) obtained solutions for the turbulent boundary layer flow beneath a converging vortex. In contrast to most other investigations, they allowed the radial velocity above the boundary layer, u_∞, to be the same order as the tangential velocity there, v_∞. They found that, as u_∞ / v_∞ increases, the importance of the secondary flow generated in the boundary layer decreases. When $u_\infty / v_\infty \approx 1$, the boundary layer interaction is not significant to the essential structure of the vortex.

Jischke and Parang also made some computations which showed that the characteristic time for condensation to occur is comparable to the characteristic

advection time for air parcels in a tornado. It has been commonly assumed that the condensation time is small compared to the advection time so that, given other assumptions, the tornado funnel coincides with the condensation pressure isobar (see Davies-Jones and Kessler, 1974, for discussion). However, utter devastation has been wreaked by some large tornadoes, which, at the time, had condensation funnels which did not span the entire distance from the (quite low) cloud base to ground. A possible explanation is that condensation occurs in an air parcel one to two seconds after the pressure of the parcel has been reduced to its condensation pressure, during which time the parcel may travel 100 meters or further upwards. Thus, in these cases the funnel surface differs markedly from the condensation pressure surface, and fails to portray the true intensity of the vortex.

5.3.4 Theoretical Implications of Dual-Doppler Radar Data

Ray (1976) and Ray et al. (1976) have evaluated the convergence and tilting terms in the vertical vorticity equation, using dual-Doppler radar data on a tornadic storm, in attempts to learn more about the vorticity production processes which are important for tornado maintenance. Their data showed that, in a mature mesocyclone, the convergence and tilting terms contribute about equally to the production of mesoscale cyclonic vorticity. Scale analysis indicates that the solenoidal generation of vertical vorticity is probably just a minor influence in the formation and maintenance of mesocyclones and tornadoes. The remaining term represents the eddy transport of vorticity. Although this process has been proposed by Starr (1974) as a means of vorticity concentration, the intense vertical velocities observed around tornadoes would seem to preclude angular momentum transport by turbulent eddies as the prime mechanism for vorticity concentration. Thus, it appears that the tornado's large vorticity is produced from background vorticity through the stretching of vortex tubes. Note that the orientation of the tubes may be changed appreciably in the process, and that both the tilting and convergence terms can amplify vorticity through the stretching mechanism if the background vorticity has both vertical and horizontal components. The observed asymmetries in vertical velocity fields around tornadoes (see Section 4.2) indicate that the tilting term may be important in tornadogenesis, as well as in mesocyclonegenesis.

5.4 Special Problems

5.4.1 Plutonium Dispersal by Tornado

In June 1975, NSSL sent representatives (Davies-Jones and Golden) to the Workshop on Dispersion and Deposition of Entrained Materials after a Tornado Strike held at Argonne National Laboratory. The purpose of this workshop was to help Argonne National Laboratory formulate a statement on how plutonium would be dispersed following a tornado strike. The findings of this workshop were scheduled to be published in due course in an edited proceedings volume, but so far have not been released.

5.4.2 Water Removal from Ponds

Accounts in the literature of water removal by tornadoes fall into three categories:

(a) Evacuation of water ponds.

(b) "Partings" of rivers and streams (similar to the biblical "parting of the Red Sea").

(c) Wells sucked dry.

Historical reports of such phenomena have been compiled from various sources[14] by Golden (in a 1975 letter to AEC). Such accounts usually cannot be verified or refuted because of the passage of time. However, Gordon (1971) has noted a tendency for historical texts and newspaper reports to exaggerate. An aerial survey begun five days after the 3 April 1974 tornado outbreak revealed that, out of 50 ponds which lay in damage paths, less than 10% showed signs of any significant drop in water level, with one or two small ponds having indications of near total water removal. During the five or more days between the tornadoes and the surveys, it is possible that heavy rains may have refilled some of the ponds again. However, NSSL during its surveys has never discovered a well documented case of substantial water removal from large ponds.

Spray generation by the wind over a water surface begins as the surface wind speeds increase above 22 m s^{-1}. There are accounts of waterspouts moving onshore and depositing large quantities of fish and seaweed. Also, heavy saline showers have been reliably reported in association with waterspouts. Waterspouts have a high concentration of very large spray drops in the lowest ten meters above the water surface, but most of the large drops are centrifuged out of the vortex below 15 m. A hollow sheath of small droplets continues upward to heights of 50-300 m (Golden, 1974a,c).

Davies-Jones (in same 1975 letter) has estimated the rate at which a tornado might remove water. The following is a revised version of that investigation. The first factor considered is the hydrostatic rise, h, in the water surface due to an applied pressure differential, Δp. From the hydrostatic equation

$$\Delta h = - \frac{\Delta p}{\rho_w g}$$

where ρ_w, the density of water, = 10^3 kg m^{-3}, and g = 9.8 m s^{-2}. For Δp = -200 mb = -2 x 10^4 MKS units, $\Delta h \sim 2$ m. The core of the tornado is typically 50 m in radius, so that roughly 10,000 to 20,000 m^3 of water might be raised above the initial water level. If the volume of the pond is much larger than 20,000 m^3, or if the sides of the pond extend 2 m or more above the undisturbed water level, the hydrostatic effect can be neglected safely. [Note that swimming pools and wells, which are small compared to tornadoes, experience only a small differential pressure across them, and thus their water surfaces will be displaced only a few centimeters by the hydrostatic effect.] In actual waterspouts and tornadoes, observed over large bodies of water, dynamical forces displace water outwards from the tornado, so that the surface near the vortex core appears to be depressed rather than elevated (Golden, 1974a,c). Thus, the hydrostatic effect may be even less significant than indicated above.

The second water removal mechanism considered here is the centrifuging of large drops out of the vortex in the lowest 10-15 meters. For a potential vortex, the tangential velocity as a function of radius

$$v = \frac{M}{r}$$

---

[14] e.g., Flora (1954), Ludlam (1970), Weather, Weatherwise, Storm Data.

where $2\pi M$ is the circulation. Neglecting differences in tangential velocity between the drops and surrounding air, the radial equation of motion for the drops is

$$u \frac{\partial u}{\partial r} = \frac{v^2}{r} = \frac{M^2}{r^3} \quad ,$$

where u is the radial velocity. If r_m denotes the radius of maximum tangential winds and v_m the maximum tangential velocity, and if $u = 0$ at $r = r_m$, integrating the above equation yields

$$u(r) = v_m \sqrt{1 - \frac{r_m^2}{r^2}} \quad ,$$

or

$$\frac{dr_*}{dt} = \frac{v_m}{r_m} \frac{\sqrt{r_*^2 - 1}}{r_*}$$

where $r_* \equiv r/r_m$. Integrating this equation yields

$$\sqrt{r_*^2 - 1} = \frac{v_m t}{r_m} \quad ,$$

assuming that $r_* = 1$ at $t = 0$. Solving for r_* gives

$$r_* = \sqrt{1 + \frac{v_m^2 t^2}{r_m^2}} \quad ,$$

i.e.,

$$r = \sqrt{r_m^2 + v_m^2 t^2} \quad .$$

In the absence of vertical velocities, a large drop ($\geq$1 mm) released at a height, h, of 15 m reaches the ground in roughly 3 seconds (the exact value depends on its terminal velocity). If NRC's design basis tornado values, v_m = 130 m s^{-1}, r_m = 50 m, are substituted in the above formula, we find that the drops can be centrifuged out considerable distances (~400 m) from the tornado axis. While the above model is crude and contains dubious assumptions, it does indicate that the mechanism it describes is potentially a serious source of water loss. Without knowledge of the water content of the low level "spray fountain," it is impossible to estimate the water loss.

The third mechanism pertains to water droplets carried upwards in a "spray sheath" around the vortex. These spray droplets have small enough fall velocities that, even though the centripetal accelerations are 10 to 30 g at the radius of maximum winds, the droplets are not centrifuged out of the vortex (the terminal velocity of a drop in the radial direction is v^2/rg times the fall velocity). Large upward velocities have been measured photogrammetrically in regions surrounding tornado cores. Assume that air rises at an average rate, W, within a

cylinder of radius, R', centered about the tornado's axis. Also, let the equivalent radius of the pond (i.e., the radius of the circle having the same surface area as the pond) be P, and let R denote the smaller of R' and P. If the liquid water content of the spray sheath is σ (in kg of water per m^3), then the water removal rate is $\pi R^2 W\sigma$.

A circular pond of radius P and depth h has a water mass of $\pi P^2 h\rho_w$ where $\rho_w (= 10^3 \text{ kg m}^{-3})$ is the density of water. A tornado travelling at a velocity V affects the pond for a time $\frac{2P}{V}$. In this time, the fraction of water removed, L, is

$$L = \frac{2R^2 W\sigma}{PVh\rho_w} \quad .$$

There are two cases according to whether R' (which can be thought of as the radius of the spray sheath) is greater than or less than the pond radius P. In the former case, R = P and $L \propto P$, while in the latter case, R = R' and $L \alpha P^{-1}$.

Based on Goldman's (1965) data of the 1963 Kankakee, Illinois tornado, $W = 50 \text{ m s}^{-1}$ and R' = 250 m. [For the 1957 Dallas tornado, measured by Hoecker (1960a), R' is much smaller, ~100 m.] The sheath's liquid water content is estimated to be $10^{-2} \text{ kg m}^{-3}$ (i.e., 10 gm m^{-3}), equivalent to a heavy shower (a reasonable upper bound in the absence of any data). The minimum translation speed of the design basis tornado is 2.23 m s^{-1} (USNRC, 1974), so $V = 2.23 \text{ m s}^{-1}$ represents the worst possible design case. A 5 acre circular pond has a radius, P = 80 m. If it is 3 m deep, then the fractional water loss for the above parameters is roughly 1%. Only for a very large, shallow pond (50 acre with h = 1 m and R' = P = R = 250 m) does the water loss becomes significant (roughly 30%). Thus, the water loss due to transport of small droplets in the spray sheath is negligible except in the unlikely case of a slow-moving tornado with a very large spray sheath affecting a large and very shallow pond.

The fourth way in which water loss might occur is through seiches and by splashing and spray caused by breaking waves. Seiches are resonant standing waves in enclosed or partially enclosed water bodies, in which the water has a natural period of oscillation. Wind and atmospheric pressure gradients are two of the agents which generate seiches. For a 5 acre ($2.02 \times 10^4 \text{ m}^2$) square pond, which is 1 m deep, the approximate periods of the fundamental mode and second harmonic are 50 and 25 s, respectively. Local drops in water level of a few feet have been observed in lakes after the passage of a tornadic storm. Organized wave-trains, generated by waterspouts, have been reported by Golden (1974a,c), Wave generation is proportional to both wind speed and fetch. The wave and seiche problems are not amenable to simple calculations.

In conclusion, water losses due to the "fountain effect" and due to seiches and waves (i.e., the second and fourth mechanisms) may be significant but are very difficult to estimate. Losses due to the hydrostatic effect and the spray sheath are generally negligible. Deep ponds should be affected less than shallow ones.

5.4.3 Some Comments on the Design Basis Tornado

The design basis tornado (DBT) currently in use over the United States (for each of the three regions shown in Fig. 32) is given in Table 5. Some scientists and engineers have considered the design basis tornado to be overly conservative;

nevertheless, attempts over the last decade to revise the values have been resisted. The following commentary on the DBT is based on theoretical and observational evidence.

Assuming that the tornado's energy source is the potential energy available in a conditionally unstable atmosphere, then an upper bound on tornado winds and pressure drops have been estimated from proximity soundings (Lilly, 1969, 1976; Kessler 1970; Davies-Jones and Kessler, 1974; Michaud, 1977). The maximum pressure drop that can be supported is roughly 150 mb according to this method. If the relationship, $\Delta p = \rho v_{max}^2$, which holds strictly only for a combined Rankine vortex, is invoked, then the 150 mb pressure deficit translates into maximum tangential winds of 115 m s^{-1}. However, Lewellen (1976) has questioned the upper bound given by this method because of the dynamic terms neglected in the derivation. He concludes that the central pressure deficit near the ground can be greater than that supported hydrostatically. Thus, no existing model adequately provides a reliable upper bound on the maximum tornadic wind velocity derivable from observed atmospheric soundings. However, there is little "hard evidence" for tornadic wind speeds in excess of 130 m s^{-1} (Davies-Jones and Kessler, 1974; Davies-Jones, 1981).

The full surface pressure deficit in an intense tornado has never been reliably measured, but can be estimated from the maximum wind speed through the formula

$$\Delta p = c\rho v_{max}^2 \quad ,$$

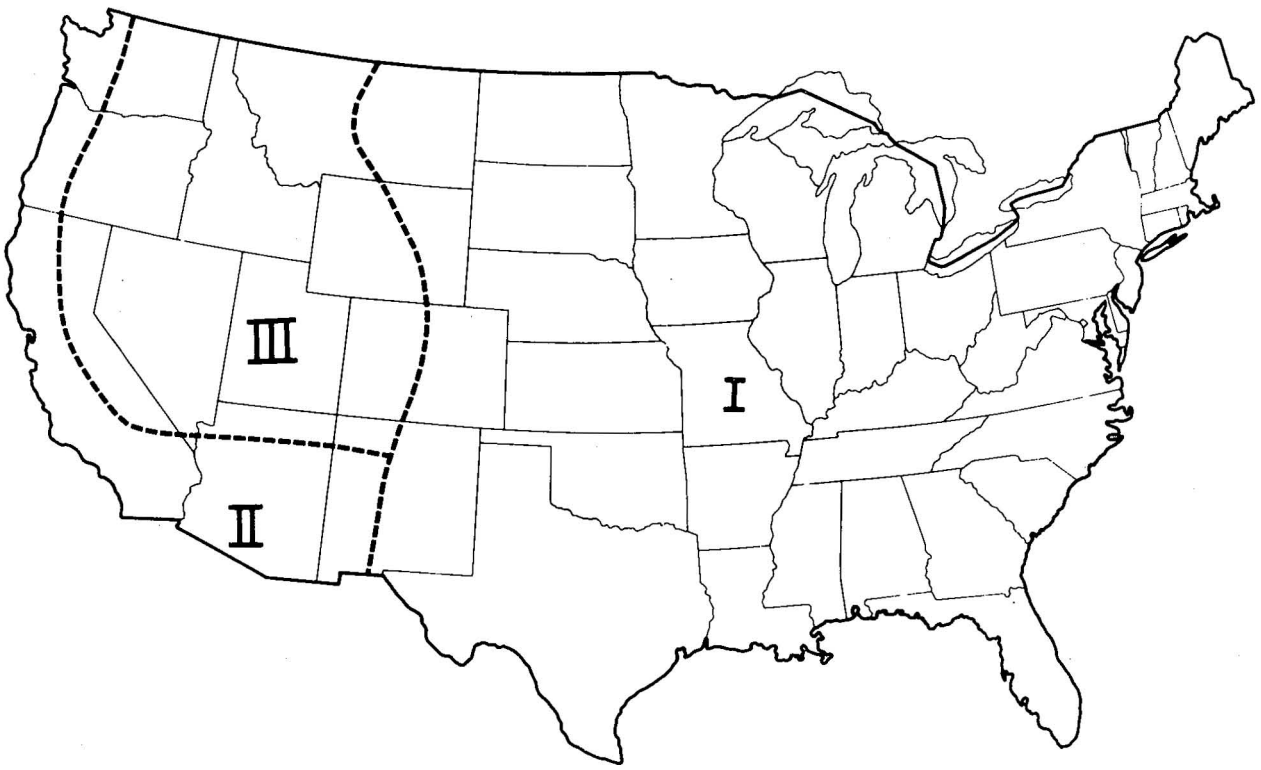

Figure 32. Tornado intensity regions.

Table 5. Design-Basis Tornado Characteristics

Region	Maximum wind speed, m s^{-1} *	Rotational speed, m s^{-1}	Translational speed, ms^{-1}		Radius of maximum rotational wind, m	Pressure drop, mb	Rate of pressure drop, mb/sec
			Maximum	Minimum+			
I	161	130	31	2.2	46	207	138
II	134	107	27	2.2	46	155	83
III	107	85	22	2.2	46	103	41

*The maximum wind speed is the sum of the rotational speed component and the maximum translational speed component.

+The minimum translational speed, which allows maximum transit time of the tornado across exposed plant features, is to be used whenever low travel speed (maximum transit time) is a limiting factor in the design.

where c = 1 for a combined Rankine vortex and for the DBT. In theory, c = 0.5 is the lowest value possible corresponding to an inviscid vortex flow with a stagnant core and an irrotational outer region. Core rotation increases c. Solid body rotation (as in the combined Rankine vortex) raises c to 1.0, but the change in c is not as large if the core vorticity increases outward from the axis rather than being constant with radius. Two more effects which amplify c in nature are the smoothing out of the cusp in the combined Rankine tangential velocity profile, and outward increasing (instead of constant) angular momentum in the outer region of the vortex. Turbulent and viscous energy losses would also act to enlarge c. For Kuo's (1966) one-cell and two-cell vortex solutions c = 1.74 and 1.14, respectively. Unfortunately, c has been found to have even wider latitude in Ward's vortex chamber (Leslie, 1979), ranging from 8 at low swirl ratio to 0.5 at high swirl ratio.

A more reliable pressure deficit estimate was obtained by Hoecker (1961), who integrated the cyclostrophic equation and used the observed tangential velocity field of the Dallas tornado. The maximum pressure drop was 60 mb and was located at the ground. Inserting v_{max} = 75 m s^{-1} (as observed) and ρ = 1.18 kg m^{-3} (a representative value of air density at sea level) in the above formula yields c = 0.90. If the Dallas tornado winds are simply scaled up to the intensity of the DBT, the pressure deficit corresponding to 130 m s^{-1} maximum tangential velocity is 180 mb. However, this procedure assumes that the swirl ratios for the two tornadoes are the same, a constraint which is unreasonable. A summary of pressure drops recorded by microbarographs when tornadoes passed over them has been given by Davies-Jones and Kessler (1974). The full deficit apparently has never been recorded because the instrument responded too sluggishly; also, there is always doubt whether the microbarograph lay in the exact path of the lowest pressure. Unofficial readings of barometers made by citizens during tornadoes in 1896 and 1904 indicated pressure deficits of 82 and 192 mb. However, the authenticity of these measurements is not well established. More dependable estimates of the maximum pressure deficit in tornadoes awaits direct measurements with fast response instruments and better numerical models.

The translation speeds of tornadoes have been measured by photogrammetry and Doppler radar. The DBT range of 2.2 to 31 m s^{-1} covers the vast majority of tornadoes. There are a few accounts of almost stationary tornadoes, however (Wolford, 1960).

Given the maximum tangential velocity and the radius of maximum winds, the maximum rate of pressure change can be estimated theoretically. For a vortex in cyclostrophic balance,

$$\frac{\partial p}{\partial r} = \frac{\rho v^2}{r} \quad .$$

Thus, for a tornado travelling toward a point at (translation) speed, T, the rate of pressure change (pressure tendency) at that point is

$$\frac{\partial p}{\partial t} = T \frac{\rho v^2}{r} \quad .$$

The maximum rate of pressure change occurs when v^2/r is a maximum. For a combined Rankine vortex

$$\left(\frac{v^2}{r}\right)_{max} = \frac{v_m^2}{r_m} \quad ,$$

i.e., the maximum pressure change rate occurs at the radius of maximum winds. For other vortex solutions, this is approximately true.[15] Thus,

$$\left(\frac{\partial p}{\partial t}\right)_{max} \approx T\rho \frac{v_m^2}{r_m} \quad ,$$

For the design basis tornado, T = 31 m s^{-1} (worst case), v_m = 130 m s^{-1}, r_m = 46 m,

$$\left(\frac{\partial p}{\partial t}\right)_{max} \approx 136 \text{ mb } s^{-1} \quad ,$$

which roughly agrees with the value listed in Table 4. The value for ρ used in this evaluation is 1.18 kg m^{-3}, the sea level density associated with the average tornado (the average tornado is associated with a sea level pressure of 1007 mb, a surface temperature of 23°C and a surface dewpoint of 17°C; Williams, 1976). Note that the design basis tornado specifies the maximum rotational wind, v_{rot}, (i.e., the maximum resultant horizontal velocity[16]) whereas the formula requires the maximum tangential velocity. Some models assume that the radial velocity, u, equals v/2 and neglect the $\frac{1}{2}\rho u^2$ dynamic pressure term, thereby underestimating the rate of pressure change by 10 to 20% (since $v_m^2 = 0.8\, v_{rot}^2$ in this case). In vortex flows, u << v at the radius of maximum winds, except close to the ground. Near the surface, cyclostrophic balance does not apply anyway, so that it seems appropriate to insert the full maximum rotational wind speed into the formula without any reduction.

The model predicts that the maximum rate of pressure change varies inversely as the radius of maximum winds, r_m. Since the design basis tornadoes for Regions I-III all have the same r_m despite the tendency for weak tornadoes to be smaller than strong ones, the maximum rates of pressure change for Regions II and III may be underestimated. Some values of r_m deduced from observations are listed in Davies-Jones and Kessler (1974). For an intense waterspout, Golden (1971) measured maximum tangential velocity of 85 m s^{-1} at 10 m from the axis. Such a vortex moving at 22 m s^{-1} (the maximum translation speed for Region III) would produce a maximum pressure tendency of 190 mb s^{-1}, considerably higher than the design value of 41 mb s^{-1}. However, it must be pointed out that the area affected by such large pressure changes is quite small. For a combined Rankine vortex, $\frac{\partial p}{\partial t}$ varies as $(\frac{r}{r_m})^{-3}$ and $(\frac{r}{r_m})^{+1}$ outside and inside the radius of maximum winds, respectively. The design value would be exceeded only in an annulus defined by radii, 2 m and 17 m. Obviously, at any one instant, only the components of a large structure not the structure as a whole, would feel the loads associated with such localized, extreme pressure changes.

---

[15] Examination of the cyclostropic equation reveals that, at the point of maximum pressure change rate, $\partial v/\partial r > 0$ but $\partial^2 v/\partial r^2 < 0$. Thus, for typical vortex flows with smooth tangential velocity profiles, the maximum pressure change rate occurs close to, but inside, the radius of maximum winds.

[16] Relative to the vortex.

Thus far, only the case of a single vortex tornado has been discussed. However, large tornadoes often are not a single vortex, but consist of several "suction" vortices revolving around a common center. The suction vortices locate the extremes of wind, pressure deficit and pressure tendency in the tornado. The formula

$$\left(\frac{\partial p}{\partial t}\right)_{max} = T\,\rho\,\frac{v_m^2}{r_m}$$

still applies, but r_m is now the radius of a suction vortex (not the whole tornado), v_m is the maximum tangential velocity around the suction vortex axis, and T is the translation speed of the suction vortex (the resultant of the tornado's overall translation velocity and the translation of the suction vortex around the tornado's center). Since suction vortices are narrow and rapidly moving, the appropriate values of T and r_m are much larger and smaller, respectively, than the corresponding values for a single vortex tornado.

The maximum wind speed, V, occurs where the velocity vectors are aligned. Thus, $V \equiv T + v_m$. Inspection of the above relationship reveals that the worst possible case (i.e., largest $\frac{\partial p}{\partial t}$) arises, for a given design speed, V, when $T = V/3$, $v_m = 2V/3$. For the DBT (Region I), $V = 161$ m s^{-1}; thus $T = 54$ m s^{-1}, $v_m = 107$ m s^{-1} yields the worst case. The radius of a suction vortex has seldom been measured, but a reasonable value for r_m is 25 m (based on Forbes, 1978). The corresponding maximum pressure tendency (for a multi-vortex DBT) is 293 mb s^{-1}. Such a large rate of pressure change would affect a given point for only a fraction of a second, and affect only a small area at any given instant. Thus, from the structural design standpoint, such large pressure tendencies are probably insignificant. Also, the value of v_m inserted into the formula appears to be extreme. For instance, the intense 1974 Parker, Indiana tornado, which was analyzed photogrammetrically by Forbes (1978), had the same values of T and r_m as used above, but v_m was 45 m s^{-1}. This value of v_m reduces the maximum pressure tendency to 52 mb s^{-1}.

6. WATERSPOUT RESEARCH

6.1 Geographical Distribution

A comprehensive assessment of waterspout statistics along the U.S. East and Gulf Coasts was completed in early 1975, and a report was transmitted to the NRC (addressed to Dr. Harbour). Also attached to this report was an overview letter and appendixes on waterpond evacuation problems posed by intense vortices. The primary purpose of the report was to assess statistically the threat posed by waterspouts, especially to floating offshore nuclear power plants. The analysis was restricted to the East and Gulf Coasts, although waterspouts have been reliably reported along the West Coast and the lee shores of the Great Lakes and a few of these are intense. More research is certainly needed on the frequency and damage potential of waterspouts in the latter two regions.

There can be no doubt that waterspouts pose a threat to the integrity of man-made structures (Golden, 1973; Fujita et al., 1972; Macky, 1953). Many of the

damaging tornadoes affecting the central and eastern Gulf Coast during the late fall and early spring originate over the northern Gulf of Mexico as intense waterspouts.

Maximum rotational wind speeds as high as 85 m s^{-1} (190 kts) have been measured by photogrammetric techniques in the lowest 10-15 m MSL for large Florida Keys waterspouts (Golden, 1971, 1974a,c). Objects weighing up to five tons have been carried 30 m or more by tornadoes moving over coastal waterways out to sea (Golden, 1969, 1971). Large amounts of sea spray are generated at the vortex column's base and circulated helically upward to heights of 300 m. Wave-trains of considerable extent and amplitude are generated as the spray vortex travels over the sea surface (Golden, 1971, 1974a,b). The wind forces in waterspouts should therefore be accounted for in designing offshore nuclear facilities.

Two primary data sources were utilized in the compilation of the NRC waterspout climatology for the U.S. East and Gulf Coasts. All Storm Data reports from coastal counties during the period 1959-73 were examined for waterspouts, tornadoes and funnel clouds. Tornadoes which passed over coastal lakes or waterways, or crossed a coastline and continued out to sea are included in the waterspout statistics and plots. Based upon the first two stages of the waterspout life cycle discovered by Golden (1973, 1974a,c), funnel clouds which were likewise reported over water bodies were also included as probable waterspouts. The second data source was a large file of mariners' reports covering almost a century, 1850-1940, for the entire western North Atlantic and Gulf of Mexico. This file was kept by past editors of the Mariner's Weather Log, and is therefore probably biased toward United States vessel reports. All definite and probably waterspouts from Storm Data and the mariners' reports were plotted on U.S. Coast and Geodetic Survey maps. There are frequency maps for three regions of interest: the Gulf of Mexico and coastal environs from Brownsville, Texas, to Cape Sable, Florida, and northward to Jacksonville, Florida; the lower U.S. East Coast northward to Cape Hatteras, South Carolina; and the upper U.S. East Coast northward to Maine. These maps of recent waterspout frequency distributions are given in Golden (1977). Details of waterspout locations within demographically-partitioned coastline segments, damaging waterspouts and directions of movement are given on the original base map plots, on permanent file at NSSL.

Waterspouts probably occur more frequently in the Florida Keys than anywhere else in the world. In addition, Golden (1973) also demonstrated that conventional data sources for the Keys underestimate the actual yearly waterspout population by nearly an order of magnitude. This tendency is likely present in the Storm Data used for the Gulf and East Coasts; public apathy and lack of understanding about potential waterspout hazards are contributing factors. In addition, the public has the mistaken impression that funnel clouds not reaching the water surface are of no interest to local National Weather Service Offices. Golden (1974a) has shown that definite closed circulation often exists at the surface without visible waterspout funnels aloft.

Table 6 gives a list of the ten most active areas along the entire U.S. Gulf and East Coasts in decreasing order of reported waterspout frequency for the 15-year period. Note that the Florida Keys experience from 50-500 waterspouts each year (at least 400 waterspouts were documented during the 1969 Lower Keys Waterspout Project--Golden, 1974a). Total waterspouts and the number producing damage are given for each coastal area. Tampa Bay has the greatest number of damaging waterspouts, and it is known that half or more of these originate over the Gulf of Mexico during midlatitude disturbances. Note that the area-averaged

TABLE 6. Top ten coastal areas for waterspout occurrence: U. S. East and Gulf Coasts, 1959–73 (all values are 15-year totals).

Location* (areal coverage)	Total spouts	Spouts per unit area ($\times 10^{-4}$ km^{-2})	Damaging cases
1. Florida Keys** (22809 km²)	>1000	>6572	15
2. Greater Miami, Fla. (10 138 km²)	335 (++)	330	16
3. Tampa Bay, Fla. (6970 km²)	235 (++++)	363	33
4. Palm Beach, Fla. (5069 km²)	234	462	7
5. Corpus Christi, Tex. (6246 km²)	211 (++++++++++)	338	≥10
6. Ft. Lauderdale-Del Rey Beach, Fla. (5069 km²)	180 (++)	355	10
7. Galveston Bay, Tex. (11 560 km²)	161 (++++++++++)	139	12
8. Mississippi River Delta*** N. Orleans (South of Lake Maurepas to Mississippi Delta) (14 790 km²)	142 (++)	96	12
9. Pensacola Bay, Fla. (4164 km²)	110 (+)	264	13
10a. Ft. Myers, Fla. (12 672 km²)	104	82	12
10b. Mississippi Sound, Miss. (5651 km²)	103 (+++)	182	16
10c. Port Arthur, Tex., to Sabine Lake (5711 km²)	102 (+)	179	10

* Compare these data with Figs. 1 and 4.
** Estimated from field data in Golden (1973) and Rossow (1970).
*** Lake Pontchartrain, north of New Orleans, had 96 (++++) total waterspout reports, one damaging (*not* included here).
Note: Each + indicates one observation of several or numerous waterspouts and was counted as only one event in the tabulations.

waterspout frequencies alter the order of the waterspout "top ten" areas of occurrence in Table 6. In terms of waterspouts per unit area, the most active region after the Florida Keys is the entire southeast Florida coast from Stuart to Homestead. Next, Tampa Bay and Corpus Christi are comparably waterspout-active, and are followed by Pensacola, Mississippi Sound and Port Arthur to Sabine Lake and Galveston Bay. The central Georgia coast is another rather active waterspout region with 118 x 10^{-4} km^{-2}. Lake Pontchartrain (north of New Orleans) also has a very high concentration of reported waterspouts.

In summary, the Gulf Coast and southeast Florida are highly active waterspout regions. The southeast U.S. Coast north of Jacksonville has comparatively light and sporadic waterspout activity. The frequency of waterspout occurrence along the upper Eastern Seaboard tends to steadily diminish northward. A maximum does, however, clearly extend from Cape Hatteras, North Carolina, northward through Pamlico Sound to Norfolk, Virginia, and to the headwaters of Chesapeake Bay. Numerous waterspouts were reported by ships east of Nags Head, South Carolina, to Norfolk, Virginia, in the Gulf Stream.

6.2 Summary of Florida Keys' Waterspout Experiments

The first systematic field experiments in the Florida Keys to investigate waterspouts and their parent cloud systems were undertaken during the summers of 1967-68 by V. J. Rossow of NASA. His results were never published in the formal literature, but are available in a NASA report (Rossow, 1970) and in conference preprints (Rossow, 1969). Rossow was unable to reach his primary objective, i.e., finding a relationship between waterspouts or their parent clouds and unusual electrical activity. He did demonstrate, however, that instrumented aircraft

could be used very efficiently to study waterspouts safely at close range, with a high frequency of occurrence in the Florida Keys. Golden (1973) published a comprehensive survey on the statistical aspects of waterspout formation in the Florida Keys, including annual frequency, seasonal distribution, diurnal occurrences, duration, multiple funnels, favored areas and the local weather situation.

Based on the favorable logistics and high waterspout frequency indicated by Rossow's work, Golden organized the Lower Keys Waterspout Project in Key West during May-September, 1969 (Golden, 1970). Several papers were published (Golden, 1974a,b,c) on the results of photogrammetric and other analyses of waterspouts. The most important of these results from NRC's standpoint, i.e., those on waterspout structure and intensity, are summarized below. Waterspouts are most destructive during the mature and early decay stages. Peak rotational wind speeds occur at small radii (10-15 m) in the spray vortex, and maxima derived from photogrammetry range from 65-88 m s^{-1}. However, it should be emphasized that only about 10-20% of all waterspouts observed each year in the Keys have intensity typical of the median tornado (i.e., peak rotational wind speeds above about 50 m s^{-1}). About 10% of the waterspouts are anticyclonic, and a few of these reach the above intensity also. Photogrammetrically-derived radial profiles of tangential winds across the spray vortices of mature waterspouts indicate close agreement with the Rankine-combined model; however, some larger waterspouts exhibit pronounced non-steady asymmetries in the circulation around the spray vortex and in the funnel, similar to secondary vortices in tornadoes. In such cases, the Rankine-combined model and cyclostrophic wind assumption cannot be used.

Additional details of the circulation within the condensation funnel were revealed by the 1969 data. Even the larger funnels had hollow cores, and cloud tags on the sloping collar cloud walls rose rapidly. Well-defined condensate filaments could be seen rotating cyclonically around the hollow core and spiralling upward in the funnel wall (w = 5-10 m s^{-1} for intense waterspouts). Therefore, although the strongest rising motions occur outside the visible funnel, air parcels are also rising in helical fashion in the funnel walls.

During the summers of 1970-73, Golden collaborated with the Purdue Tornado Group on waterspout probing. A sensor package for pressure, temperature and humidity was pulled behind a light aircraft on a trailing electrical cable. The pilot had to execute a very difficult, sharp turn of the aircraft as it passed to within 50 ft or so of the waterspout funnel just below cloudbase, to swing the trailing wire probe through the funnel. Preliminary analyses of temperature traces from the Purdue probe gave positive temperature anomalies in the double peaks averaging 0.3 to 0.6C, ranging up to about 2.2C for large waterspouts (see Church, et al., 1973, and Golden, 1974a). These data may not be reliable however, because of sensor problems uncovered by the Purdue Group after the completion of the field experiments. An additional difficulty of their trailing-wire approach was the residual uncertainty about the exact path of the sensor package viz a viz the core of the waterspout funnel on each pass. The first year of the Purdue work was sponsored by NASA, and subsequent years by NOAA/ERL--a final report was completed for NSSL in 1974 (Church and Ehresman, 1974).

A more direct approach for the probing of waterspouts, and one that proved to be more accurate and successful was developed by P. C. Sinclair of Colorado State University, with the collaboration of Golden and NSSL. This approach utilized a heavily-instrumented, highly-stressed aircraft to penetrate waterspout funnels directly. Experiments sponsored by NOAA were carried out in 1974 and again in 1975-77 with partial support from NRC. Data on waterspout velocity, temperature

and pressure fields obtained during 1974 in the near-cloud base environment show: (1) a core of rising motion of 5-10 m s^{-1}; (2) a horizontal circular flow field that is broader in weaker waterspouts and spatially concentrated in more intense waterspouts; (3) a central core region about 0.3°K warmer than the environment (in agreement with the Purdue results); and (4) a core pressure deficit on the order of 1-10 mb depending on waterspout intensity. Based on these data, some simplifications to the cylindrical, incompressible equations of motion have been made by a scale analysis of each term. While the present form of the reduced equations represent only a rough approximation, it has been shown that the cyclostrophic equation and a Rankine-combined vortex model account for about 75% of the measured total pressure deficit. A final report of the 1974 waterspout penetration experiments has been prepared by Sinclair (1978) for NOAA, and the results have also been published by Leverson et al. (1975, 1977).

The Wave Propagation Laboratory's portable Doppler Lidar System (see Section 4.3.1) was used to measure waterspout winds in the Florida Keys during the summers of 1975-77 with assistance from Golden and NSSL. The maximum horizontal velocity measured in 20 waterspouts was 25 m s^{-1} (Schwiesow et al., 1977). The data sometimes showed a double peak in tangential velocity, an observation which is consistent with the double-walled funnel seen in some waterspouts.

7. TORNADO AND WATERSPOUT CLIMATOLOGY

Climatological aspects of tornadoes have been addressed in several ways. NSSL assisted in review of the Dames and Moore report, "A Meteorological and Engineering Approach to the Regionalization of Tornado Wind Criteria for Nuclear Power Plant Design." AEC contract AT(11-1)-2396 (1975) complimented an in-house study by Kessler (1974), published in an AIAA paper entitled "Survey of Boundary Layer Winds with Special Reference to Extreme Values." In addition, all recorded tornadoes from 1953 through 1974 were analyzed, and statistics on property damage and human casualties were normalized by reference to estimated property values and populations at risk. Results were first published as NOAA Technical Memorandum ERL NSSL-77 (Kessler and Lee, 1976), entitled "Normalized Indices of Destruction and Deaths by Tornadoes," and later summarized in a short article (Kessler and Lee, 1978).

Waterspout climatology concerned a search of all waterspout reports obtainable for the United States Atlantic Ocean and Gulf of Mexico shorelines (see Section 6.1).

8. ACKNOWLEDGMENTS

The pulsed-Doppler tornado spectra have been realized through the dedicated effort of Mr. Dale Sirmans, who developed NSSL's Doppler radar into a harmonious system. Glen Anderson was instrumental in bringing the high PRF system on line, while Larry Hennington conceived the multi-moment display and developed tracking techniques. Mr. Bill Bumgarner has provided valuable computer support, and the color display system reflects the work of Allen Zahrai. Dr. R. J. Doviak contributed much to the overall wind speed measurement from Doppler spectra.

Oklahoma University's Meteorology Department has made important contributions towards the Tornado Intercept Project's success under the guidance of Drs. Yoshi

Sasaki, Jeff Kimpel, and Howie Bluestein. Don Burgess, Ed Brandes, Les Lemon, and John Weaver have filled the exacting roles of Storm Chase Coordinator and Nowcaster. In addition, Don Burgess provided most of the real-time information on Doppler radar signatures. Roughly fifty people, too many to list individually, have been regular members of the field teams. The efforts of D. Purcell and K. Droegemeier in pre-season preparations and post-season documentation are especially appreciated.

The photogrammetric results are due to the painstaking work of D. Purcell, R. Zipser, G. Moore, and K. Droegemeier. R. Pettit assisted in the compilation of the waterspout statistics. Thanks are also due to the numerous people who took part in damage surveys, and to members of NSSL's staff who have contributed in many different ways to the work described in this report.

Typing of this report and its preliminary drafts was performed by Ms. Sandy Mudd and Ms. Barbara Franklin. The graphics were drafted by Ms. Joan Kimpel, and Mr. Charles Clark and Mr. Robert Goldsmith prepared the photographic prints.

9. REFERENCES AND PUBLICATIONS AUTHORED WITH SUPPORT FROM NRC (NON-NRC SUPPORTED REFERENCES INDICATED BY ASTERISKS)

*Agee, E. M., C. Church, C. Morris, and J. Snow, 1975: Some synoptic aspects and dynamic features of vortices associated with the tornado outbreak of 3 April 1974. Mon. Wea. Rev., 103, 318-333.

*Armstrong, G. M., and R. J. Donaldson, 1969: Plan shear indicator for real-time Doppler radar identification of hazardous storm winds. J. Appl. Meteor., 8, 376-383.

*Auer, A. H., and J. D. Marwitz, 1972: Hail in the vicinity of organized updrafts. J. Appl. Meteor., 11, 748-752.

*Bates, F. C., 1962: Tornadoes in the Central United States. Transactions Kansas Academy of Science, 65, 215-246.

*_____, 1963: An aerial observation of a tornado and its parent cloud. Weather, 18, 12-18.

Bluestein, H. B., 1979: The University of Oklahoma Severe Storms Intercept Project--1979. Final Report, NOAA, NA79RAD00012, Dept. of Meteorology, Univ. of Oklahoma, Norman, Okla., 39 pp.

_____, 1980: The University of Oklahoma Severe Storms Intercept Project--1979. Bull. Amer. Meteor. Soc., 61, 560-567.

_____, J. McGinley, D. Bowman, D. Carmichael, D. Engles, M. Jain, C. Kessinger, B. Moyer, E. Rasmussen, and D. Rusk, 1978: A contribution to the Severe Storms Intercept Project--1978. Final Report, NSSL Grant No. 04-78-B01-11, Dept. of Meteorology, U. of Oklahoma, Norman, Okla., 66 pp.

*_____, and D. Metzler, 1980: Dual-Doppler analysis of the Oklahoma City severe thunderstorm of 21 May 1974. Preprints, 19th Conf. on Radar Meteorology, Miami Beach, Fla., Amer. Meteor. Soc., 350-356.

Brandes, E. A., 1975: Severe thunderstorm flow characteristics revealed by dual-Doppler observations: 6 June 1974. Preprints, 9th Conf. on Severe Local Storms, Norman, Okla., Amer. Meteor. Soc., 85-90.

_____, 1978: Mesocyclone evolution and tornadogenesis: some observations. Mon. Wea. Rev., 106, 995-1011.

Brown, J. M., and K. R. Knupp, 1980: The Iowa cyclonic-anticyclonic tornado pair and its parent thunderstorm. Mon. Wea. Rev., 108, 1626-1646.

Brown, R. A., Ed., 1976: The Union City, Oklahoma Tornado of 24 May 1973. NOAA Tech. Memo. ERL NSSL-80, National Severe Storms Lab., Norman, Okla., 235 pp.

_____, D. W. Burgess, J. K. Carter, and D. Sirmans, 1975: NSSL dual-Doppler radar measurement in tornadic storms: A preview. Bull. Amer. Meteor. Soc., 56, 524-526.

_____, _____, and K. Crawford, 1973: Twin tornado cyclones within a severe thunderstorm: Single Doppler radar observation. Weatherwise, 26, 63-71.

_____, and L. R. Lemon, 1976: Single Doppler radar vortex recognition: Part II - tornadic vortex signatures. Preprints, 17th Conf. on Radar Meteorology, Seattle, Wash., Amer. Meteor. Soc., 104-109.

_____, _____, and D. W. Burgess, 1978: Tornado detection by pulsed Doppler radar. Mon. Wea. Rev., 106, 29-38.

*Browning, K. A., J. Hallett, T. W. Harold, and D. Johnson, 1968: The collection and analysis of freshly fallen hailstones. J. Appl. Meteor., 7, 603-612.

Burgess, D. W., 1976a: Anticyclonic tornado. Weatherwise, 29, p. 167.

_____, 1976b: Single Doppler radar vortex recognition: Part I - Mesocyclone signatures. Preprints, 17th Conf. on Radar Meteorology, Seattle, Wash., Amer. Meteor. Soc., 97-103.

*_____, J. D. Bonewitz, and D. R. Devore, 1978: Operational Doppler radar experiments: results year 1. Preprints, 18th Conf. on Radar Meteorology, Atlanta, GA, Amer. Meteor. Soc., 442-448.

_____, and R. A. Brown, 1976: Tornado and mesocyclone detection with single Doppler radar. Proceedings, Symposium on Tornadoes: Assessment of Knowledge and Implications for Man. Texas Tech. Univ., Lubbock, Texas, 557-564.

_____, _____, L. R. Lemon, and C. R. Safford, 1977: Evolution of a tornadic storm. Preprints, 10th Conf. on Severe Local Storms, Omaha, Nebr., Amer. Meteor. Soc., 84-89.

_____, and R. P. Davies-Jones, 1977: Unusual tornadic storms in eastern Oklahoma on 5 December 1975. Preprints, 10th Conf. on Severe Local Storms, Omaha, Nebr., Amer. Meteor. Soc., 487-492.

_____, and _____, 1979: Unusual tornadic storms in eastern Oklahoma on 5 December 1975. Mon. Wea. Rev., 107, 451-457.

_____, and D. R. Devore, 1979: Doppler radar utility in severe weather warnings. Preprints, 11th Conf. on Severe Local Storms, Kansas City, Mo., Amer. Meteor. Soc., 577-579.

_____, and R. J. Donaldson, 1979: Contrasting tornadic storm types. Preprints, 11th Conf. on Severe Local Storms, Kansas City, Mo., Amer. Meteor. Soc., 189-192.

*_____, _____, T. Sieland, and J. Hinkelman, 1979: Final Report on the Joint Doppler Project (JDOP) 1976-1978. Part I. NOAA Tech. Memo. ERL NSSL-86, National Severe Storms Lab., Norman, Okla., 84 pp.

_____, L. D. Hennington, R. J. Doviak, and P. S. Ray, 1976: Multi-moment Doppler display for severe storm identification. J. Appl. Meteor., 15, 1302-1306.

_____, L. R. Lemon, and R. A. Brown, 1975: Evolution of a tornado signature and parent circulation as revealed by single Doppler radar. Preprints, 16th Conf. on Radar Meteorology, Houston, Texas, Amer. Meteor. Soc., 99-106.

_____, and _____, 1975: Tornado characteristics revealed by Doppler radar. Geophys. Res. Letts., 2, 183-184.

Burggraf, O. R., and M. R. Foster, 1977: Continuation or breakdown in tornado-like vortices. J. Fluid Mech., 80, 685-703.

Church, C. R., and C. M. Ehresman, 1974: Final Report on the Purdue waterspout program. Final Report, NOAA Grant No. N22-32-72(G). Purdue Univ., West Lafayette, Ind., 97 pp.

_____, _____, and J. H. Golden, 1973: Instrumentation for probing waterspouts. Preprints, 8th Conf. on Severe Local Storms, Denver, Colo., Amer. Meteor. Soc., 169-172.

*Danielsen, E. F., 1975: A conceptual theory of tornadogenesis based on macro-, meso-, and microscale processes. Preprints, 9th Conf. on Severe Local Storms, Norman, Okla., Amer. Meteor. Soc., 376-383.

Davies-Jones, R. P., 1973: The dependence of core radius on swirl ratio in a tornado simulation. J. Atmos. Sci., 30, 1427-1430.

_____, 1974: Discussion of measurements inside high speed thunderstorm updrafts. J. Appl. Meteor., 13, 710-717.

_____, 1976: Laboratory simulation of tornadoes. Proceedings, Symposium on Tornadoes: Assessment of Knowledge and Implications for Man, Texas Tech Univ., Lubbock, Texas, 151-174.

_____, 1979: Dual-Doppler radar coverage area as a function of measurement accuracy and spatial resolution. J. Appl. Meteor., 18, 1229-1233.

_____, 1981: Tornado dynamics. Chapter IX, Thunderstorms: A Social, Scientific and Technological Documentary, Vol. 2, E. Kessler (Ed.), U. S. Government Printing Office, Wash. D.C. (to be published).

_____, D. W. Burgess, and L. R. Lemon, 1975: Analysis of the 4 June 1973 Norman tornadic storm. Preprints, 9th Conf. on Severe Local Storms, Norman, Okla., Amer. Meteor. Soc., 384-388.

_____, _____, and _____, 1976: An atypical tornado-producing cumulonimbus. Weather, 31, 336-347.

_____, _____, _____, and D. Purcell, 1976: Interpretation of surface marks and debris patterns from Union City tornado. Chapter 13, The Union City, Oklahoma Tornadic Storm of 24 May 1973, NOAA Tech. Memo. ERL NSSL-80, R. Brown (Ed.), National Severe Storms Lab., Norman, Okla., 141-156.

_____, _____, _____, and _____, 1978: Interpretation of surface marks and debris patterns from the 24 May 1973, Union City tornado. Mon. Wea. Rev., 106, 12-21.

_____, and J. H. Golden, 1975a: On the relation of electrical activity to tornadoes. J. Geophys. Res., 80, 1614-1616.

_____, and _____, 1975b: Reply to comments on "On the relation of electrical activity to tornadoes," by S. A. Colgate. J. Geophys. Res., 80, 4557.

_____, and _____, 1975c: Reply to comments on "On the relation of electrical activity to tornadoes," by B. Vonnegut. J. Geophys. Res., 80, 4561.

_____, and J. Henderson, 1973: Characteristics of thunderstorm updraft soundings. Preprints, 8th Conf. on Severe Local Storms, Denver, Colo., Amer. Meteor. Soc., 1-5.

_____, and _____, 1974: Updraft properties deduced from rawinsoundings. NOAA Tech. Memo. ERL NSSL-72, National Severe Storms Lab., Norman, Okla., 117 pp.

_____, and _____, 1975: Updraft properties deduced statistically from rawinsoundings. Pure and Appl. Geoph., 113, 787-801.

_____, and E. Kessler, 1974: Tornadoes. Chapter 16 (pp. 552-595), Weather and Climate Modification. Ed., W. N. Hess, John Wiley and Sons, New York, 842 pp.

*Deissler, R. G., 1977: Models for some aspects of atmospheric vortices. J. Atmos. Sci., 34, 1502-1517.

*Donaldson, R. J., and W. E. Lamkin, 1964: Visual observations beneath a developing tornado. Mon. Wea. Rev., 92, 326-329.

Doviak, R. J., D. W. Burgess, L. R. Lemon, and D. Sirmans, 1974: Doppler velocity and reflectivity structure observed within a tornadic storm. J. de Recherches Atmospheriques, VO/VIII, Nos. 1-2, 235-243.

_____, _____, _____, and _____, 1974: Observations of Doppler isotach and reflectivity structure within tornadic storms. Preprints, Inter-Union Commission of Radio Meteorology Colloquium, Nice, France, 23-31 October 1973, Collique de i-IURCR, Vol I, Ch II-9, 7 pp.

_____, and D. Sirmans, 1973: Doppler radar with polarization diversity. J. Atmos. Sci., 30, 737-738.

_____, D. S. Zrnic, and D. S. Sirmans, 1979: Doppler weather radar. Proceedings, IEEE, 67, 1522-1553.

*Eskridge, R. E., and P. Das, 1976: Effect of a precipitation-driven downdraft on a rotating wind field: a possible trigger mechanism for tornadoes. J. Atmos. Sci., 33, 70-84.

*Flora, S. D., 1954: Tornadoes of the United States. University of Oklahoma Press, Norman, Okla., 194 pp.

*Forbes, G. S., 1978: Three scales of motion associated with tornadoes. Contract Report NUREG/CR-0363, U.S. Nuclear Regulatory Commission, Washington D.C., 359 pp.

*Fujita, T. T., 1971: Proposed characterization of tornadoes and hurricanes by area and intensity. SMRP Res. Paper 69, Dept. of Geophys. Sciences, The University of Chicago, Chicago, Ill., 42 pp.

*_____1975: New evidence from April 3-4, 1974 tornadoes. Preprints, 9th Conf. on Severe Local Storms, Norman, Okla., Amer. Meteor. Soc., 248-254.

*_____, 1979: Objectives, operation and results of project Nimrod. Preprints, 11th Conf. on Severe Local Storms, Kansas City, Mo., Amer. Meteor. Soc., 259-266.

*_____, D. L. Bradbury, and P. G. Black, 1967: Estimation of tornado wind speeds from characteristic ground marks. SMRP Res. Pap. 67, Dept. of Geophys. Sciences, The University of Chicago, Chicago, Ill., 19 pp.

*_____, K. Watanabe, K. Tsuchiya, and M. Schimada, 1972: Typhoon-associated tornadoes in Japan and the new evidence of suction vortices in a tornado near Tokyo. J. Meteor. Soc. of Japan, 50, 431-453.

*Gannon, R., 1973: Tornado! How science tracks down the dread twister. Popular Science, September, 64-66, 122-125.

Gillespie, E. S., and D. S. Zrnic', 1978: Maximum wind speeds in two tornadic storms. Preprints, 18th Conf. on Radar Meteorology, Atlanta, GA, Amer. Meteor. Soc., 197-202.

*Golden, J. H., 1969: The Dinner Key 'Tornadic-Waterspout' of June 7, 1968. Mariner's Weather Log, 13, 139-147.

*_____, 1970: The lower Florida Keys waterspout project, May-September, 1969. Bull. Amer. Meteor. Soc., 51, 235-236.

*_____, 1971: Waterspouts and tornadoes over south Florida. Mon. Wea. Rev., 99, 146-154.

_____, 1973: Some statistical aspects of waterspout formation. Weatherwise, 26, 108-117.

_____, 1974a: The life cycle of Florida Keys' waterspouts. I. J. Appl. Meteor., 13, 676-692.

_____, 1974b: Scale-interaction implications for the waterspout life-cycle. II. J. Appl. Meteor., 13, 693-709.

_____, 1974c: Life cycle of Florida Key's waterspouts. NOAA Tech. Memo. ERL NSSL-70, National Severe Storms Lab., Norman, Okla., 147 pp.

_____, 1976a: Tornado intercept strategy and morphological observations. Appendix A, The Union City, Oklahoma tornado of 24 May 1973. NOAA Tech. Memo. ERL NSSL-80, R. Brown (Ed.), National Severe Storms Lab., Norman, Okla., 185-189.

_____, 1976b: Comparison of Union City tornado life-cycle with Florida Keys waterspout life-cycle. Chapter 12, The Union City, Oklahoma tornado of 24 May 1973. NOAA Tech. Memo. ERL NSSL-80, R. Brown (Ed.), National Severe Storms Lab., Norman, Okla., 135-140.

_____, 1976c: An assessment of windspeeds in tornadoes. Proceedings, Symposium on Tornadoes: Assessment of Knowledge and Implications for Man, Texas Tech Univ., Lubbock, Texas, 5-42.

_____, 1977: An assessment of waterspout frequencies along the U.S. East and Gulf Coasts. J. Appl. Meteor., 16, 231-236.

_____, and R. P. Davies-Jones, 1975: Photogrammetric windspeed analysis and damage interpretation of the Union City, Oklahoma tornado, May 24, 1973. Proceedings, 2nd U.S. Natl. Conf. on Wind Engineering Research, Fort Collins, Colo., II-2-1 to II-2-4.

_____, and J. McCarthy, 1975: Some tornado characteristics over Kentucky, southern Indiana and southern Ohio on April 3, 1974 from aerial damage surveys. Paper presented at the 55th Annual Meeting of the Amer. Meteor. Soc., Denver, Colo., 20-23 January.

_____, and B. J. Morgan, 1972: The NSSL/Notre Dame tornado intercept program, spring 1972. Bull. Amer. Meteor. Soc., 53, 1178-1179.

_____, and D. Purcell, 1975: Photogrammetric velocities for the Great Bend, Kansas tornado: acceleration and asymmetries. Preprints, 9th Conf. on Severe Local Storms, Norman, Okla., Amer. Meteor. Soc., 336-343.

_____, and _____, 1976: Airflow characteristics around the Union City tornado. Chapter 14, The Union City, Oklahoma tornado of 24 May 1973. NOAA Tech. Memo. ERL NSSL-80, R. Brown (Ed.), National Severe Storms Lab., Norman, Okla., 141-156.

_____, and _____, 1977: Photogrammetric velocities for the Great Bend, Kansas tornado of 30 August 1974: accelerations and asymmetries. Mon. Wea. Rev., 105, 485-492.

_____, and _____, 1978a: Life cycle of the Union City, Oklahoma tornado and comparison with waterspouts. Mon. Wea. Rev., 106, 3-11.

_____, and _____, 1978b: Airflow characteristics around the Union City tornado. Mon. Wea. Rev., 106, 22-28.

*Goldman, J. L., 1965: The Illinois tornadoes of 17 and 22 April 1963. SMRP Res. Paper No. 39, Dept. of Geophys. Sciences, U. of Chicago, Chicago, Ill., 80 pp.

*Gordon, H., 1971: Comment on a unique tornado report. Mon. Wea. Rev., 99, 649.

*Hoecker, W. H., 1960a: Wind speed and airflow patterns in the Dallas tornado of April 2, 1957. Mon. Wea. Rev., 88, 167-180.

*_____, 1960b: The dimensional and rotational characteristics of the tornadoes and their parent cloud system. The tornadoes at Dallas, Tex., April 2, 1957. U.S. Weather Bureau Res. Paper No. 41, Washington, D.C., U.S. Govt. Printing Office, 53-113.

*_____, 1961: Three-dimensional pressure pattern of the Dallas tornado and some resultant implications. Mon. Wea. Rev., 89, 533-542.

Jischke, M., and M. Parang, 1974: Properties of simulated tornado-like vortices. J. Atmos. Sci., 31, 506-512.

_____, and _____, 1975: Fluid dynamics of a tornado-like vortex flow. Final Report NOAA Grants N22-200-72(G) and 04-4-022-13, School of Aerospace, Mechanical and Nuclear Engineering, U. of Oklahoma, Norman, Okla., 198 pp.

*Kessler, E., 1970: Tornadoes. Bull. Amer. Meteor. Soc., 51, 926-936.

*_____, 1972: On tornadoes and their modification. Mass. Inst. Technol. Rev., 74, May, 48-55.

_____, 1974: Survey of boundary layer winds with special reference to extreme winds. AIAA 7th Fluid and Plasma Dynamics Conf., Palo Alto, Calif., AIAA Paper No. 74-586, 19 pp.

_____, 1976: Recent development in tornado research. Proceedings, Symposium on Tornadoes: Assessment of Knowledge and Implications for Man, Texas Tech Univ., Lubbock, Texas, 431-435.

_____, 1978: Tornadoes: state of knowledge. J. of the Structural Division, ASCE, 104, 352-357.

_____, and J. T. Lee, 1976: Normalized indices of destruction and deaths by tornadoes. NOAA Tech. Memo. ERL NSSL-77, National Severe Storms Lab., Norman, Okla., 47 pp.

_____, and ___, 1978: Distribution of the tornado threat in the United States. Bull. Amer. Meteor. Soc., 59, 61-62.

Kimpel, J., H. Bluestein, J. McGinley, L. Ruthi, D. Engles, and S. Somers, 1977: A contribution to the tornado intercept project 1977. Final Report, NOAA Grant 04-7-022-44018, Dept. of Meteorology, U. of Oklahoma, Norman, Okla. 53 pp.

_____, L. Ruthi, B. Smull, S. George, C. Sohl, S. Young, H. Crowther, and R. Garvin, 1976: A severe storm forecast and intercept project. Final Report, NOAA Grant 04-6-022-44024, Dept. of Meteorology, U. of Oklahoma, Norman, Okla., 59 pp.

*Knight, C. A., and N. C. Knight, 1974: Drop freezing in clouds. J. Atmos. Sci., 31, 1174-1176.

*_____ and _____, 1976: Hail embryo studies. Preprints, International Cloud Physics Conf., Boulder, Colo., Amer. Meteor. Soc., 222-226.

*Kuo, H. L., 1966: On the dynamics of convective atmospheric vortices. J. Atmos. Sci., 23, 25-42.

Lemon, L. R., D. W. Burgess, and R. A. Brown, 1975: Tornado production and storm sustenance. Preprints, 9th Conf. on Severe Local Storms, Norman, Okla., Amer. Meteor. Soc., 100-104.

_____, _____, and _____, 1978: Tornadic storm airflow and morphology derived from single-Doppler radar measurements. Mon. Wea. Rev., 106, 48-61.

*_____, and C. A. Doswell, 1979: Severe thunderstorm evolution and mesocyclone structure as related to tornadogenesis. Mon. Wea. Rev., 107, 1184-1197.

*Leslie, F. W., 1977: Surface roughness effects on suction vortex formation: a laboratory simulation. J. Atmos. Sci., 34, 1022-1027.

*_____, 1979: Dynamic behaviour of single and multiple vortex tornadoes inferred from laboratory simulation. Ph.D. Dissertation, Dept. of Meteorology, U. of Oklahoma, Norman, Okla., 139 pp.

Leverson, J. H., P. Sinclair, and J. H. Golden, 1975: Waterspout wind, temperature, and pressure structure deduced from aircraft measurements. Preprints, 9th Conf. on Severe Local Storms, Norman, Okla., Amer. Meteor. Soc., 350-357.

_____, _____, and _____, 1977: Waterspout wind, temperature, and pressure structure deduced from aircraft measurements. Mon Wea. Rev., 105, 725-733.

*Lewellen, W. S., 1976: Theoretical models of the tornado vortex. Proceedings, Symposium on Tornadoes: Assessment of Knowledge and Implications for Man, Texas Tech Univ., Lubbock, Texas, 107-143.

*Lilly, D. K., 1965: Experimental generation of convectively driven vortices. Geofisica Internacional, 5, 43-48.

*_____, 1969: Tornado dynamics. NCAR Manuscript 69-117, National Center for Atmospheric Research, Boulder, Colo., 39 pp.

*_____, 1975: Severe storms and storm systems: scientific background, methods and critical questions. Pure and Appl. Geoph., 113, 713-734.

*_____, 1976: Sources of rotation and energy in the tornado. Proceedings, Symposium on Tornadoes: Assessment of Knowledge and Implications for Man, Texas Tech Univ., Lubbock, Texas, 145-150.

*Long, R. R., 1961: A vortex in an infinite fluid. J. Fluid Mech., 11, 611-624.

*Ludlam, D. M., 1970: Early American Tornadoes. Amer. Meteor. Soc., Boston, Mass., 219 pp.

*Macky, W. A., 1953: The Easter tornadoes at Bermuda. Weatherwise, 6, 74-75.

Martner, B. E., 1975: Final report on the University of Wyoming's participation in NSSL Project Storm Intercept, 1975 (data analysis). Final Project Report under NSSL Contract No. 03-5-022-66, Dept. Atmospheric Sciences, U. of Wyoming, Laramie, Wyoming, 14 pp. + figs.

*Michaud, L. M., 1977: On the energy and control of atmospheric vortices. J. Rech. Atmos., 11, 99-120.

Minor, J. E., J. R. McDonald, and K. C. Mehta, 1977: The tornado: an engineering-oriented perspective. NOAA Tech. Memo. ERL NSSL-82, National Severe Storms Lab., Norman, Okla., 196 pp.

*Moller, A., C. Doswell, J. McGinley, S. Tegtmeier, and R. Zipser, 1974: Field observations of the Union City tornado in Oklahoma. Weatherwise, 27, 68-77.

Morgan, B. J., 1972: Severe storm detection and tracking-photographic mission. Final Project Report, NSSL Grant No. N22-149-72(G), Dept. Civil Eng., Notre Dame Univ., South Bend, Ind., 34 pp.

_____, 1974: Tornado photographic analysis. Final Report, NSSL-NOAA Grant No. 04-4-022-8, Dept. Civil Eng., Notre Dame Univ., South Bend, Ind., 47 pp.

*Morton, B. R., 1966: Geophysical vortices. Progress in Aeronautical Sciences, 7, Pergamon Press, New York, 145-193.

NOAA, 1977: Tornadoes: a spotter's guide. Movie available from Disaster Preparedness Office, National Weather Service, NOAA, Silver Spring, Maryland.

*NOAA, 1980: A slide series supplement to tornado: "A Spotters Guide." Slides available from Weather and Flood Warnings Coordination Program, National Weather Service, NOAA, Silver Spring, Maryland.

*NWS, 1972: Programs and accomplishments, Systems Development Office, Fiscal Year 1972, NOAA, National Weather Service, 40 pp.

Ray, P. S., 1976: Vorticity and divergence fields within tornadic storms from dual-Doppler observations. J. Appl. Meteor., 15, 879-890.

___, R. J. Doviak, G. A. Walker, D. Sirmans, J. K. Carter, and W. C. Bumgarner, 1975: Dual-Doppler observation of a tornadic storm. Preprints, 16th Conf. on Radar Meteorology, Houston, Texas, Amer. Meteor. Soc., 115-120.

___, _____, _____, _____, _____, and _____, 1975: Dual-Doppler observations of a tornadic storm. J. Appl. Meteor., 14, 1521-1530.

___, C. E. Hane, R. P. Davies-Jones, and R. Alberty, 1976: Tornado-parent storm relationship deduced from a dual-Doppler radar analysis. Geophys. Res. Letts., 3, 721-723.

___, and K. Wagner, 1975: Multiple Doppler radar observation of tornadic storms. Preprints, 10th International Symposium on Remote Sensing of Environment, Ann Arbor, Mich., October 6-10, 163-172.

*Rossman, F. O., 1960: On the physics of tornadoes. Cumulus Dynamics, Pergamon Press, New York, 167-174.

*Rossow, V. J., 1969: On the electrical nature of waterspouts. Preprints, 6th Conf. on Severe Local Storms, Chicago, Ill., Amer. Meteor. Soc., 182-187.

*_____, 1970: Observations of waterspouts and their parent clouds. NASA Tech. Note D-5854, National Aeronautics and Space Administration, Washington, D.C., 63 pp.

*Saunders, P. M., 1963: Simple sky photogrammetry. Weather, 18, 8-11.

*Schwiesow, R. L., and R. E. Cupp, 1976: Remote Doppler velocity measurements of atmospheric dust devil vortices. Appl. Opt., 15, 1-2.

*_____, ____, M. J. Post, R. F. Abbey, and P. C. Sinclair, 1977: Velocity structure of waterspouts and dust devils as revealed by Doppler lidar measurements. Preprints, 10th Conf. on Severe Local Storms, Omaha, Nebr., Amer. Meteor. Soc., 116-119.

*Silberg, P. A., 1966: Dehydration and burning produced by the tornado. J. Atmos. Sci., 23, 202-205.

Sinclair, P. C., 1978: Vortex structure and dynamics of Florida Keys waterspouts. 1974 Field Experiment, Final Report, NOAA Grant 04-5002-8 and NRC Grant AT49-24-0197, Dept. of Atmospheric Science, Colorado State Univ., Fort Collins, Colo., 158 pp.

Sirmans, D., 1973: Real-time estimate of mean velocity by averaging quantized phase displacement of Doppler radar echoes. 1973 SWIEECO Record of Tech. Reports, 25th Annual Southwestern IEEE Conf. & Exhibition, Houston, Texas, IEEE Catalog No. 73CH0719-5-SWIECO, 71-72.

_____, and W. C. Bumgarner, 1975: Estimation of spectral density mean and variance by covariance argument techniques. Preprints, 16th Radar Meteor. Conf., Houston, Texas, Amer. Meteor. Soc., 6-13.

_____, and _____, 1975: Numerical comparison of five mean frequency estimators. J. Appl. Meteor., 14, 991-1003.

_____, and R. J. Doviak, 1973: Pulsed Doppler velocity isotach displays of storm winds in real time. J. Appl. Meteor., 694-697.

_____, _____, D. W. Burgess, and L. R. Lemon, 1974: Real-time Doppler isotach and reflectivity signature of a tornado cyclone. Bull. Amer. Meteor. Soc., 55, 1126-1127.

*Smith, M., 1974: Visual observations of a tornadic thunderstorm. Weatherwise, 27, 256-258.

*Smith, R. K., and L. M. Leslie, 1979: A numerical study of tornadogenesis in a rotating thunderstorm. Quart. J. Roy. Meteor. Soc., 105, 107-127.

*Starr, V. P., 1974: The tornado mechanism and its possible artificial duplication. Revista Italiana di Geofisica, 23, 267-271.

*Tegtmeier, S. A., 1974: The role of the surface, subsynoptic system in severe weather forecasting. Master's Thesis, Univ. of Oklahoma, Norman, Okla., 66 pp.

*USNRC, 1974: USNRC Regulatory Guide 1.76. U.S. Nuclear Regulatory Commission, Washington, D.C.

*Vonnegut, B., 1960: Electrical theory of tornadoes. J. Geophys. Res., 65, 203-212.

*_____, and R. E. Passarelli, 1978: Modified cine sound camera for photographing thunderstorms and recording lightning. J. Appl. Meteor., 17, 1079-1081.

*Ward, N. B., 1961: Radar and surface observations of tornadoes on May 4, 1961. Proceedings, 9th Weather Radar Conf., Kansas City, Mo., Amer. Meteor. Soc., 175-180.

*____, 1972: The exploration of certain features of tornado dynamics using a laboratory model. J. Atmos. Sci., 29, 1194-1204.

Weaver, J. F., and C. R. Safford, 1977: A case study of mesocyclone formation. Preprints, 10th Conf. on Severe Local Storms, Omaha, Nebr., Amer. Meteor. Soc., 505-510.

Wilk, K., and R. A. Brown, 1975: Applications of conventional and Doppler radar measurements in severe storm research. Preprints, 3rd Symposium of Meteor. Observations and Instrumentation, Amer. Meteor. Soc., 165-174; also Proceedings, IEEE 1975 Electronics and Aerospace Conf., Washington D.C., 75 CHO 998-5 EASCON.

*____, and E. Kessler, 1970: Quantitative radar measurements of precipitation. Met. Monographs, 11, No. 33, 315-329.

*Williams, R. J., 1976: Surface parameters associated with tornadoes. Mon. Wea. Rev., 104, 540-545.

*Wolford, L. V., 1960: Tornado occurrences in the United States. Tech. Paper No. 20, Rev. Ed., U.S. Weather Bureau, Washington, D.C. 71 pp.

Wood, V. T., D. W. Burgess, and R. A. Brown, 1979: Single Doppler radar evolution of the Del City, Oklahoma tornado cyclone. Preprints, 11th Conf. on Severe Local Storms, Kansas City, Mo., Amer. Meteor. Soc., 545-548.

Zahrai, F. A., 1980: Real-time Doppler radar data processing and display. Preprints, 19th Conf. on Radar Meteorology, Miami Beach, Fla., Amer. Meteor. Soc., 211-215.

Zipser, R. A., 1976: Photogrammetric studies of a Kansas tornado and a Hawaiian tornadic-waterspout. Master's Thesis, Dept. of Meteorology, Univ. of Oklahoma, Norman, Okla., 75 pp.

Zrnic', D. S., 1975: Simulation of weatherlike Doppler spectra and signals. J. Appl. Meteor., 14, 619-620.

_____, 1979: Estimation of spectral moments for weather echoes. IEEE Trans. on Geosci. Electr., 17, 113-128.

_____, and R. J. Doviak, 1975: Velocity spectra of vortices scanned with a pulsed Doppler radar. J. Appl. Meteor., 14, 1531-1539.

_____, and _____, 1976: Tornado probing with a pulse-Doppler radar. Proceedings, Symposium on Tornadoes: Assessment of Knowledge and Implications for Man. Texas Tech Univ., Lubbock, Texas, 465-473.

_____, _____, and D. W. Burgess, 1978: Probing tornadoes with pulse-Doppler radar. Quart. J. Roy. Meteor. Soc., 103, 707-720.

_____, _____, _____, and D. Sirmans, 1976: Tornado characteristics revealed by a pulse-Doppler radar. Preprints, 16th Conf. on Radar Meteorology, Seattle, Wash., Amer. Meteor. Soc., 110-117.

_____, and M. Istok, 1980: Maximum wind speeds and tornado parameters deduced from Doppler spectra. Preprints, 19th Conf. on Radar Meteorology, Miami Beach, Fla., Amer. Meteor. Soc., 376-383.

_____, and _____, 1980: Wind speeds in two tornadic storms and a tornado deduced from Doppler spectra. J. Appl. Meteor., 19, 1405-1415.

NATIONAL SEVERE STORMS LABORATORY

The NSSL Technical Memoranda, beginning at No. 28, continue the sequence established by the U. S. Weather Bureau National Severe Storms Project, Kansas City, Missouri. Numbers 1-22 were designated NSSP Reports. Numbers 23-27 were NSSL Reports, and 24-27 appeared as subseries of Weather Bureau Technical Notes. These reports are available from the National Technical Information Service, Operations Division, Springfield, Virginia 22151, a microfiche version for $3.50 or a hard copy, cost depending upon the number of pages. NTIS numbers are given below in parenthesis.

No. 1 National Severe Storms Project Objectives and Basic Design. Staff, NSSP. March 1961, 16 p. (PB-168207)

No. 2 The Development of Aircraft Investigations of Squall Lines from 1956-1960. B. B. Goddard. 34 p. (PB-168208)

No. 3 Instability Lines and Their Environments as Shown by Aircraft Soundings and Quasi-Horizontal Traverses. D. T. Williams. February 1962. 15 p. (PB-168209)

No. 4 On the Mechanics of the Tornado. J. R. Fulks. February 1962. 33 p. (PB-168210)

No. 5 A Summary of Field Operations and Data Collection by the National Severe Storms Project in Spring 1961. J. T. Lee. March 1962. 47 p. (PB-165095)

No. 6 Index to the NSSP Surface Network. T. Fujita. April 1962. 32 p. (PB-168212)

No. 7 The vertical structure of Three Dry Lines as Revealed by Aircraft Traverses. E. L. McGuire. April 1962. 10 p. (PB-168213)

No. 8 Radar Observations of a Tornado Thunderstorm in Vertical Section. Ralph J. Donaldson, Jr. April 1962. 21 p. (PB-174859)

No. 9 Dynamics of Severe Convective Storms. Chester W. Newton. July 1962. 44 p. (PB-163319)

No. 10 Some Measured Characteristics of Severe Storms Turbulence. Roy Steiner and Richard H. Rhyne. July 1962. 17 p. (N62-16401)

No. 11 A Study of the Kinematic Properties of Certain Small-Scale Systems. D. T. Williams. October 1962. 22 p. (PB-168216)

No. 12 Analysis of the Severe Weather Factor in Automatic Control of Air Route Traffic. W. Boynton Beckwith. December 1962. 67 p. (PB-168217)

No. 13 500-Kc./Sec. Sferics Studies in Severe Storms. Douglas A. Kohl and John E. Miller. April 1963. 36 p. (PB-168218)

No. 14 Field Operations of the National Severe Storms Project in Spring 1962. L. D. Sanders. May 1963. 71 p. (PB-168219)

No. 15 Penetrations of Thunderstorms by an Aircraft Flying at Supersonic Speeds. G. P. Roys. Radar Photographs and Gust Loads in Three Storms of 1961 Rough Rider. Paul W. J. Schumacher. May 1963. 19 p. (PB-168220)

No. 16 Analysis of Selected Aircraft Data from NSSP Operations, 1962. T. Fujita. May 1963. 29 p. (PB-168221)

No. 17 Analysis of Methods for Small-Scale Surface Network Data. D. T. Williams. August 1963. 20 p. (PB-168222)

No. 18 The Thunderstorm Wake of May 4, 1961. D. T. Williams. August 1963. 23 p. (PB-168223)

No. 19 Measurements by Aircraft of Condensed Water in Great Plains Thunderstorms. George P. Roys and Edwin Kessler. July 1966. 17 p. (PB-173048)

No. 20 Field Operations of the National Severe Storms Project in Spring 1963. J. T. Lee, L. D. Sanders, and D. T. Williams. January 1964. 68 p. (PB-168224)

No. 21 On the Motion and Predictability of Convective Systems as Related to the Upper Winds in a Case of Small Turning of Wind with Height. James C. Fankhauser. January 1964. 36 p. (PB-168225)

No. 22 Movement and Development Patterns of Convective Storms and Forecasting the Probability of Storm Passage at a Given Location. Chester W. Newton and James C. Fankhauser. January 1964. 53 p. (PB-168226)

No. 23 Purposes and Programs of the National Severe Storms Laboratory, Norman, Oklahoma. Edwin Kessler. December 1964. 17 p. (PB-166675)

No. 24 Papers on Weather Radar, Atmospheric Turbulence, Sferics and Data Processing. August 1965. 139 p. (AD-621586)

No. 25 A Comparison of Kinematically Computed Precipitation with Observed Convective Rainfall. James C. Fankhauser. September 1965. 28 p. (PB-168445)

No. 26 Probing Air Motion by Doppler Analysis of Radar Clear Air Returns. Roger M. Lhermitte. May 1966. 37 p. (PB-170636)

No. 27 Statistical Properties of Radar Echo Patterns and the Radar Echo Process. Larry Armijo. May 1966. The Role of the Kutta-Joukowski Force in Cloud Systems with Circulation. J. L. Goldman. May 1966. 34 p. (PB-170756)

No. 28 Movement and Predictability of Radar Echoes. James Warren Wilson. November 1966. 30 p. (PB-173972)

No. 29 Notes on Thunderstorm Motions, Heights, and Circulations. T. W. Harrold, W. T. Roach, and Kenneth E. Wilk. November 1966. 51 p. (AD-644899)

No. 30 Turbulence in Clear Air Near Thunderstorms. Anne Burns, Terence W. Harrold, Jack Burnham, and Clifford S. Spavins. December 1966. 20 p. (PB-173992)

No. 31 Study of a Left-Moving Thunderstorm of 23 April 1964. George R. Hammond. April 1967. 75 p. (PB-174681)

No. 32 Thunderstorm Circulations and Turbulence from Aircraft and Radar Data. James C. Fankhauser and J. T. Lee. April 1967. 32 p. (PB-174860)

No. 33 On the Continuity of Water Substance. Edwin Kessler. April 1967. 125 p. (PB-175840)

No. 34 Note on the Probing Balloon Motion by Doppler Radar. Roger M. Lhermitte. July 1967. 14 p. (PB-175930)

No. 35 A Theory for the Determination of Wind and Precipitation Velocities with Doppler Radars. Larry Armijo. August 1967. 20 p. (PB-176376)

No. 36 A Preliminary Evaluation of the F-100 Rough Rider Turbulence Measurement System. U. O. Lappe. October 1967. 25 p. (PB-177037)

No. 37 Preliminary Quantitative Analysis of Airborne Weather Radar. Lester P. Merritt. December 1967. 32 p. (PB-177188)

No. 38 On the Source of Thunderstorm Rotation. Stanley L. Barnes. March 1968. 28 p. (PB-178990)

No. 39 Thunderstorm - Environment Interactions Revealed by Chaff Trajectories in the Mid-Troposphere. James C. Fankhauser. June 1968. 14 p. (PB-179659)

No. 40 Objective Detection and Correction of Errors in Radiosonde Data. Rex L. Inman. June 1968. 50 p. (PB-180284)

No. 41 Structure and Movement of the Severe Thunderstorms of 3 April 1964 as Revealed from Radar and Surface Mesonetwork Data Analysis. Jess Charba and Yoshikazu Sasaki. October 1968. 47 p. (PB-183310)

No. 42 A Rainfall Rate Sensor. Brian E. Morgan. November 1968. 10 p. (PB-183979)

No. 43 Detection and Presentation of Severe Thunderstorms by Airborne and Ground-based Radars: A Comprehensive Study. Kenneth E. Wilk, John K. Carter, and J. T. Dooley. February 1969. 56 p. (PB-183572)

No. 44 A Study of a Severe Local Storm of 16 April 1967. George Thomas Haglund. May 1969. 54 p. (PB-184970)

No. 45 On the Relationship Between Horizontal Moisture Convergence and Convective Cloud Formation. Horace R. Hudson. March 1970. 29 p. (PB-191720)

No. 46 Severe Thunderstorm Radar Echo Motion and Related Weather Events Hazardous to Aviation Operations. Peter A. Barclay and Kenneth E. Wilk. June 1970. 63 p. (PB-192498)

No. 47 Evaluation of Roughness Lengths at the NSSL-WKY Meteorological Tower. Leslie D. Sanders and Allen H. Weber. August 1970. 24 p. (PB-194587)

No. 48 Behavior of Winds in the Lowest 1500 ft in Central Oklahoma: June 1966-May 1967. Kenneth C. Crawford and Horace R. Hudson. August 1970. 57 p. (N71-10615)

No. 49 Tornado Incidence Maps. Arnold Court. August 1970. 76 p. (COM-71-00019)

No. 50 The Meteorologically Instrumented WKY-TV Tower Facility. John K. Carter. September 1970. 18 p. (COM-71-00108)

No. 51 Papers on Operational Objective Analysis Schemes at the National Severe Storms Forecast Center. Rex L. Inman. November 1970. 91 p. (COM-71-00136)

No. 52 The Exploration of Certain Features of Tornado Dynamics Using a Laboratory Model. Neil B. Ward. November 1970. 22 p. (COM-71-00139)

No. 53 Rawinsonde Observation and Processing Techniques at the National Severe Storms Laboratory. Stanley L. Barnes, James H. Henderson and Robert J. Ketchum. April 1971. 245 p. (COM-71-00707)

No. 54 Model of Precipitation and Vertical Air Currents. Edwin Kessler and William C. Bumgarner. June 1971. 93 p. (COM-71-00911)

No. 55 The NSSL Surface Network and Observations of Hazardous Wind Gusts. Operations Staff. June 1971. 20 p. (COM-71-00910)

No. 56 Pilot Chaff Project at the National Severe Storms Laboratory. Edward A. Jessup. November 1971. 36 p. (COM-72-10106)

No. 57 Numerical Simulation of Convective Vortices. Robert P. Davies-Jones and Glenn T. Vickers. November 1971. 27 p. (COM-72-10269).

No. 58 The Thermal Structure of the Lowest Half Kilometer in Central Oklahoma: December 9, 1966-May 31, 1967. R. Craig Goff and Horace R. Hudson. July 1972. 53 p. (COM-72-11281)

No. 59 Cloud-to-Ground Lightning Versus Radar Reflectivity in Oklahoma Thunderstorms. Gilbert D. Kinzer. September 1972. 24 p. (COM-73-10050)

No. 60 Simulated Real Time Displays of Velocity Fields by Doppler Radar. L. D. Hennington and G. B. Walker. November 1972. 10 p. (COM-73-10515)

No. 61 Gravity Current Model Applied to Analysis of Squall-Line Gust Front. Jess Charba. November 1972. 58 p. (COM-73-10410)

No. 62 Mesoscale Objective Map Analysis Using Weighted Time-Series Observations. Stanley L. Barnes. March 1973. 60 p. (COM-73-10781)

No. 63 Observations of Severe Storms on 26 and 28 April 1971. Charles L. Vlcek. April 1973. 19 p. (COM-73-11200)

No. 64 Meteorological Radar Signal Intensity Estimation. Dale Sirmans and R. J. Doviak. September 1973. 80 p. (COM-73-11923/2AS)

No. 65 Radisonde Altitude Measurement Using Double Radiotheodolite Techniques. Stephan P. Nelson. September 1973. 20 p. (COM-73-11932/9AS)

No. 66 The Motion and Morphology of the Dryline. Joseph T. Schaefer. September 1973. 81 p. (COM-74-10043)

No. 67 Radar Rainfall Pattern Optimizing Technique. Edward A. Brandes. March 1974. 16 p. (COM-74-10906/AS)

No. 68 The NSSL/WKY-TV Tower Data Collection Program: April-July 1972. R. Craig Goff and W. David Zittel. May 1974. 45 p. (COM-74-11334/AS)

No. 69 Papers on Oklahoma Thunderstorms, April 29-30, 1970. Stanley L. Barnes, Editor. May 1974. 147 p. (COM-74-11474/AS)

No. 70 Life Cycle of Florida Key's Waterspouts. Joseph H. Golden. June 1974. 147 p. (COM-74-11477/AS)

No. 71 **Interaction of Two Convective Scales Within a Severe Thunderstorm: A Case Study and Thunderstorm** Wake Vortex Structure and Aerodynamic Origin. Leslie R. Lemon. June 1974. 43 p. (COM-74-11642/AS)

No. 72 Updraft Properties Deduced from Rawinsoundings. Robert P. Davies-Jones and James H. Henderson. October 1974. 117 p. (COM-75-10583/AS)

No. 73 Severe Rainstorm at Enid, Oklahoma - October 10, 1973. L. P. Merritt, K. E. Wilk, and M. L. Weible. November 1974. 50 p. (COM-75-10583/AS)

No. 74 Mesonetwork Array: Its Effect on Thunderstorm Flow Resolution. Stanley L. Barnes. October 1974. 16 p. (COM-75-10248/AS)

No. 75 Thunderstorm-Outflow Kinematics and Dynamics. R. Craig Goff. December 1975. 63 p. (PB-250808/AS)

No. 76 An Analysis of Weather Spectra Variance in a Tornadic Storm. Philippe Waldteufel. May 1976. 80 p. (PB-258456/AS)

No. 77 Normalized Indices of Destruction and Deaths by Tornadoes. Edwin Kessler and J. T. Lee. June 1976. 47 p. (PB-260923/AS)

No. 78 Objectives and Accomplishments of the NSSL 1975 Spring Program. K. Wilk, K. Gray, C. Clark, D. Sirmans, J. Dooley, J. Carter, and W. Bumgarner. July 1976. 47 p. (PB-263813/AS)

No. 79 Subsynoptic Scale Dynamics As Revealed By The Use Of Filtered Surface Data. Charles A. Doswell III. December 1976. 40 p. (PB-265433/AS)

No. 80 The Union City, Oklahoma Tornado of 24 May 1973. Rodger A. Brown, Editor. December 1976. 235 p. (PB-269443/AS)

No. 81 Mesocyclone Evolution and Tornado Generation Within the Harrah, Oklahoma Storm. Edward A. Brandes. May 1977 28 p. (PB-271675/AS)

No. 82 The Tornado: An Engineering-Oriented Perspective. Joseph E. Minor, James R. McDonald, and Kishor C. Mehta. December 1977. 196 p. (PB-281860/AS)

No. 83 Spring Program '76. R. L. Alberty, J. F. Weaver, D. Sirmans, J. T. Dooley, and B. Bumgarner. December 1977. 130 p. (PB280745/AS)

No. 84 Spring Program '77. P. S. Ray, J. Weaver, and NSSL Staff. December 1977. 173 p. (PB-284953/AS)

No. 85 A Dual-Doppler Variational Objective Analysis as Applied to Studies of Convective Storms. Conrad L. Ziegler. November 1978. 116 p. (PB-293581/AS)

No. 86 Final Report on the Joint Doppler Operational Project (JDOP) 1976-78. Prepared by Staff of the National Severe Storms Laboratory, Environmental Research Laboratories; Weather Radar Branch, Air Force Geophysics Laboratory; Equipment Development Laboratory, National Weather Service; and Air Weather Service, United States Air Force. March 1979. 84 p. (PB80-107188/AS)

No. 87 An Analysis of the Clear Air Planetary Boundary Layer Wind Synthesized from NSSL's Dual Doppler-Radar Data. Myron I. Berger and R. J. Doviak. June 1979. 55 p. (PB-300865/AS)

No. 88 The Relationship of the 300-mb Jet Stream to Tornado Occurrence. Carolyn M. Kloth and Robert P. Davies-Jones. July 1980. 62 p.

No. 89 A Study of Hail Production in a Supercell Storm Using a Doppler Derived Wind Field and a Numerical Hail Growth Model. Stephan P. Nelson. December 1980. 90 p.

☆ U. S. GOVERNMENT PRINTING OFFICE 1980 - 777-002/1226 Reg. 8